THE TEMPERATURE PREDICTION IN DEEPWATER DRILLING OF VERTICAL WELL

A Dissertation

by

MING FENG

Submitted to the Office of Graduate Studies of
Texas A&M University
in partial fulfillment of the requirements for the degree of

DOCTOR OF PHILOSOPHY

May 2011

Major Subject: Petroleum Engineering

THE TEMPERATURE PREDICTION IN DEEPWATER DRILLING OF VERTICAL WELL

A Dissertation

by

MING FENG

Submitted to the Office of Graduate Studies of
Texas A&M University
in partial fulfillment of the requirements for the degree of

DOCTOR OF PHILOSOPHY

Approved by:

Co-Chairs of Committee,	Jerome Schubert
	Catalin Teodoriu
Committee Members,	Hans Juvkam-Wold
	Benchun Duan
Head of Department,	Stephen A. Holditch

May 2011

Major Subject: Petroleum Engineering

ABSTRACT

The Temperature Prediction in Deepwater Drilling of Vertical Well. (May 2011)
Ming Feng, B. S., Southwest Petroleum University, China;
M. S., Southwest Petroleum University, China;
M. S., University of Louisiana at Lafayette
Chair of Advisory Committee: Dr. Jerome Schubert

The extreme operating conditions in deepwater drilling lead to serious relative problems. The knowledge of subsea temperatures is of prime interest to petroleum engineers and geo-technologists alike. Petroleum engineers are interested in subsea temperatures to better understand geo-mechanisms; such as diagenesis of sediments, formation of hydrocarbons, genesis and emplacement of magmatic formation of mineral deposits, and crustal deformations. Petroleum engineers are interested in studies of subsurface heat flows. The knowledge of subsurface temperature to properly design the drilling and completion programs and to facilitate accurate log interpretation is necessary. For petroleum engineers, this knowledge is valuable in the proper exploitation of hydrocarbon resources.

This research analyzed the thermal process in drilling or completion process. The research presented two analytical methods to determine temperature profile for onshore drilling and numerical methods for offshore drilling during circulating fluid down the drillstring and for the annulus. Finite difference discretization was also introduced to predict the temperature for steady-state in conventional riser drilling and riserless drilling. This research provided a powerful tool for the thermal analysis of wellbore and rheology design of fluid with Visual Basic and Matlab simulators.

DEDICATION

To my family for their love and support

ACKNOWLEDGMENTS

During these four years at Texas A&M University I have tried my best to adhere to the requirements of being a qualified graduate student. I got tons of help in the process of pursuing my Ph.D. degree. I want to acknowledge these people for their generosity and kindness.

First of all, my gratitude goes to my advisors, Dr. Jerome Schubert and Dr. Catalin Teodoriu, for their academic advice to me in these years, and in years to come. Their inspiration, encouragement, guardianship, and patience were essential for my research and study.

I would also like to express my sincere appreciation to my committee member, Dr. Hans Juvkam-Wold, for his advice, knowledge, and priceless assistance during these years.

Thanks are also extended to a member of my supervising committee, Dr. Benchun Duan, of the Department of Geology and Geophysics, for managing time out of his busy schedule to provide valuable comments and suggestions.

I wish to express my appreciation to the faculty and staff of the Department of Petroleum Engineering at Texas A&M University. I am indebted to my colleagues because they made the whole study more enjoyable. I truly appreciate my family, without their support I would not have realized my dream.

TABLE OF CONTENTS

Page

Page

LIST OF TABLES

Page

Page

LIST OF FIGURES

Page

Page

Page

Page

Page

CHAPTER I

INTRODUCTION AND OBJECTIVES

The petroleum industry is exploring extensively and quickly into deep-water oil and gas reservoirs to meet the energy demand. Offshore drilling structures, which are placed in the ocean for the exploration beneath the ocean floor, are at the mercy of the environment they are subject to hostile environments of such areas as the North Sea and the high arctic. The search for the oil has made the drilling of a well a highly complicated and expensive operation. The environments that the structures may face are the ocean current, the oceanography conditions (Chakrabarti 2005). The strong loop ocean currents and induced eddies can pose significant problems for deep-water drilling. Broadly divided ocean currents, surface currents, bottom currents and vertical currents, interact with the deep water drilling structures as one of environmental forces.

One of the engineering challenges in deep water drilling is temperature gradient. In the past the temperature in the wellbore was ignored and an isothermal system was assumed because no practical means existed to determine the well bore temperature profile. But the fact is that the negative thermal gradient exists between surface to seafloor and it becomes positive below the seafloor. The extreme values observed at the seafloor could be as low as 40^{o}F and as high as 150~200^{o}F at the wellbore annulus. Unfortunately, deepwater environments combine low temperatures, high pressures, gas and water that can induce hydrate formation. Hydrates can lead to tubing blockages and affect valves and BOP operation. The low temperatures due to the hydrate or ocean current affect the properties of cement, which indicates to redesign cement slurry composition required.

This dissertation follows the style and format of the *SPE Journal*.

In addition to low temperature condition, the significant heat exchange also occurs for high temperature and geothermal reservoirs. Generally speaking, an accurate model of estimating the temperature distribution and its variation with time would have a variety of applications as follow:

- Enable the dynamic temperature profile and bottom-hole temperature to be determined rather than the static temperatures presently available from electric logging tools.
- Improve cementing program design, particularly with regard to the amount of retarder or actual work required and the setting time.
- Improve drilling fluid design by providing information on the actual circulating temperatures to enable high temperature modifications to be made to the drilling fluid program.
- Enable casing thermal stresses to be determined.
- Provide improved well design in permafrost regions.
- Improve injection and production operations.
- Logging tool design and log interpretation.
- Well control or dynamic kill operations.

In the offshore drilling, fluid flows through the drill pipe, drill bit and goes back up through the annular space, riser or return line to the surface. As long as there always is temperature difference between them, heat exchange occurs inevitably. The heat exchange between the drilling system and ocean currents exists because the continuous flowing colder currents carry the heat away due to the external convection heat transfer interacted with relatively stationary drilling system. The internal forced convection heat transfer also exists extensively in the fluid of the drillpipe, annulus, riser and return line while mud circulating. The friction across the drilling system caused by hydraulic pressure loss also is one of the heat sources which are transferred by the force. The temperature information available at the well site is the inlet and outlet fluid temperature without logging tool.

Although various heat transfer models have been formulated to enable certain parameters to be estimated, most have been oversimplified so as to enable their use at the well site in the form of simple equation, solvable by a slide rule, monographs or plots. As a result the practical application of the relevant theory is minimal. In the present era of powerful computer system, this can no longer be justified and it is becoming increasingly more feasible to utilize the complicated theory that exists in the literature at the well site. Models is developed from such theory with subsequent improvements in an accuracy are probably most useful at the well planning and design stage in view of the fact that large powerful computers are available with virtually no limitations on solution time or storage space for all practical purpose.

The objectives of this research are to develop a hydraulic and temperature simulator to compute the pressure and temperature distribution during routine drilling operations. One of the purposes of this research is to use the existing theory in the steady-state and transient heat flow in a well bore to develop a computer model to estimate the temperature distribution and its variation with circulating time. Unlike previous modes, it will be feasible to use this model at a remote well site without a significant loss of accuracy. Furthermore this model incorporates a number of improvements over previous model in terms of both accuracy and applicability. A further aim of this study was to use the computer model to simulate wellbore temperature distributions so that a complete parametric sensitivity analysis could be carried out to indicate which parameters have the most significant effect on the temperature.

CHAPTER II

LITERATURE REVIEW

The wellbore temperature during drilling depends on many factors such as wellbore geometry, wellbore depth, flow rate, the properties of the formation, the properties of the fluid, the geothermal gradients etc. Although a lot of work has been done, most of them focus on the onshore drilling area.

2.1 Downhole Circulating Mud Heat Transfer Models

Ramey(Ramey JR. 1962) estimated the temperature of fluids, tubing and casing as a function of depth and time. The result was expressed in simple algebraic form suitable for slide-rule calculation. The solution assumed that heat transfer in the wellbore was steady-state, while heat transfer to the earth would be unsteady radial conduction. Allowances were made for heat resistances in the wellbore. The method used might be applied to derivation of other heat problems such as flow through multiple strings in a wellbore.

Raymond(Raymond 1969) calculated drilling temperature. The position and time showed that circulation lowered considerably the temperatures of both the bottom-hole fluid and the rock and that the maximum circulating fluid temperatures happened at a fourth to a third of the way up the annulus. With the trend toward deeper and consequently hotter holes, measurements of drilling mud properties at atmospheric temperatures were becoming increasingly inadequate.

Holmes(Holmes and Swift 1970) developed an analytical mathematical model that could be used to predict the mud temperature in the drill pipe and annulus while drilling at any depth in the well. His modeling was a solution of the steady-state equation for the heat transfer between the fluids in the annulus and the fluids in the drill pipe. The model

in this study was based upon the assumption that the heat transfer between the annular fluid and the formation could be approximated by steady-state linear heat transfer. The Edwardson's work (Edwardson, Girner et al. 1962) had shown that the temperature was relatively constant at any point sufficiently removed from the drill bit. This effect showed that the steady-state assumption appeared to be a close enough approximation of this phenomenon. Other simplifying assumptions were that the heat generated by the drill bit was negligible and that a linear geothermal profile exists.

Schoeppel(Schoeppel and Bennett 1971) developed the numerical simulation of borehole and formation temperature distributions. The method was developed to model numerically the unsteady temperature distributions in a circulating drilling fluid and the surrounding formation. The model was based on a set of fourth-order partial differential equations describing heat flow by forced convection in the wellbore and by conduction in the adjacent formation. Finite-difference representations of these equations were formulated implicitly, and the resulting algebraic equations solved by modified methods of Gaussian elimination. Computer simulation time for solution of the numerical model was reasonably short. The method was found to provide an accurate solution to the problem of predicting non-steady temperature distributions associated with drilling of a well.

Oster(Oster and Scheffler 1976) derived a method described to determine the temperature distribution in a circulating drilling fluid when aquifers are present in the formation. His quasi steady-state model was used to predict the temperature distributions in the drill pipe, annulus and in the rock formation when water from the rock formation was entering the annulus and/or where drilling fluid is flowing from the annulus to the formation.

Wooley(Wooley 1980) presented his model for predicting downhole wellbore temperatures in flowing or shut-in fluid streams, in casing and cement, and in

formations. Flowing options include injection/production, forward/reverse circulation, and drilling. Model predictions agree with field temperature data. The influences of temperature, flow rate, and depth on downhole temperatures were presented.

Zijsling(Zijsling 1984) analyzed temperature distribution and performance of polycrystalline diamond compact bits under field drilling conditions. A thermal model had been developed on the basis of these results to predict the temperature distribution in the PDCs under quasi-static drilling conditions. The maximum temperature was found to occur at the PDC's cutting edge and was virtually independent of PDC position under normal rotary drilling conditions. At elevated rotary speeded however, the maximum cutting edge temperature occurred in PDCs at the gauge of the bit. This temperature could exceed the boiling point of water-based drilling fluids, resulting in higher cutting edge temperatures and wear rates of the PDCs which might lead to premature failure of the bit.

Durrant(Durrant and Thambynayagam 1986) presented a straightforward iterative procedure for the wellbore heat transmission problem during upward or downward flow of a steam/water mixture. The mathematical model was taken directly from the literature and was based on material and momentum balances in the wellbore and a heat balance on the entire system including the surrounding media. The transient heat conduction equation was solved analytically by the application of successive Fourier and Laplace transforms. A simple super-positioning in the time domain permits a matching procedure similar to multiphase flow calculations in pipelines.

Mitchell, R.F(Mitchell and Wedelich III 1989) described an advanced method to predict downhole temperatures during operations. Two specific field cases, tubing movement during stimulation and well deliverability, were investigated in detail. The objective was to determine the range of effects that unknown operating conditions had

on flowing temperatures and pressures, and not assumed that temperatures and pressures were the unknowns.

Kashikar, S.V(Kashikar and Arnold 1991) developed a new method that utilizes temperature recordings from short time flow tests to accurately determine formation temperatures, The temperature distribution prior to production was obtained by solving the diffusivity equation for conductive heat transfer during the circulation period. This provided the initial condition for solving the continuity equation for convective heat transfer during production by the method of characteristics.

Sagar(Sagar, Doty et al. 1991) developed a model with measured temperature data from 392 wells, assumed that the heat transfer within the wellbore is steady-state. Comparisons between the model's predictions and field data indicated that the model was highly accurate within its range of application. Temperature profiles helped calculate accurate two-phase-flow pressure-drop predictions, which in turn could improve an artificial-lift system design.

Marshall(Marshall and Lie 1992) provided a finite difference approach, simultaneously solving all the heat transfer equations. Predictions of bottom hole and return temperatures from this model were shown to closely agree with the presently available field data.

Brown(Brown, Clapham et al. 1996) developed a transient heat transfer model in pipeline bundles. The model was coupled to the transient, multiphase flow simulator OLGA. The lines containing the multiphase production fluids were modeled by OLGA, and the heat transfer between the internal lines, carrier pipe, and surroundings was handled by the bundle model. The model had been applied extensively to the design of a subsea, heated bundle system for the Britannia gas condensate field in the North Sea.

A.R. Hasan(Hasan and Kabir 1996) presented a mechanistic model for the flowing temperature of the annular gas and the gas/liquid two-phase mixture in the tubing as a function of both well depth and production time, regardless of the well deviation angle. The model was based on energy balance between the formation and fluids flowing through each conduit. While flowing down the annulus, the cold gas injected at the wellhead continues to gain heat. The results showed that the temperature profiles in both flow conduits were nonlinear, unlike those used previously, particularly in the annulus.

Kabir, C.S.(Kabir, Hasan et al. 1996) estimated fluid temperature in both flow conduits (drillpipe or tubing and the annulus) to ascertain the fluid density and viscosity, and in turn to calculate the pressure-drop or the maximum allowable pumping rate for a number of operations. Steady-state heat transfer was assumed in the wellbore while transient heat transfer took place in the formation. A limited sensitivity study showed that all the models gave comparable solutions, with the exception of line-source solution at early times.

George J. Zabaras(Zabaras and Zhang 1997) addressed the thermal performance of the subsea equipment that could provide weak thermal links for the subsea system. While subsea insulated flowlines could eliminate or reduce the risk of hydrate formation during steady-state production, they might not provide sufficient cool down time before hydrates were formed during an emergency shutdown. Subsea wellheads, pipe field joints, manifold and flowline tubing jumpers were very difficult to insulate effectively. As a result, these pieces of equipment exhibited faster cool down to hydrate formation temperature than either the wellbore or the flowline. A two-dimensional general purpose finite-element partial differential equation solver was utilized to analyze the steady state and transient thermal behavior at different cross-sections of the subsea tree. In contrast to the intuitive common belief that a subsea tree cool down time to hydrate formation temperature was of the order of several hours. A cool down time less than two hours was determined after a system shutdown. Steady-state analysis of a flowline field joint

indicated that the joint degrades the flowline thermal performance causing up to a 20% increase in the flowline overall heat transfer coefficient.

Calvert, D.G.(Calvert and Griffin 1998) described temperatures in wells drilled in deep water. Computer simulations of wellbore temperatures were presented. Additionally, the simulations showed the effects of factors not taken into account by the API correlation. These factors included circulation rate and time, temperature of the injected fluid and sea temperature and currents, to name a few. Failure to account for the correct temperature could result in greatly extended cement setting times and led to long delays in continued rig operations.

Zhang, Yong(Zhang and Duan 1998) reviewed the high temperature and high pressure well drilling operations conducted by China Offshore Oil Nanhai West Corporation in the Ying-Qiong Area South China Sea and probed the technology applied to the high temperature and high pressure well drilling operation. It emphasized on the prediction of formation pore pressure, well casing program design, casing wear prevention and well drilling technical measures.

Bernt S. Aadnøy(Aadnøy 1999) developed an analytical model by describing the energy balance in a circulating well. Input of energy due to rotation of the drillstring and pumping of the mud were included. The effect of having a riser in offshore applications was also included. It was shown that for most cases there was a net flow of energy from the formation to the surface. In offshore applications there would always be a heat loss in the riser. Calculating the energy balance provided important information on temperature- and fluid density behavior. The new analytical model gave improved temperature profiles throughout the well. In addition to well pressure this information was also important for cement program design, and in some cases, reservoir PVT analysis. The new models were also different from the older numerical approached as

simple model calibration procedures were developed, making the model useful on-site. This paper aimed at implementing these models in a field operation.

Y.D. Chin(Chin, Perera et al. 2000) investigated the thermal interaction among the flowlines and its effects on the overall thermal performance of the bundle, and on the product arrival temperature. Multiphase flow and thermal analysis procedures were conducted for the Garden Banks 216 field pipeline bundle located in the Gulf of Mexico. The investigated bundle had three flowlines that carry multiphase product fluid and heating fluid. The flowlines were enclosed with insulation and encased in a steel casing pipe. The model should be solved using a multiphase flow simulator, OLGA, combined with a modified conduction heat transfer model. The numerical analytical results were compared with the field data.

E. Duret(Duret, Lebreton et al. 2000) developed a transient pipeline bundle numerical module to analyze the thermal interactions between several single phase lines and the main production line. The SYSTUS code developed by SYSTUS International was currently used at Stolt Offshore to solve thermal engineering problems including pipeline bundles. The simulation resulted demonstrate that it was important to take accurately into account thermal effects in case of deep-water production to predict phenomena such as hydrate formation or wax deposition.

M. Ward(Ward, Granberry et al. 2001) monitored the cooling effect of the sea through the measurement of the fluid temperature at the mud line depth. All temperature data were measured by a sensor deployed inside the bottomhole assembly while circulating or drilling. This method was selected for its low cost and lack of interference with drilling operations. Data were collected in the Gulf of Mexico, Brazil, Indonesia and West Africa with an average water depth of 1200 m. The outcome of this study helped to define better cement slurry testing procedures for deepwater applications. As a result the technology that was best suited for these specific conditions could be selected

on a more rigorous technical basis. During drilling operations the cool-down of the fluid in the riser could affect mud rheology, especially for synthetic based mud (SBM), and cause high circulating pressure when pumping was resumed after shut-down, or excessive surge and swab pressures when the pipe was run in or pulled out of the hole. Low fluid temperature combined with relatively high pressures, as might occur in deepwater drilling conditions, could also cause formation of gas hydrates resulting in several adverse effects such as plugging at the BOP's or in the riser.

J.T. Finger(Finger, Jacobson et al. 2002) used software to predict wellbore temperature and to calculate sensitivity in IDP design differences with a comparison of calculated and measured wellbore temperatures in the field test. The analysis was based on mixed (IDP and CDP) drillstrings.

Zhongming Chen(Chen and Novotny 2003) developed a finite difference methods to determine the bottom hole circulating temperature (BHCT) for the proper design of cementing slurries. It also provided the information on temperature recovery after the cement slurry becomes static. Emphasis was placed on evaluation of wells with multiple temperature gradients, multiple fluid circulation schedule, and wellbore deviations. The effect of offshore water currents was also discussed. The predictions of the wellbore temperature profiles and returned temperatures from this model were validated through actual measured wellbore temperature profile history, including offshore and onshore cases.

M. Ward(Ward, Granberry et al. 2003) discussed the importance of temperature in deepwater drilling. All temperature data were measured by a sensor deployed inside the bottomhole assembly (BHA) while circulating or drilling. Data were collected in the Gulf of Mexico, Brazil, Indonesia, and West Africa in an average water depth of 1200 m. A summary of the temperature measurements was presented, and comparison was also made with the predictions of a numerical simulator. Detailed interpretation of the

data gathered pinpoints the importance of correctly accounting for the exact temperature profile in the sea as well as the velocity of sea currents vs. depth.

Fouad Fleyfel(Fleyfel, Hernandez et al. 2004) reviewed active heat in pipe-in-pipe .

Ajay P. Mehta(Mehta, Zabaras et al. 2004) reviewed the prospective of the flow assurance in deepwater exploration. Development of a robust flow assurance strategy would play a central role in the system selection, detailed design, and operation of deepwater heavy oil fields. They had focused our attention on viscosity management techniques and emulsion formation tendencies of heavy oils and also assessed the risk posed by solids such as hydrates, wax and asphaltenes.

Alexander F Zazovsky(Zazovsky, Haddad et al. 2005) developed a new method for estimating formation temperature from wireline formation tester temperature measurements. This method was based on the reconstruction of thermal history, which involves drilling, no-mud-circulation and pumping-out phases, using the model of heat transport in the formation. The model calibration was achieved by fitting the predicted temperature at some intermediate distance from the borehole for the temperature data measured in flowline during pumping-out. The temperature found in intermediate zone was then extrapolated to the boundary of cooled zone surrounding borehole for estimating initial formation temperature. The forward model used for thermal history simulation was simple and robust. It did not involve the borehole temperature modeling during drilling and can be calibrated with a single parameter - either the average mud temperature opposite the tested interval or the average heat flux from the formation during drilling. Although this model could not predict accurately the initial phase of thermal history (drilling and no-mud-circulation), it became adequate for the pumping-out phase when the details of borehole temperature variation with time during drilling became insignificant.

Fernando Ascencio-Cendejas(Ascencio-Cendejas, Reyes et al. 2006) did conceptual studies for the design of thermally bundled wells to optimize the heavy oil production of the offshore fields in the Gulf of Mexico. Heat transfer management achieved through novel and clever thermal design, operation and maintenance of the wells, pipelines and process equipment, maintains the viscosity of the oil at acceptable levels.

Michael Piber(Piber, Prohaska et al. 2006) developed a model for these cyclic temperature/pressure load test and the impact of temperature. The ability of Xanthan and Bentonite fluids to break and reestablish viscosity under cyclic temperature and pressure loads was evaluated. When using these findings, the accuracy of hydraulic modeling and nozzle optimization could be improved. Better predictions of critical viscosity breakdowns and additive requirements to maintain fluid viscosity could be done.

Richard F. Vargo(Vargo, Heathman et al. 2006) studied the improved deepwater cementing practices . Real-time monitoring and detailed pressure analysis were used to manage cementing operations and the correct application of SSR plugs. Feedback of these processes from operators and service tool personnel had resulted in improved job performance as measured through reduced NPT and well construction costs.

Barkim Demirdal(Demirdal, Miska et al. 2007) developed a way to estimate equivalent circulating density (ECD) and circulating bottom hole pressure (CBHP). Normally, calculated frictional pressure losses did not match actual frictional losses recorded during drilling operations. Discrepancies between calculated and measured pressure losses were more severe in operations where synthetic based drilling fluids were used because synthetic based drilling fluid theologies vary with changes in downhole conditions. An empirical relation for density as a function of pressure and temperature was introduced. The rheological model that defined the shear stress shear rate relation of the drilling fluid used in this study at all pressure and temperature

conditions was the Yield Power Law model. The effects of downhole conditions on the rheological parameters consistency index (K), flow behavior index (n) and yield stress (to) were analyzed.

David Stiles(Stiles and Trigg 2007) developed a mathematical simulators to model wellbore temperatures. The input parameters for this study were based upon a typical deepwater well in West Africa. In some of the cases studied, differences among the simulated cementing temperatures were significant enough to warrant performance of risk analysis and implementation of risk mitigation measures. Part two of this paper presented the circulating temperature model and temperature surveillance program utilized to drill and test a deepwater high temperature high pressure (HTHP) well. The predictions from the model were used to evaluate design considerations such as the selection of blowout preventer (BOP) elastomers and qualification of downhole drilling and testing tools. The model aided in completion fluid selection to optimize hydrate prevention and influence flowing wellhead and surface temperatures. A comparison of modeled parameters and measured field data was included. In addition to the model results, the functionalities of each of the temperature simulators and how those functionalities might influence the results are discussed.

Farzad Tahmourpour(Tahmourpour and Quinton 2009) discussed how best practices in combination with optimized downhole temperature modeling could potentially reduce the number of hours in WOC-time without introducing any additional risk factors into the cementing/drilling operations. Calculating accurate downhole temperature and pressure profiles, which were also used for pipe-body movement and casing-and tubing-load analysis, assists cementing, drilling, and completion engineers to produce highly effective solution.

Bulent Izgec(Izgec, Hasan et al. 2010) used a wellbore model handling steady flow of fluids but unsteady-state heat transfer to estimate production rate, given wellhead

pressure and temperature. The model rigorously accounted various thermal properties of the fluid and the formation, including Joule-Thompson (J-T) (Thompson and Joule 1853) heating and/or cooling. In the single-point approach, a single-point-temperature measurement made anywhere in the wellbore, including at the wellhead, was needed to estimate the mass rate at a given time step. Good correspondence between the measured and calculated resulted demonstrates the robustness of the proposed methods.

2.2 Drilling Fluid Properties At High Temperature And High Pressure

At high temperature and pressure, the densities of water/oil base drilling or completion fluids can be significantly different from those properties measured at surface conditions. To predict the density of drilling fluid, the differential pressure at high temperature and high pressure is significantly necessary to reduce the unintentional underbalance or kick (Kutasov 1999).

Hoberock (Hoberock and Stanbery 1981) presented his simulator for the dynamic pressure while the mud is circulating in the well. To predict pressure and flow propagation in the drill-pipe, it was necessary to make suitable modifications to reflect the non-Newtonian nature of the drilling mud. It could be shown that the steady-state frictional pressure drop per unit length for the flow of a Bingham plastic in a smooth circular pipe was given by fluid density, pipe diameter, mean fluid velocity, Fanning friction factor. Herberock's work also indicated that the predicted bottomhole pressure with constant densities to be in error by hundreds of psig.

L. E. Bartlett et al.(Bartlett 1967) developed some conclusions for the effects of temperatures on the properties of drilling mud. Present drilling fluids did not behave as Bingham plastics data obtained at surface temperatures could not be used to determine flow conditions at higher temperatures encountered in the well.

Carney(Carney and Meyer 1976) obtained a drilling fluid capable of withstanding temperatures in the ultra-high range. This included a study on the rheology of sepiolite slurries that have been subjected to temperatures up to 800 ^{o}F. Data was given showing that slurries prepared from sepiolite and other additives had favorable rheological and fluid loss properties over wide temperature ranges properties over wide temperature ranges.

McMordie(McMordie Jr., Bland et al. 1982) presented on the changes in the densities of 11-18 lb/gal oil and water base drilling fluids in the temperature and pressure ranges of 70 deg. -400 deg. F and 0-14,000 psig. Results indicated that the change in density of a given type of drilling fluid appeared to be independent of the initial density of the fluid, and as oil base drilling fluids were subjected to high temperatures and pressures, they became more dense than water base drilling fluids.

Sorelle(Sorelle, Jardiolin et al. 1982) provided a mathematical model requiring a minimum of input data to predict the variation of downhole density and hydrostatic-pressure in static drilling fluids. The model took into account volumetric changes in the solid, oil, and water phases due to temperature, hydrostatic pressure, and any imposed surface pressure. The behavior of each component, with changes in temperature and pressure, was determined separately; equations were developed to express this behavior. These equations were combined into a general equation to describe the behavior of a drilling fluid made up of any of these three components-oil, water, and solids.

Moussa(Moussa and Al-Marhoun 1985) developed reliable flow loop which could measure these parameters efficiently at high temperature which had been considered as one of the main contaminants . Also it showed how the experimental data could be of value in solving difficult mud properties control problems. A laboratory investigation of the effect of temperature and time and mud composition on these properties was made with a modified scaled flow loop.

J. W. Galate(Galate and Mitchell 1986) presented an analysis of the behavior of diesel-oil- based muds with an advanced thermal and hydraulic wellbore mathematical simulator. As rheological correlations were developed for other oil-based muds, such as mineral-oil-based muds, they could also be incorporated into the model. A specific deep-well application of the model illustrated the behavior of oil-based muds and showed the differences between water-based mud and oil-mud local fluid densities during drilling, circulating, and static conditions. The behavior of any drilling fluid under flowing conditions was a complex function of the sizes of the drillstring, return annulus, and bit nozzles, and of the flow rate.

Peters, Ekwere J.(Peters, Chenevert et al. 1990) measured the densities of diesel oil, two mineral oils, and calcium chloride solutions from 78 to 350 ^{o}F and from 0 to 15,000 psig. The measured densities were used in an existing compositional psig. The measured densities were used in an existing compositional material-balance model to predict the densities of 11 lbm/gal and 17 lbm/gal oil-based muds. He also measured the densities of these muds at elevated pressures and temperatures and compared them with the predicted values. The results showed excellent agreement between measured and predicted densities. The experimental density data were used to predict downhole densities and static wellbore pressures for the oil-based muds. Results showed that the mineral-oil muds were not only more compressible than the diesel-oil muds, but also more susceptible to thermal expansion. Therefore, all the oil-based muds tended to give essentially the same static-wellbore-pressure profile. To plan well control adequately, to prevent lost circulation, and to analyze fracture-gradient test data accurately, one must be able to predict the densities of these muds at elevated pressures and temperatures.

Zilch(Zilch, Otto et al. 1991) described both laboratory and field results when using these drilling fluids, including the third generation fluid that was first used successfully in an exploratory well drilled in 1980. To evaluate these fluids in the laboratory, standard API test procedures were performed in conjunction with a battery of procedures

were performed in conjunction with a battery of evaluations to simulate actual field contaminates and temperatures.

Cesaroni(Cesaroni and Repetti 1993) developed drilling fluid systems which were applied on the Villafortuna/Trecate Oilfield in the Po valley. The necessity to provided adequate environmental protection and at the same time facilitate optimum drilling performance is described. Well conditions required drilling fluids of high density which were stable to high temperatures. The technology that was discussed in the paper described the water base fluid that was eventually used, the solids control equipment and the actions taken to operate in accordance with the environmentally protective approach.

Carlson(Carlson and Hemphill 1994) provided an ester-based drilling fluid system. This particular system had exhibited increased performance in terms of penetration rates and reduced drilling costs. In this paper, field applications of the ester-based drilling fluid in water depths between 1,000 and 4,000 feet (305-1,220 m) were discussed.

G.J. Zabaras (Zabaras 1994) presented for predicting pressure profiles in oil and gas wells. The method combined mechanistic low pattern transition criteria with physical models for pressure loss and liquid holdup calculations for each of the flow patterns considered. In contrast, the new method was universally applicable to all types of wells under all operating scenarios since it was based on fundamental physics rather than curve-fit of field data. Its prediction performance had been demonstrated by extensive comparison to field data from a variety of wells. Profitable production of many offshore oil and gas fields relied on accurate prediction of the multiphase well tubing flow.

Isambourg, P.(Isambourg, Anfinsen et al. 1996) measured volumetric changes of high density muds at high pressure and high temperature, up to 1500 bars and 200 C, developed as part of a HPHT research program.

Maglione(Maglione, Gallino et al. 1996) characterized the real influence of pressure and temperature upon the rheology of the drilling fluids, circulation tests were performed and repeated at different depths inside cased hole (9 5/8" csg at 2973 m) with the 8 1/2" bit off bottom, while making trip (e. g. for the drilling out task of the casing shoe).

W.W. White(White, Zamora et al. 1997) attempted to compensate for these sensitivity effects with oil-based muds. Similar difficulties were encountered with synthetic-based muds (SBM); however, concerns were more acute. Pump-pressure calculations with SBM's can be off as much as 35%. The primary goal of this project was to collect sufficient data to resolve discrepancies concerning pump pressures and ECD's. Secondary targets included measuring and evaluating surge/swab pressures, bit pressure loss, equivalent static density (ESD), and mud-temperature profile.

Karstad, Eirik(Karstad and Aadnoy 1998) presented an analytical model for the density-pressure-temperature dependence for drilling fluids. This generalized equation of state was valid for oil- and water based drilling fluids and also for completion fluids. The model was compared to other models already proposed, and was found to represent the measured data more accurately than the other models. In the application of the model we studied the transient density behavior during drilling operations.

Davison(Davison 1999) also provided an option of rheology of various Drilling Fluid systems under deepwater drilling conditions and the importance of accurate predictions of downhole Fluid Hydraulics.

Haige Wang(Wang and Su 2000) studied the effects of formation temperature gradient, wellbore inlet mud temperature, and mud type on the equivalent static density (ESD). Computing results showed that temperature gradient has large effect on ESD, pressure, flowing pressure, Equivalent Circulating Density (ECD) and surge and swab

pressure. The results showed that errors resulting from ignoring variations in mud properties were small in relatively shallow wells. However in HTHP wells, especially in those wells with narrow safe mud margins available, to ensure the wellbore stable, changes in mud density due to elevated temperature and pressure and its influence on wellbore pressure system must be taken into accounts.

E.A. Osman(Osman and Aggour 2003) provided accurate predictions of mud density as a function of mud type, pressure and temperature. Available experimental measurements of water-base and oil-base drilling fluids at pressures ranging from 0 to 1400 psi and temperatures up to 400 °F were used to develop and test the ANN model.

Samuel Olusola Osisanya(Osisanya and Harris 2005) studied the effects of the temperature and pressure conditions in high temperature/high pressure wells on drilling fluid equivalent circulating density and consequently bottom-hole pressure were presented in this paper. High temperature conditions caused the fluid in the wellbore to expand, while high pressure conditions in deep wells caused fluid compression. Failure to take these two opposing effects into account could lead to errors in the estimation of bottom-hole pressure. The rheological behavior drilling fluids was also affected by the temperature and pressure conditions. A simulator called DDSimulator was developed to simulate the wellbore during circulation. The results of the simulation showed that higher geothermal gradients led to lower bottom-hole pressure. The inlet pipe temperature did not have a significant effect on the bottom-hole temperature and pressure, and higher circulation rates resulted in lower bottom-hole temperature and higher bottom-hole pressure.

Ronald G. Bland (Bland, Mullen et al. 2006) identified and discussed the major HP/HT drilling fluid challenges, recent innovations in fluid viscosity measurements under HP/HT conditions, drilling fluid designs stable to extreme HP/HT conditions, and other considerations in HP/HT drilling.

Eirik Kaarstad(Kaarstad, Aadnoy et al. 2009) conducted friction research , trying to further understand mechanical, viscous, temperature and material frictional effects. Many water and oil based drilling muds from several mud vendors had been measured. The test equipment used included a heat element to study the temperature effect on friction. The data reported covered a temperature range of 10°- 100°C. As expected, oil based fluids had lower friction coefficient than water based fluids. The coefficient of friction increased with temperature for all fluids, except for one mud which showed nearly constant friction above 50 °C. There was considerable variation between the different fluids.

CHAPTER III

BASIC HEAT TRANSFER AND HYDRAULIC CALCULATION

Heat transfer could be classified as three categories, conduction, convection and radiation. To describe the temperature profile in drilling, what we can do is to apply these three heat transfer phenomena to build up the governing equations and to solve the equation by analytical or numerical methods. The difficulty to solve this problem depends on the complicated of the governing equations, the properties of the fluid modeling such density, viscosity and rheology etc.

3.1 Conduction

Conduction is the energy transferred from the higher energy state particles of a substance to the adjacent lower energy ones interacted between the particles. Fourier's Law tells us that, the geothermal gradient proves that rocks have some finite ability to conduct heat and the earth must be conducting heat from its interior to its exterior (Banks 2008).

The conduction equation, Fourier's law, implies the heat flux is a vector quantity, the general heat conduction rate equation as follows;

$$q'' = -k\nabla T = -k\left(i\frac{\partial T}{\partial x} + j\frac{\partial T}{\partial y} + k\frac{\partial T}{\partial z} \right) \qquad \text{Eq(3-1)}$$

where ∇ is the three-dimensional del operator and T(x,y,z) is the scalar temperature field. For the cylindrical coordinates, the general form of the heat flux vector and hence of Fourier's law is

$$q'' = -k\nabla T = -k\left(i\frac{\partial T}{\partial r} + j\frac{1}{r}\frac{\partial T}{\partial \phi} + k\frac{\partial T}{\partial z} \right) \qquad \text{Eq(3-2)}$$

Applying an energy balance to the differential control volume, the following general form of the heat equation in cylindrical coordinate system is obtained, which

could be used to describe the temperature change versus time in the solids with internal heat source.

$$\frac{1}{r}\frac{\partial}{\partial r}\left(kr\frac{\partial T}{\partial r}\right)+\frac{1}{r^2}\frac{\partial}{\partial \phi}\left(k\frac{\partial T}{\partial \phi}\right)+\frac{\partial}{\partial z}\left(k\frac{\partial T}{\partial z}\right)+q=\rho c_p\frac{\partial T}{\partial t} \qquad \text{Eq(3-3)}$$

Fourier's Law implies that various conductivities of formation lead to different geothermal gradient. Assuming a constant flux of heat from the earth's interior, a layer of rock with a low thermal conductivity must possess a high geothermal temperature gradient otherwise the geothermal gradient will be even. The geothermal gradient in the lower conductivity mudstone layer must be higher than in the sand layer in the Figure 3-1 (Banks 2008).

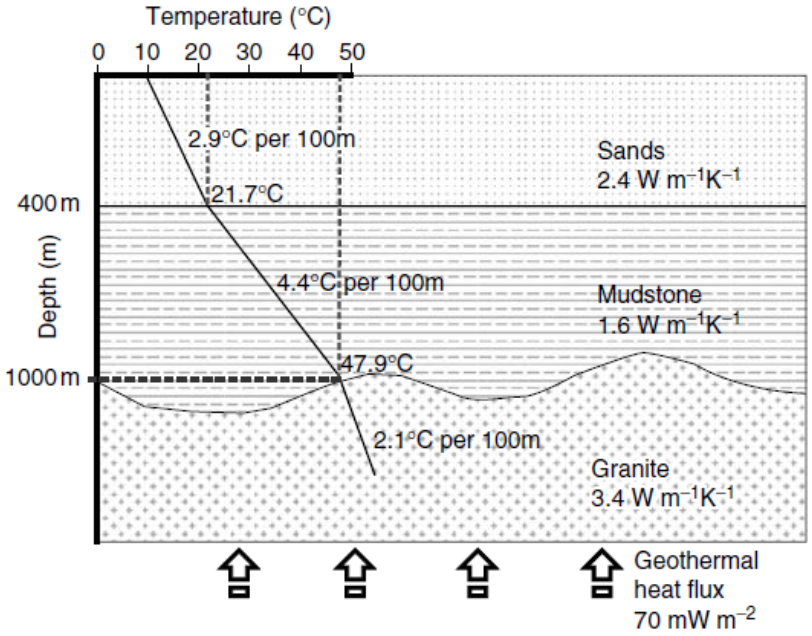

Figure 3-1 Schematic cross section through a three layer 'sandwich' of different rock types

The thermal conductivity describes how good the medium is at conducting heat: steel is very good, rocks are less good and plastics are generally poor in Table 3-1(Banks 2008). Thus, the thermal conductivity of rocks and sediments depends to a large extent on their quartz content.

Table 3-1 Thermal conductivity and volumetric heat capacity of selected rocks and minerals

	Thermal conductivity (W m^{-1} K^{-1})	Volumetric heat capacity (MJ m^{-3} K^{-1})
Rocks and sediments		
Coal	*0.3*	*1.8*
Limestone	1.5–3.0 (*2.8, massive limestone*)	1.9–2.4 (*2.3*)
Shale	1.5–3.5 (*2.1*)	*2.3*
Wet clay	0.9–2.2 (*1.6*)	*2.4*
Basalt	1.3–2.3 (*1.7*)	*2.4*–2.6
Diorite	1.7–3.0 (*2.6*)	*2.9*–3.3
Sandstone	2.0–6.5 (*2.3*)	*2.0*–2.1
Gneiss	2.5–4.5 (*2.9*)	2.1–2.6 (*2.1*)
Arkose	2.3–3.7 (*2.9*)	*2.0*
Granite	3.0–4.0 (*3.4*)	1.6–3.1 (*2.4*)
Quartzite	5.5–7.5 (*6.0*)	1.9–2.7 (*2.1*)
Minerals		
Plagioclase	1.5–2.3	1.64–2.21
Mica	2.0–2.3	2.2–2.3
K-feldspar	2.3–2.5	1.6–1.8
Olivine	3.1–5.1	2.0–3.6
Quartz	7.7	1.9–2.0
Calcite	3.6	2.24
Pyrite	19.2–23.2	2.58
Galena	2.3–2.8	1.59
Haematite	11.3–12.4	3.19
Diamond	545	–
Halite	5.9–6.5	1.98
Other		
Air	0.024	1.29×10^{-3} at 1 atm.
Glass	0.8–1.3	1.6–1.9
Concrete	0.8 (*1.6*)	*1.8*
Ice	1.7–2.0 (*2.2*)	*1.9*
Water	*0.6*	4.18
Copper	390	3.5
Freon-12* at 7°C (liquid)	0.073	1.3
Oak	0.1–0.4	1.4
Polypropene	0.17–0.20	1.7
Expanded polystyrene	0.035	–

3.2 Convection

Convectional heat transfer can also take place from a hot body in a fluid that is initially static, with no externally imposed forces (Banks 2008). We need the forced convection (advection) of heat that occurs with drilling fluid, rock, drillstring, riser and returnline.

There are two categories of convection heat transfer in practical calculation, internal flow convection heat transfer and external flow convection heat transfer. The external flow convection heat transfer is due to the ocean current. The environmental conditions in design are obtained from the site-specific data. Therefore, it is difficult to be too specific in terms of the magnitude of current in offshore locations (Chakrabarti 2005). An example of 100-yr environment for a few offshore deepwater sites of the world are included in Table 3-2 (Chakrabarti 2005). These metocean conditions can be based on information for a general region or an area near the well site. Table 3-3 (Chakrabarti 2005) lists thermal conductivity data for lithology.

Table 3-2 Extreme environment for various locations

Location	Type	Water Depth(m)	Hs (m)	Windspeed (m/s)	Surface current(m/s)	Seabed current(m/s)
Gulf of Mexico	Hurricane	3000	12.9	42	1.1	0.1
Gulf of Mexico	Loop	3000	4.9	32.9	2.57	0.51
Brazil	Foz de Amazon	3000	6	20	2.5	0.3
Northern Norway	Nyk High	1500	15.7	38.5	1.75	0.49
West Africa	Girrasol	1350	4	19	1.5	0.5
Atlantic Frontier	Faeroe-shetland Channel	1000	18	40	1.96	0.63

Table 3-3 Thermal conductivity data for selected lithology in the UK

Formation	Lithology	*N*	Thermal conductivity (W m^{-1} K^{-1})
London Clay (Palaeogene)	Sandy mudstone	5	2.45 ± 0.07
Reading Beds (Palaeogene)	Sandy mudstone	4	2.33 ± 0.04
	Mudstone	10	1.63 ± 0.11
Chalk (Cretaceous)	Limestone	41	1.79 ± 0.54
Upper Greensand (Cretaceous)	Sandstone	18	2.66 ± 0.19
Gault (Cretaceous)	Sandy mudstone	32	2.32 ± 0.04
	Mudstone	4	1.67 ± 0.11
Kimmeridge Clay (Jurassic)	Mudstone	58	1.51 ± 0.09
Oxford Clay (Jurassic)	Mudstone	27	1.56 ± 0.09
Mercia Mudstone (Triassic)	Mudstone	225	1.88 ± 0.03
Sherwood Sandstone (Permo-Triassic)	Sandstone	64	3.41 ± 0.09
Magnesian Limestone (Permian)	Limestone	12	3.32 ± 0.17
Westphalian (Coal Measures)	Sandstone	37	3.31 ± 0.62
	Siltstone	12	2.22 ± 0.29
	Mudstone	25	1.49 ± 0.41
	Coal	8	0.31 ± 0.08
Namurian (Millstone Grit)	Sandstone	7	3.75 ± 0.16
Lower Carboniferous limestone	Limestone	14	3.14 ± 0.13
Upper Old Red Sandstone (Devonian)	Sandstone	27	3.26 ± 0.11
Silurian slates near Selkirk	Slate	67	3.33 ± 0.05
Hercynian granites	Granite	895	3.30 ± 0.18
Basalt	Basalt	17	1.80 ± 0.11

3.2.1 External Flow

A common external flow involves fluid motion normal to the axis of a circular cylinder. The free stream fluid is brought to rest at the forward stagnation point, with an accompanying rise in pressure.

The occurrence of boundary layer transition depends on the Reynolds number and influence the position of the separation point. The empirical correlation due to Knudsen and Katz (Ozisik. 1977) is

$$\overline{Nu_D} = \frac{\bar{h}}{k} D = C \,\mathrm{Re}_D^m \,\mathrm{Pr}^{\frac{1}{3}} \qquad \text{Eq(3-4)}$$

The corresponding constants are shown in the Table 3-4.

Table 3-4 Constants of Hilpert equation for the circular cylinder in cross flow

Re_D	C	m
0.4-4	0.989	0.330
4-40	0.911	0.385
40-4000	0.683	0.466
4000-40000	0.193	0.618
40000-400000	0.027	0.805

The external correlation in crossflow could be used in the ocean current on the drillpipe, marine drilling riser or return line to get the heat transfer convection coefficient. Figure 3-2 indicates the ocean currents velocity and temperatures versus depth in various locations (Chakrabarti 2005).

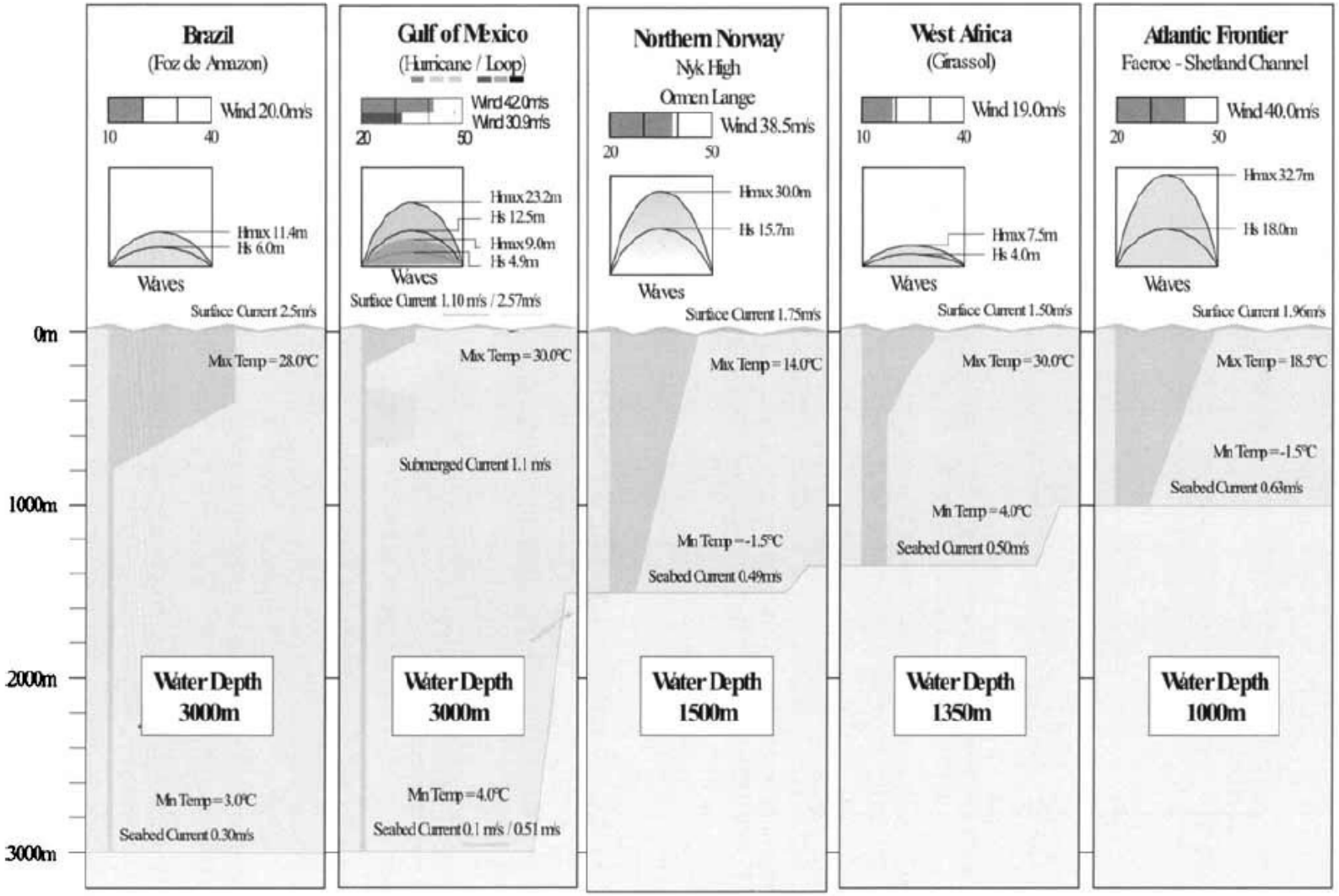

Figure 3-2 Environmental conditions at several deep water sites

3.2.2 Internal Flow

The Nussult number in a circular tube characterized by uniform surface heat flux and laminar, fully developed conditions is a constant, independent of Renold number.

$$\overline{Nu_D} = \frac{\bar{h}}{k} D = 3.66 \qquad \text{Eq(3-5)}$$

The Nussult number in a circular smooth tube characterized by uniform surface heat flux and turbulent flow is recommended by Sieder and Tate (Ozisik. 1977)

$$\overline{Nu_D} = \frac{\bar{h}}{k} D = 0.027 \,\mathrm{Re}_D^{\frac{4}{5}} \,\mathrm{Pr}^{\frac{1}{3}} \qquad \text{Eq(3-6)}$$

$$0.7 \le \mathrm{Pr} \le 16{,}700$$

$$\mathrm{Re}_D \ge 10{,}000$$

$$L / D \ge 10$$

where Pr, Re_D, *L/D* are Prandtl Number, Renold Number and the ratio of Length to Diameter respectively.

The Nussult number in a concentric circular smooth annulus characterized by uniform surface heat flux and force convection is recommended by Jaco Dirker and Josua P.Meyer (Dirker and Meyer 2002)

$$\overline{Nu_D} = \frac{\bar{h}}{k} D = C \,\mathrm{Re}_D^m \,\mathrm{Pr}^{\frac{1}{3}} \left(\frac{\mu}{\mu_w} \right)^{0.14} \qquad \text{Eq(3-7)}$$

where

$$m = 1.013 \times 10^{-0.067a}$$

$$C = \frac{0.003a^{1.86}}{0.063a^3 - 0.674a^2 + 2.225a - 1.157}$$

The values of m and C were reaffirmed. From the experimental results, the behavior of P and C can be described relatively precisely for annular diameter ratios.

3.3 Radiation

Heat can be transferred radiatively by the emission and absorption of thermal photons. Thermal photons are similar to light photons (380–750 nanometers), but fall at the longer wavelength (approximately 700 to beyond 15,000 nanometers) infrared portion of the electromagnetic spectrum. It is for that reason that radiation contributes relatively little in the way of energy or mass transfer within the Earth(Glassley 2010) .

3.4 Geothermal Gradient

Temperature gradients change widely over the earth. The temperature in the ocean decreases naturally with depth largely controlled by the annual average ambient temperature and the temperature at the surface of earth is dominantly ultimately derived from solar energy absorbed. Below the seafloor, the geothermal gradient is positive because the constant migrating geothermal heat flux from the earth's interior towards the earth's surface, which could be referred to Figure 3-3 (Banks 2008).

3.5 Overall Heat Transfer Coefficient

For multi-layer coaxial cylinder, the overall heat transfer coefficient is defined as

$$U = \frac{1}{\left(\frac{1}{A_i h_i} + \sum_{m=1}^{n} \frac{\ln(r_{m+2} / r_{m+1})}{2\pi L k_m} + \frac{1}{A_o h_o} \right) A_r} \qquad \text{Eq(3-8)}$$

3.6 Hydraulic Calculation

Fluid densities generally vary with depth as functions of temperature, pressure, and salinity. For liquids, the temperature and pressure dependence of density can be approximated as

$$\rho = \rho_o\left[1 - \alpha\left(T - T_0\right) + \beta\left(P - P_0\right)\right] \quad \text{Eq(3-9)}$$

Here, α is the expansivity and β the compressibility of the fluid. When fluid density varies with depth, because of generally increasing temperatures and pressures, Eq. (3-9) is no longer applicable to calculate the dependence of fluid pressure on depth (Pruess 2002).

For the practical hydraulic calculation, the API RP 13D (1995) equations are recommended as follow.

3.6.1 Pipe Flow

Pipe Flow Behavior Index

$$n_p = 3.32\log\left(\frac{R_{600}}{R_{300}}\right) \quad \text{Eq(3-10)}$$

Pipe Consistency Index

$$K_p = \frac{5.11 R_{600}}{1{,}022^{n_p}} \quad \text{Eq(3-11)}$$

Pipe Flow Mean Velocity

$$V_p = \frac{0.408\, Q}{D^2} \quad \text{Eq(3-12)}$$

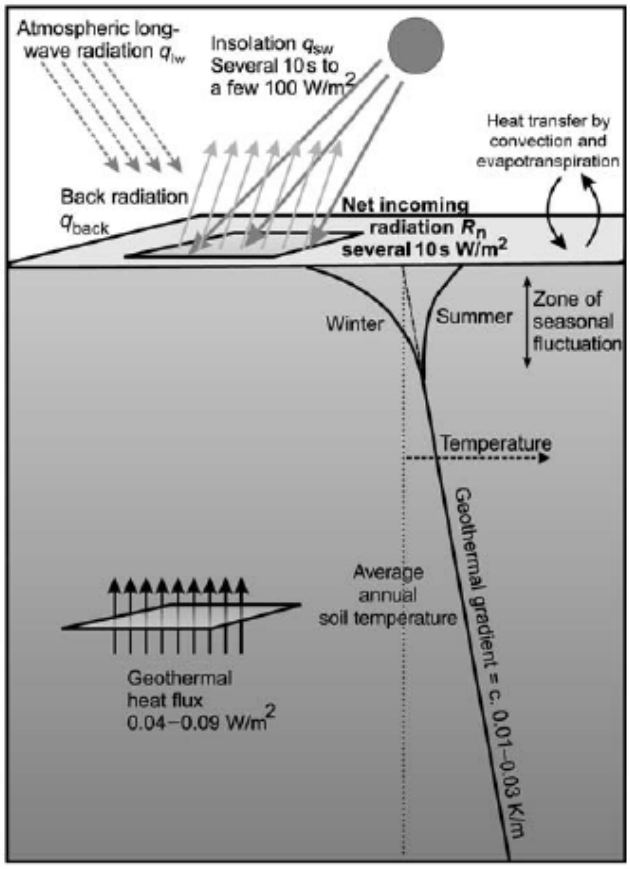

Figure 3-3 Schematic block diagram showing the downward increase in temperature in the earth due to the geothermal gradient

Effective Viscosity

$$\mu_{ep} = 100\ K_p \left(\frac{96V_p}{D} \right)^{n_p - 1} \left(\frac{3n_p + 1}{4n_p} \right)^{n_p} \qquad \text{Eq(3-13)}$$

Reynolds Number

$$N_{\mathrm{Re}_p} = \frac{928\, D V_p \rho}{\mu_{ep}} \qquad \text{Eq(3-14)}$$

For Laminar Flow, the Friction Factor

$$f_p = \frac{16}{N_{\mathrm{Re}_p}} \qquad \text{Eq(3-15)}$$

For turbulent flow, the Friction Factor

$$a = \frac{\log\ n_p + 3.93}{50} \qquad \text{Eq(3-16)}$$

$$b = \frac{1.75 - \log n_p}{7} \qquad \text{Eq(3-17)}$$

$$f_p = \frac{a}{N_{\mathrm{Re}_p}{}^{b}} \qquad \text{Eq(3-18)}$$

Pressure Loss

$$\left(\frac{dP}{dL}\right)_{dp} = \frac{f_p V_p{}^2 \rho}{25.81 D} \qquad \text{Eq(3-19)}$$

$$\Delta P_{dp} = \left(\frac{dP}{dL}\right)_{dp} \Delta L_{dp} \qquad \text{Eq(3-20)}$$

3.6.2 Annular Flow

Annulus Flow Behavior Index

$$n_a = 0.657 \log\left(\frac{R_{100}}{R_3}\right) \qquad \text{Eq(3-21)}$$

Annulus Consistency Index

$$K_a = \frac{5.11 R_{100}}{170.2^{n_a}} \qquad \text{Eq(3-22)}$$

Annulus Flow Mean Velocity

$$V_a = \frac{0.408Q}{D_2{}^2 - D_1{}^2} \qquad \text{Eq(3-23)}$$

Effective Viscosity

$$\mu_{ea} = 100\ K_a \left(\frac{144 V_a}{D_2 - D_1}\right)^{n_a - 1} \left(\frac{2n_a + 1}{3n_a}\right)^{n_a} \qquad \text{Eq(3-24)}$$

Reynolds Number

$$N_{\mathrm{Re}_a} = \frac{928 (D_2 - D_1) V_a \rho}{\mu_{ea}} \qquad \text{Eq(3-25)}$$

The Friction Factor for Laminar Flow

$$f_a = \frac{24}{N_{\mathrm{Re}_a}} \qquad \text{Eq(3-26)}$$

The Friction Factor for Turbulent Flow

$$a = \frac{\log\ n_a + 3.93}{50} \qquad \text{Eq(3-27)}$$

$$b = \frac{1.75 - \log n_a}{7} \qquad \text{Eq(3-28)}$$

$$f_a = \frac{a}{N_{\mathrm{Re}_a}{}^{b}} \qquad \text{Eq(3-29)}$$

Pressure Loss

$$\left(\frac{dP}{dL}\right)_a = \frac{f_a V_a{}^2 \rho}{25.81\left(D_2 - D_1\right)} \qquad \text{Eq(3-30)}$$

$$\Delta P_a = \left(\frac{dP}{dL}\right)_a \Delta L_a \qquad \text{Eq(3-31)}$$

CHAPTER IV

ONSHORE HEAT TRANSFER MODELS

The following analytical models are presented to evaluate the effects of depth, conductivity of drilling fluid on downhole and to estimate the effect of mud type on the difference between bottomhole fluid and outlet temperatures. The governing equations are second order differential partial equations. Douglas' model (D.Cline 1981) introduced dimensionless definitions to do the sensitivity analysis of various terms while Hasan and Kabir's (Hasan and Kabir 1996) did not. As a matter of fact, both models are "pseudo-steady state" axial conduction models. The configuration of onshore drilling system could be referred to Figure 4-1(www.conservation.ca.gov).

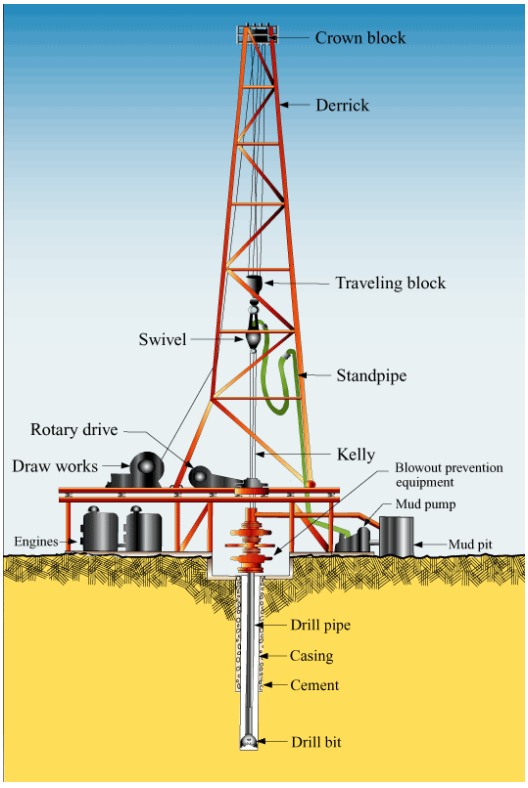

Figure 4-1 Onshore drilling rig

4.1 Hasan And Kabir's Model

Complete unsteady-state formulations were presented for both forward and reverse circulation cases. In flowing down the tubing and back up the annulus (forward circulation), or down the annulus and up the tubing (reverse circulation), the circulating fluid generally gains heat from the hotter formation. The heat transfer rate for the fluid in the annulus depends on the formation temperature from which it gains heat and on the tubing fluid temperature to which it loses heat.

Assumptions are based on

- Formation is homogeneous;
- Neglect vertical heat transfer;
- Fluid solution and mixing are negligible;
- Single Phase steady-state flow.

Based on these assumptions, a second-order linear differential equation presents the transient heat transfer model. Heat loss from the fluid decreases with time and depends on the various resistances to heat flow between the hot fluid in the tubing and the surrounding earth.

Governing Equation

$$\frac{B}{L_R}\frac{d^2T_t}{dz^2} \pm B\frac{dT_t}{d_z} - T_t + T_{es} + g_G z\sin\theta = 0 \qquad \text{Eq(4-1)}$$

Temperature of annular fluid

$$T_a = T_t \mp B\frac{dT_t}{dz} \qquad \text{Eq(4-2)}$$

$$L_R = \frac{2\pi}{c_{fl}w}\frac{r_c U_c k_e}{k_e + r_c U_c T_D} \qquad \text{Eq(4-3)}$$

$$B = \frac{wc_{fl}}{2\pi r_t U_t} \qquad \text{Eq(4-4)}$$

Temperature of tubing fluid

$$T_t = \alpha e^{\lambda_1 z} + \beta e^{\lambda_2 z} + g_G z \sin\theta \pm B g_G + T_{es} \quad \text{Eq(4-5)}$$

Temperature of annular fluid

$$T_a = (1 \mp B\lambda_1)\alpha e^{\lambda_1 z} + (1 \mp B\lambda_2)\beta e^{\lambda_2 z} + g_G z \sin\theta \pm B g_G + T_{es} \quad \text{Eq(4-6)}$$

$$\alpha = -\frac{(T_{ts} - T_{es} + B g_G \sin\theta)\lambda_2 e^{\lambda_2 L} + g_G \sin\theta}{\lambda_1 e^{\lambda_1 L} - \lambda_2 e^{\lambda_2 L}} \quad \text{Eq(4-7)}$$

$$\beta = \frac{(T_{ti} - T_{es} + B g_G \sin\theta)\lambda_1 e^{\lambda_1 L} + g_G \sin\theta}{\lambda_1 e^{\lambda_1 L} - \lambda_2 e^{\lambda_2 L}} \quad \text{Eq(4-8)}$$

$$\lambda_1 = \frac{L_R}{2} + \frac{L_R}{2}\sqrt{1 + 4(r_c U_c T_D + k_e)\frac{r_t U_t}{r_c U_c k_e}} \quad \text{Eq(4-9)}$$

$$\lambda_2 = \frac{L_R}{2} - \frac{L_R}{2}\sqrt{1 + 4(r_c U_c T_D + k_e)\frac{r_t U_t}{r_c U_c k_e}} \quad \text{Eq(4-10)}$$

Constant heat flow rate

$$T_D = \ln\left\{e^{-0.2 t_D}\right\} + \left(1.5 - 0.3719 e^{-t_D}\right)\sqrt{t_D} \quad \text{Eq(4-11)}$$

$$t_D = \frac{k_e t}{\rho_e c_e r_w^2} \quad \text{Eq(4-12)}$$

Overall heat transfer coefficient is

$$h_r = \frac{\sigma\left(T_{ins}^2 + T_{ci}^2\right)\left(T_{ins} + T_{ci}\right)}{\frac{1}{\varepsilon_{ins}} + \frac{r_{ins}}{r_{ci}}\left(\frac{1}{\varepsilon_{ci}} - 1\right)} \quad \text{Eq(4-13)}$$

$$0 \le \varepsilon \le 1$$

Table 4-1 shows the properties of fluid and wellbore geometry to calculate the temperature profile. Figure 4-2 shows the bottom hole temperatures versus fluid thermal conductivity. Figure 4-3 indicates the effects of fluid thermal conductivity on the temperature profile.

Table 4-1 Properties of fluid and wellbore geometry

t=	168	hrs
L=	9500	ft
T_{es}=	59.5	^{o}F
T_{ts}=	75	^{o}F
T_{ti}=	59.5	^{o}F
g_G=	0.0127	^{o}F/ft
$1/U_{to}$=	0.372	hr-ft^2-^{o}F/BTU
r_{ti}=	1.4375	in
r_{to}=	1.5	in
r_{in}=	1.51	in
r_{ci}=	3.13	in
r_{co}=	3.5	in
r_{wb}=	4.5	in
v_{ti}=	0.2218	ft/s
$v_{annulus}$=	0.0004235	ft/s
Re(ti)=	3553	
Re(annu)=	25	
P_r=	119.62	
h_{ti}=	289.94	Btu/hr-ft^2-^{o}F
h_{r}=	0.6236	Btu/hr-ft^2-^{o}F
h_c=	6.1899	Btu/hr-ft^2-^{o}F
k_f=	0.383	Btu/hr-ft-^{o}F
k_t=	26	Btu/hr-ft-^{o}F
k_{ins}=	0.1	Btu/hr-ft-^{o}F
k_c=	26	Btu/hr-ft-^{o}F
k_{cem}=	4.021	Btu/hr-ft-^{o}F
Mass Q=	2693.16	lb/hr
ρ_f=	74.81	lb/ft^3
v=	20	cp
Cp=	0.947	Btu/lbm-^{o}F

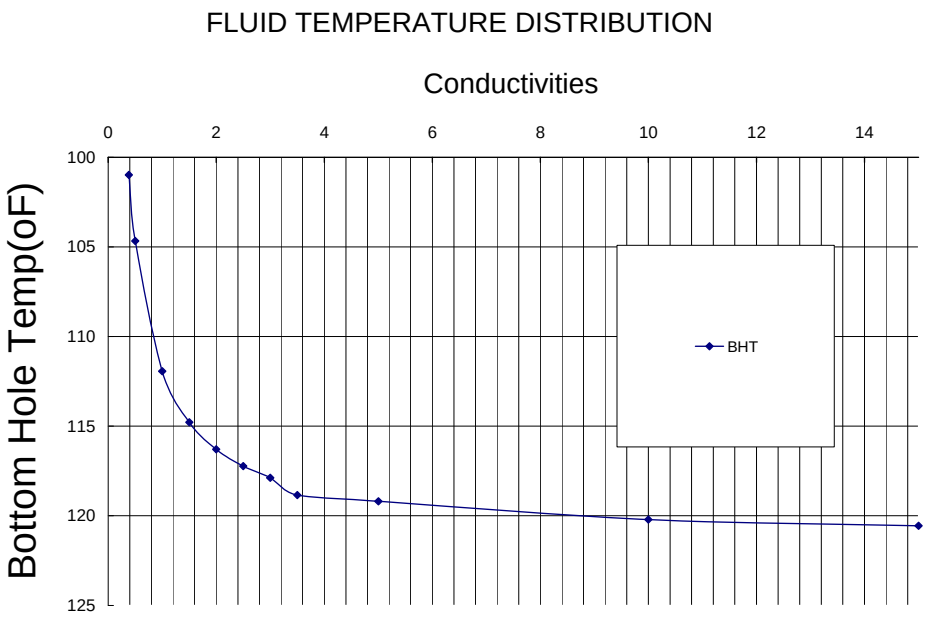

Figure 4-2 Sensitivity of fluid thermal conductivity in Hasan's model

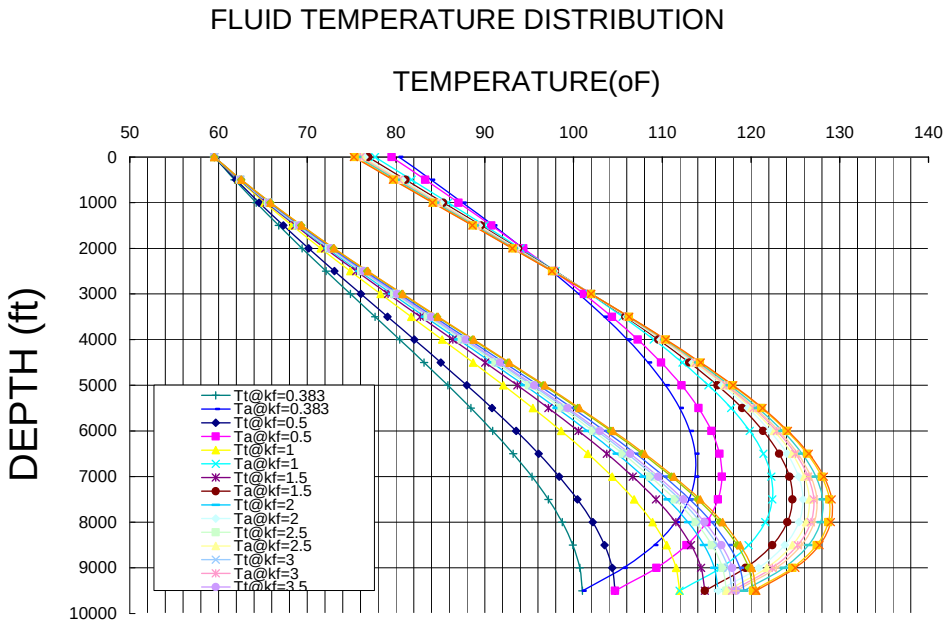

Figure 4-3 Temperature profile for different conductivities in Hasan's model

4.2 Douglas' Model

The overall heat transfer coefficient between the annulus fluid and the primary fluid is given by

$$U_{pa} = \left[\frac{1}{r_1 h_{fp}} + \frac{\ln(r_2 / r_1)}{k_{12}} + \frac{1}{r_2 h_{fa}} \right]^{-1} \qquad \text{Eq(4-14)}$$

The overall heat transfer coefficient between the outermost casing and the annulus fluid is given by

$$U_{a5} = \left[\frac{1}{r_3 h_{fa}} + \frac{\ln(r_4 / r_3)}{k_{34}} + \frac{\ln(r_5 / r_4)}{k_{45}} \right]^{-1} \qquad \text{Eq(4-15)}$$

In order to model the pseudo-steady heat transfer from the formation, the solution of Carslaw and Jaeger for the heat flux across an infinite, homogeneous medium at temperature T_∞ to an internally bounded cylinder at temperature T_5 is utilized. This relationship is given by

$$q = \frac{8}{\pi} k_\infty (T_\infty - T_5) \int_0^\infty \frac{e^{-\lambda \psi^2}}{\left[\left(\frac{\psi}{k} \right) J_1(\psi) + J_0(\psi) \right]^2 + \left[\left(\frac{\psi}{k} \right) Y_1(\psi) + Y_0(\psi) \right]^2} \frac{d\psi}{\psi} \qquad \text{Eq(4-16)}$$

where

$$\lambda = \frac{\alpha_\alpha t}{r_5^2} \qquad \text{Eq(4-17)}$$

$$k = \frac{U_{a5} r_5}{k_\infty} \qquad \text{Eq(4-18)}$$

The thermal conductivity of the infinite medium is given by k_∞ k while α_∞ represents its thermal diffusivity.

The above equation may be compared to the formulation derived by Willhite(Willhite and Griston 1987). In the nomenclature of Willhite(Willhite and Griston 1987), (as well as that of Ramey) it can be seen that

$$f(t) = F(\lambda, k) \qquad \text{Eq(4-19)}$$

where values of f(t) have been tabulated by Willhite(Willhite and Griston 1987). For long circulation times, i.e., greater than 7 days, approximate values for the function f(t) may be obtained from the following relationship.

$$f(t) = \ln\left(2\sqrt{\lambda}\right) - 0.29 \qquad \text{Eq(4-20)}$$

An effective overall heat transfer coefficient between the formation and the annulus may be defined as

$$U_{eff}(\lambda, k) = \frac{k_\infty U_{a5}}{k_\infty + U_{a5} F(\lambda, k)} \qquad \text{Eq(4-21)}$$

The dependent variables and independent coordinate are to be normalized by the following dimensionless variables,

Dimensionless temperature of primary fluid

$$\theta_p = \frac{T_P}{T_{in}} \qquad \text{Eq(4-22)}$$

Dimensionless temperature of annular fluid

$$\theta_a = \frac{T_a}{T_{in}} \qquad \text{Eq(4-23)}$$

Dimensionless depth

$$Z^* = \frac{Z}{L} \qquad \text{Eq(4-24)}$$

The appropriate relationships over each subinterval are defined below.

$$\theta_{\infty 1} = \theta_{g1} Z^* + \theta_{s1} \text{ on } 0 \le z^* \le z_0 \qquad \text{Eq(4-25)}$$

$$\theta_{\infty 2} = \theta_{g2} Z^* + \theta_{s2} \text{ on } z_0 \le z^* \le 1 \qquad \text{Eq(4-26)}$$

$$\theta_{g1} = \frac{\tilde{T} - T_s}{T_{in} z_0} \quad \text{Eq(4-27)}$$

$$\theta_{s1} = \frac{T_s}{T_{in}} \quad \text{Eq(4-28)}$$

$$\theta_{g2} = \frac{T_{bf} - \tilde{T}}{T_{in}(1 - z_0)} \quad \text{Eq(4-29)}$$

$$\theta_{s2} = \frac{\tilde{T}}{T_{in}} - \frac{T_{bf} - \tilde{T}}{T_{in}} \left(\frac{z_0}{1 - z_0} \right) \quad \text{Eq(4-30)}$$

$$z_0 = \frac{\tilde{z}}{L} \quad \text{Eq(4-31)}$$

Eliminating θ_a Sa from Equation yields a linear second order ordinary differential equation for θ_p.

$$\frac{d^2\theta_P}{dz^{*2}} - k_a \frac{d\theta_P}{dz} - \tilde{k}\,\theta_P = -\tilde{k}\,\theta_\infty(z^*) \quad \text{Eq(4-32)}$$

$$k = k_a k_P \quad \text{Eq(4-33)}$$

Primary Fluid:

$$\theta_P(z^*) = (A + \alpha)\frac{e^{AZ^*}1}{(A - B)} - (B + \alpha)\frac{e^{BZ^*}}{(A - B)} - \frac{\tilde{k}}{(A - B)} I \quad \text{Eq(4-34)}$$

Annular Fluid:

$$\theta_a(z^*) = \left\{ \frac{A(A + \alpha)}{k_P} \right\} \frac{e^{AZ^*}}{(A - B)} - \left\{ \frac{B(B + \alpha)}{k_p} \right\} \frac{e^{BZ^*}}{(A - B)} - \frac{k_a}{(A - B)} \frac{dI}{dz^*} + \theta_P(z^*) \quad \text{Eq(4-35)}$$

where

$$A = \frac{k_a}{2} + \frac{1}{2}\sqrt{k_a^2 + 4\tilde{k}} \quad \text{Eq(4-36)}$$

$$B = \frac{k_a}{2} - \frac{1}{2}\sqrt{k_a^2 + 4\tilde{k}} \quad \text{Eq(4-37)}$$

where α is a function of only ka, kp and the geothermal temperature distribution. The expression for α is given by

$$\alpha = \frac{k_a k_p}{\left(Ae^A - Be^B\right)}\left\{\begin{array}{l}\theta_{s1}\left[\left(e^A - e^{A(1-z_0)}\right) - \left(e^B - e^{B(1-z_0)}\right)\right] + \theta_{g1}\left[\left(\frac{e^A}{A} - z_0 e^{A(1-z_0)} - \frac{e^A(1-z_0)}{A}\right) - \left(\frac{e^B}{B} - z_0 e^{B(1-z_0)} - \frac{e^B(1-z_0)}{B}\right)\right] \\ + \theta_{s2}\left[e^{A(1-z_0)} - e^{B(1-z_0)}\right] + \theta_{g2}\left[\left(\frac{e^A(1-z_0)}{A}(z_0 A+1) - \frac{1}{A}\right) - \left(\frac{e^B(1-z_0)}{B}(z_0 B+1) - \frac{1}{B}\right)\right]\end{array}\right\}$$

$$- \frac{A^2 e^A - B^2 e^B}{Ae^A - Be^B}$$

Eq(4-38)

Figure 4-4 indicates the sensitivity analysis for various thermal conductivities in Douglas' Model.

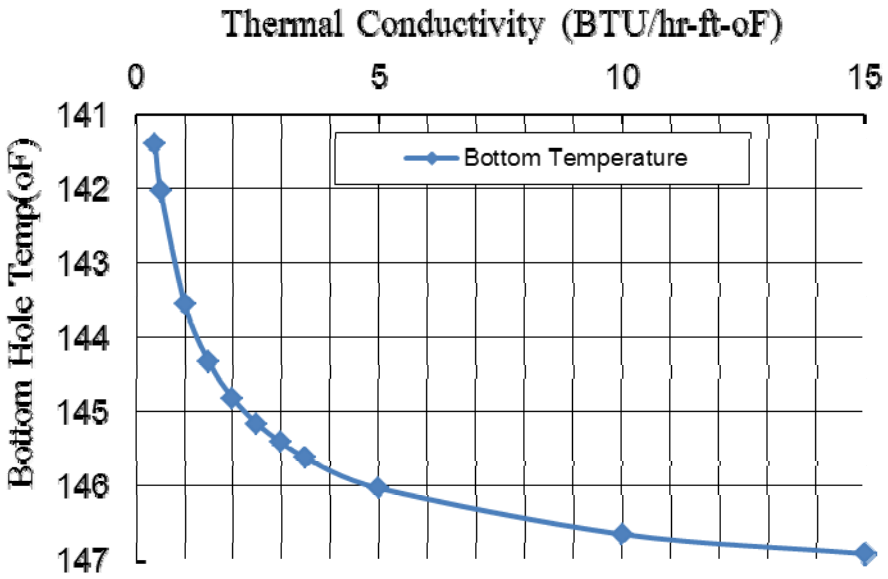

Figure 4-4 Sensitivity of fluid thermal conductivities in Douglas' Model

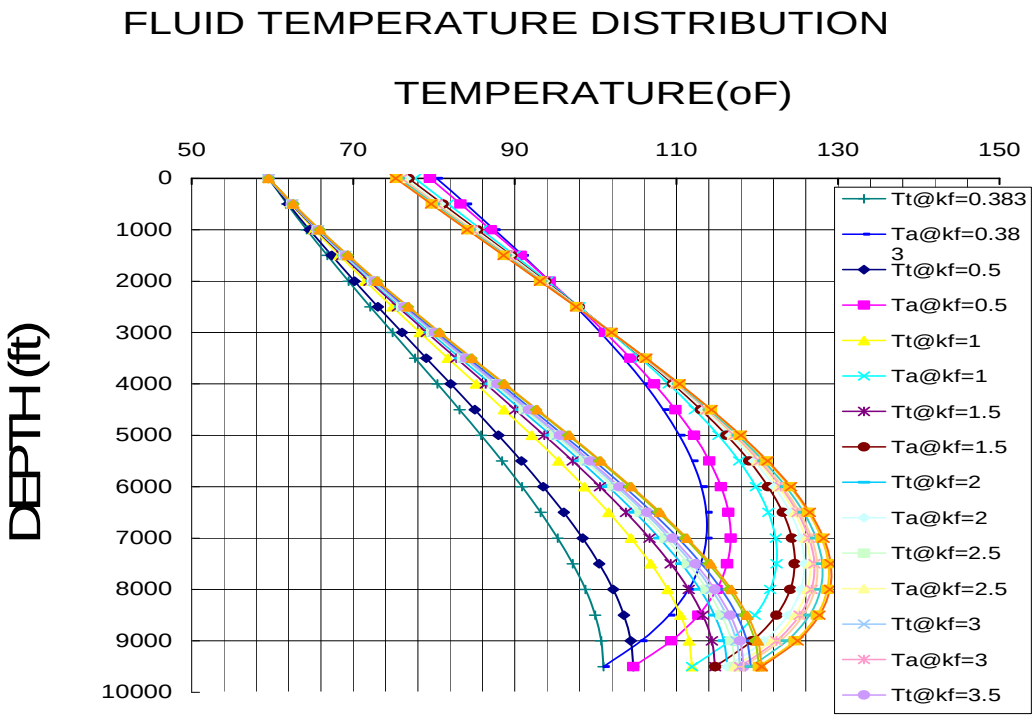

Figure 4-5 Temperature profile for different thermal conductivities in Douglas' Model

Figure 4-5 indicates the temperature profiles for various conductivities in Douglas' Model. The conductivities varies from 0.383 Btu/hr-ft-oF to 3.5 Btu/hr-ft-oF. Since the thermal conductivities are always in certain range, they can't be changed freely. Table 4-2 lists the base parameters to calculate the temperature distribution in the well system by Douglas' model. Table 4-3 lists the dimensionless temperature profile example by Douglas' model.

Table 4-2 Properties of fluid and wellbore geometry in Douglas' model

α=	1.71E-09	$1/ft^2hr^oR^4$
Qmass=	0.04	ft3/s
Mud Density=	10	ppg
viscosity=	20	cp
Cp=	0.947	Btu/lbm-^{o}F
kf=	0.383	Btu/hr-ft-^{o}F
Z_{bar}=	4750	ft
Z_0=	0.5	
T_{bar}=	119.825	^{o}F
t=	240	hrs
L=	9500	ft
s=	0.793333	
s_2=	0.793333	
g=	1.608667	
g_2=	1.608667	
T_s=	59.5	^{o}F
T_{in}=	75	^{o}F
Tbf	180.15	^{o}F
g_{G1}=	0.0127	^{o}F/ft
g_{G2}=	0.0127	^{o}F/ft
earth=	0.0476	ft^2/hr
k_{bar}=	19.5223	$BTU^2/(hr\text{-}ft\text{-}^oF)^2$
f(t)=	2.601835	
K_a=	4.376041	BTU/(hr-ft-^{o}F)
K_p=	4.461178	BTU/(hr-ft-^{o}F)
U_{eff}=	0.747911	BTU/(hr-ft-^{o}F)
U_{a5}=	1.449285	BTU/(hr-ft-^{o}F)
U_{pa}=	0.762462	BTU/(hr-ft-^{o}F)

Table 4-3 Dimensionless temperature profile Vs well depth in Douglas' Model

Z=	θp	θa
ft		
0	1	1.011495
500	1.008329	1.06658
1000	1.026872	1.125521
1500	1.054234	1.187745
2000	1.089201	1.252734
2500	1.130705	1.32
3000	1.177805	1.389071
3500	1.229654	1.459461
4250	1.314653	1.566338
4750	1.375072	1.637496
5250	1.43764	6.999841
5750	1.501564	9.547043
6250	1.565928	13.21829
6750	1.629605	18.52371
7250	1.691136	26.20538
7750	1.748553	37.34263
8250	1.799125	53.50539
8750	1.838998	76.97706
9250	1.862666	111.0788
9500	1.866068	133.5495

CHAPTER V

OFFSHORE HEAT TRANSFER MODELS

5.1 Mass Balance

Of fundamental importance for fluid flow studies, whether in porous media or in free space, is the mass balance or mass conservation equation. Simply put it states that the change in fluid mass is given by the net inflow across the surface of that volume, plus contributions. From a practical viewpoint it is best to think of them as boxes or, in two dimensions, rectangles. The centroids of the grid blocks are referred to as "nodal points," and we associate average pressure, temperature, etc. in a grid block with these nodal points. In drilling process, the flow of drilling fluid could be treated as 1-dimension flow. For simplicity, let us consider a single-phase system with a single-component fluid (Pruess 2002).

5.2 Conservation Of Energy

Energy balances are more complicated than mass balances, primarily because thermal energy is not conserved as such, but may be partially converted into mechanical work and vice versa. This is expressed by the First Law of Thermodynamics, or energy balance,

$$\Delta U = G + W$$

where the change ΔU in internal energy of a system is due to heat transfer G and mechanical work W done to the system.

For a finite (sub-)volume V of a flow system, when not only heat and work but also fluids may be exchanged with the surroundings, the energy balance can be written in the following form (Pruess 2002).

change in internal energy in volume V	=	net transfer of energy by fluid flow	+	mechanical work done to volume V	+	net heat transfer by conduction	+	net energy gain from sinks and sources

We then set up energy balances , for each of the grid blocks or control volume. In reality, the thermodynamic conditions in a flow system may vary from point to point; by discretizing into finite-size grid blocks we approximate these point-to-point variations by means of averages in each grid block. Expressed differently, we assume that (approximate) thermodynamic equilibrium prevails "locally," on the scale of a grid block. Time is also discretized into finite increments or "time steps" Δt. Suppose that at some given time t we know the thermodynamic conditions in all grid blocks. We then allow these flows to proceed for a time Δt and, using energy balances, we obtain new updated inventories of energy in each grid block corresponding to time $t + \Delta t$. This process is repeated for as many time steps as desired, to obtain a prediction of thermodynamic conditions for a time period of interest. We generalize this equation by dividing the total depth z into N small intervals of length $\Delta z = z/N$ as Figure 5-1 (Pruess 2002).

Figure 5-1 Dividing depth into small intervals Δz, numbered i = 1, 2, ..., N

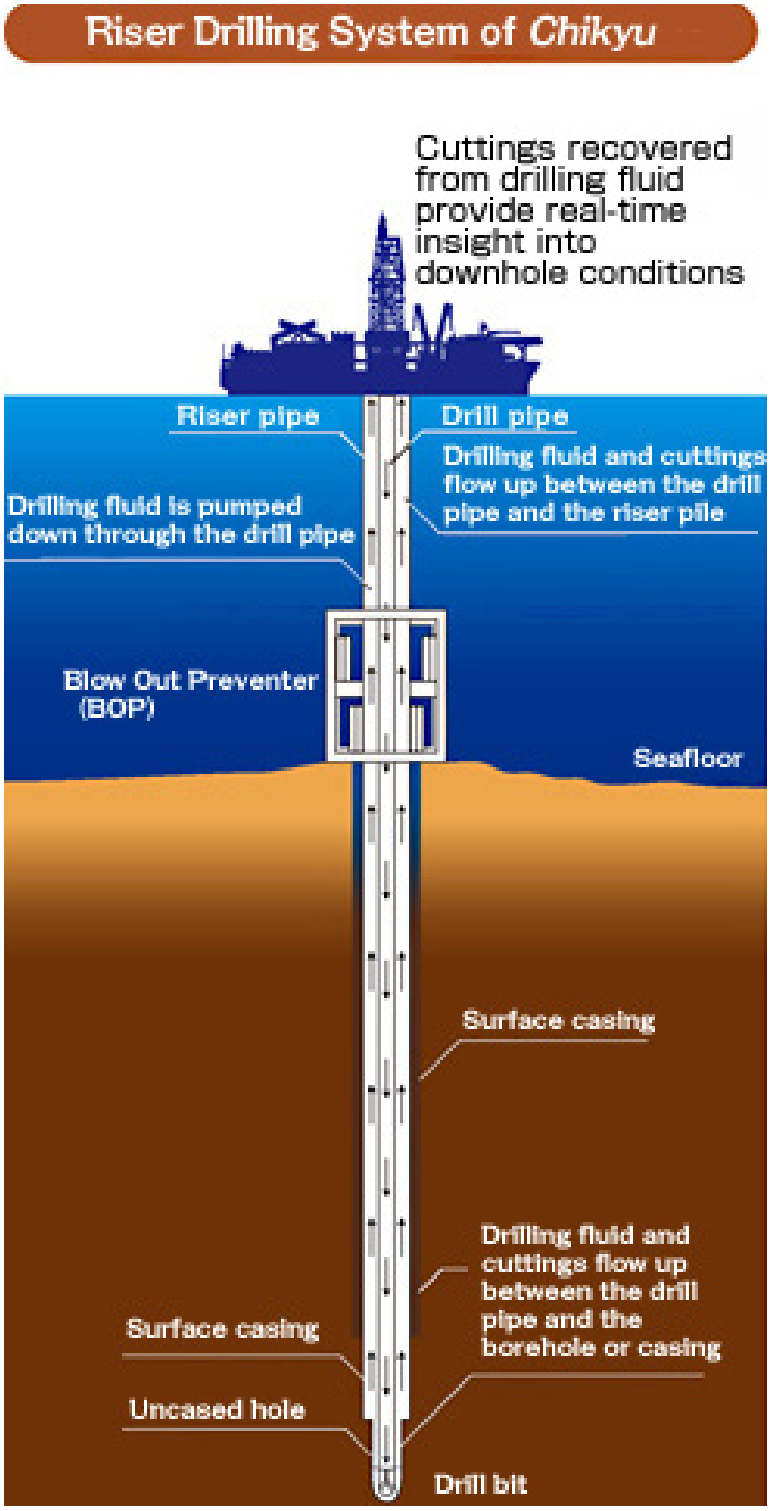

Figure 5-2 Conventional riser drilling system

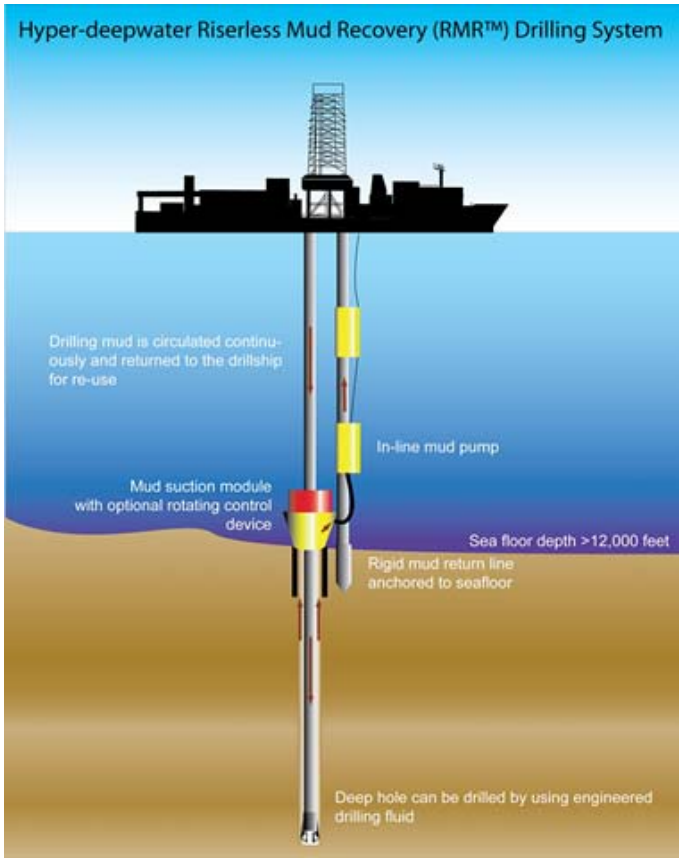

Figure 5-3 Riserless drilling system

5.3 Steady-state Heat Transfer Model

For the steady-state heat transfer modeling, the variation of temperature with time steps is ignored. As we discussed, based on the conservation of energy, every control volume or grid achieves energy equilibrium. Since it is very simple to derive the governing equations, the derivations are referred to Lima's dissertation(Lima 1998). The conventional riser drilling and riserless drilling are depicted in Figure 5-2 (www.jamstec.go.jp) and Figure 5-3 (www.maritimeandenergy.com) respectively. By

carefully choosing control volume in Figure 5-4 (Lima 1998), we can derive the governing equations for steady-state heat transfer models and transient heat transfer model.

Governing Equations for Steady-state Heat Transfer Model

For the DrillString

$$-m_p C_{p,p}\frac{\partial T_p}{\partial z}+Q_p-2\pi r_p U_p\left(T_p-T_w\right)=0 \qquad \text{Eq (5-1)}$$

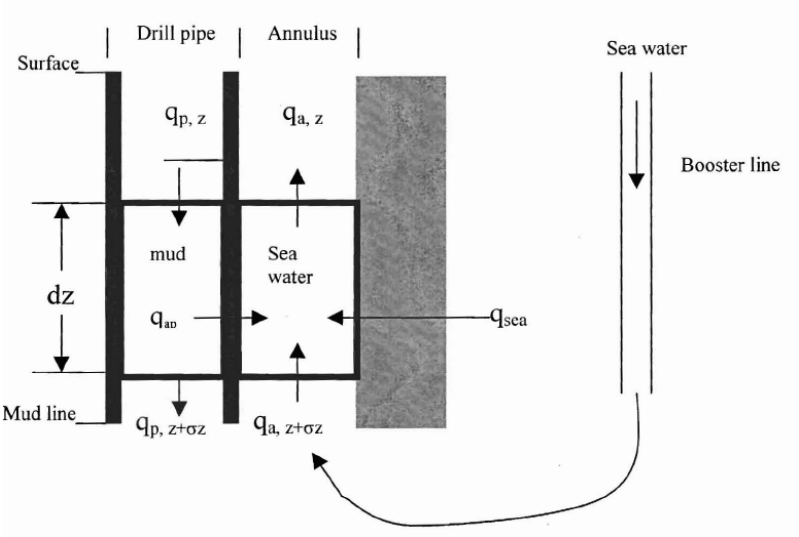

Figure 5-4 Control volume

For the Annulus

$$m_a C_{p,a}\frac{\partial T_w}{\partial z}+2\pi r_p U_p\left(T_p-T_w\right)-2\pi r_a U_a\left(T_w-T_f\right)+Q_a=0 \qquad \text{Eq (5-2)}$$

Mass Flowrate

$$m_p = \rho_p Q_{p,p} \qquad \text{Eq (5-3)}$$

$$m_a = \rho_a Q_{p,a} \qquad \text{Eq (5-4)}$$

The temperature of drillstring wall

$$T_w = T_p + \frac{1}{2\pi r_p U_p}\left(m_p C_{p,p} \frac{\partial T_p}{\partial z} - Q_p \right) \qquad \text{Eq (5-5)}$$

Substituting Eq(5-1), Eq(5-2), Eq(5-3) and Eq(5-4) to Eq(5-5), we have

$$\begin{aligned} &\frac{m_a C_{p,a} m_p C_{p,p}}{2\pi r_p U_p}\frac{\partial^2 T_p}{\partial z^2} + \left(m_a C_{p,a} - m_p C_{p,p} - \frac{r_a U_a}{r_p U_p} m_p C_{p,p} \right)\frac{\partial T_p}{\partial z} \\ &- 2\pi r_p U_p T_p + 2\pi r_a U_a T_f + \left(1 + \frac{r_a U_a}{r_p U_p} \right) Q_p + Q_a = 0 \end{aligned} \qquad \text{Eq (5-6)}$$

$$A = \frac{m_a C_{p,a} m_p C_{p,p}}{2\pi r_p U_p} \qquad \text{Eq (5-7)}$$

$$B = m_a C_{p,a} - m_p C_{p,p} - \frac{r_a U_a}{r_p U_p} m_p C_{p,p} \qquad \text{Eq (5-8)}$$

$$C = -2\pi r_p U_p \qquad \text{Eq (5-9)}$$

$$D = 2\pi r_a U_a T_f + \left(1 + \frac{r_a U_a}{r_p U_p} \right) Q_p + Q_a \qquad \text{Eq (5-10)}$$

$$A\frac{\partial^2 T_p}{\partial z^2} + B\frac{\partial T_p}{\partial z} + CT_p + D = 0 \qquad \text{Eq (5-11)}$$

For the homogeneous linear differential equation Eq(5-11) with second order, rewrite the equation as follows

$$\frac{\partial^2 T_p}{\partial z^2} + \frac{B}{A}\frac{\partial T_p}{\partial z} + \frac{C}{A}T_p + \frac{D}{A} = 0 \qquad \text{Eq (5-12)}$$

Discretizing Eq(5-12) with finite difference, we have

$$A\frac{T_{p,i+1} - 2T_{p,i} + T_{p,i-1}}{(\Delta z)^2} + B\frac{T_{p,i+1} - T_{p,i}}{\Delta z} + CT_{p,i} + D_i = 0 \qquad \text{Eq (5-13)}$$

For different grid nodes, write Eq(5-13) in matrix form of linear equations.

$$\begin{pmatrix} b & c & 0 & 0 & 0 & 0 \\ a & b & c & 0 & 0 & 0 \\ 0 & a & b & c & 0 & 0 \\ \cdots & \cdots & \cdots & \cdots & \cdots & \cdots \\ 0 & 0 & 0 & a & b & c \\ 0 & 0 & 0 & 0 & a & b \end{pmatrix} \begin{pmatrix} T_{p,1} \\ T_{p,2} \\ T_{p,3} \\ \cdots \\ T_{p,i-1} \\ T_{p,i} \end{pmatrix} = - \begin{pmatrix} aT_{p,0} + D_1 \\ D_2 \\ D_3 \\ \cdots \\ D_{i-1} \\ cT_{p,i+1} + D_i \end{pmatrix} \qquad \text{Eq (5-14)}$$

where

$$a = \frac{A}{(\Delta z)^2} + \frac{B}{\Delta z}$$

$$b = -\frac{2A}{(\Delta z)^2} - \frac{B}{\Delta z} + C$$

Now based on the derivations, what we will do it is to solve the linear equations. The special case of a system of tridiagonal linear equations has nonzero elements only on the diagonal plus or minus one column. Also common are systems that are band-diagonal, with nonzero elements only along a few diagonal lines adjacent to the main diagonal (above and below). For tridiagonal matrix, the procedures of LU decomposition are executed with forward- and back substitution. The set of equations is solved in the Visual Basic program with TDMA module.

5.4 Transient Heat Transfer Modeling

Assumptions of Transient heat transfer modeling are made as follows:

- Flow is steady state and fully developed.
- Heat transfer with the drill fluid is by axial convection axial conduction may be neglected.
- The radial temperature gradient within the drilling fluid may be neglected.
- Fluid properties such as density thermal conductivity and heat capacity are independent of temperature.

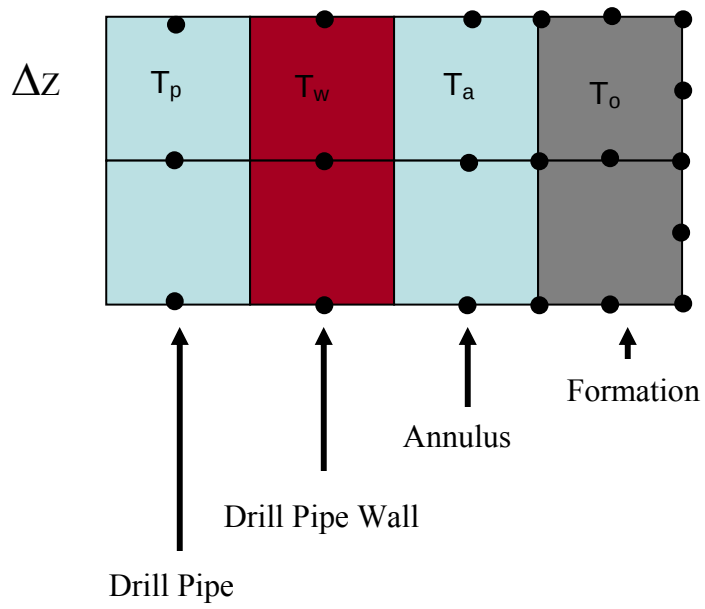

Figure 5-5 Mesh generation of heat transfer in the wellbore

Mesh generation can be greatly simplified by exploiting actual or approximate symmetries of a flow system. This allows far more efficient and potentially more accurate simulations. Considering the longitudinal symmetric volume, cylindral coordinate is the natural choice in Figure 5-5.

For the riserless drilling system, it can be divided into two parts, drilling system above the seafloor and that below the seafloor. Based on the conservation of energy, control volumes are carefully chosen.

5.4.1 Governing equations for Transient Heat Transfer Modeling

The well system above the seafloor is divided into different control volumes to derive the energy balance equations as Figure 5-6, Figure 5-7 and Figure 5-8 indicated. The well system below the seafloor can be treated in same way.

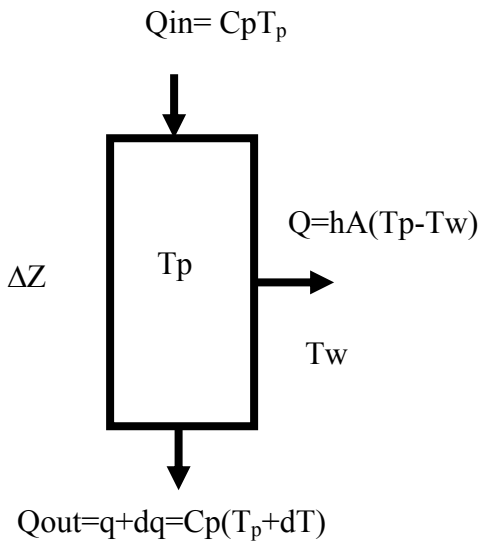

Figure 5-6 Conservation of energy for the control volume in the fluid of the drillpipe

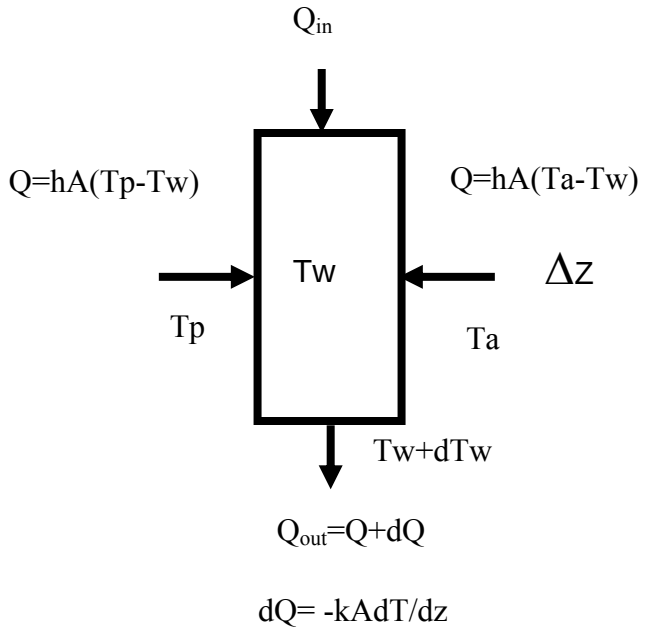

Figure 5-7 Conservation of energy for the Control Volume of drillstring wall

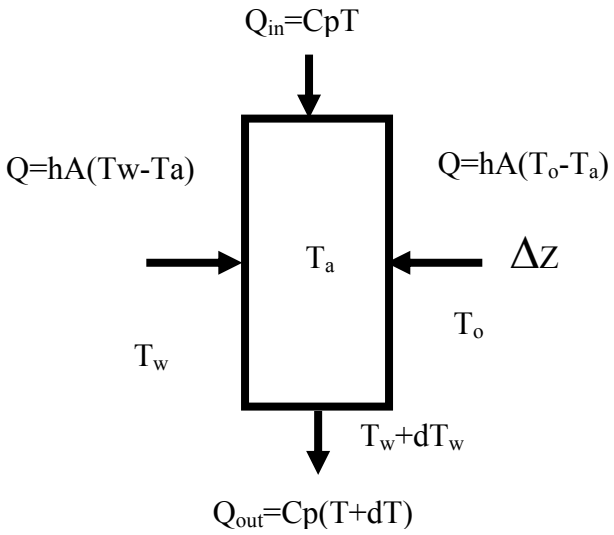

Figure 5-8 Conservation of Energy for the Control Volume of Annulus

Control volume 1: Fluid in the drill pipe

$$\rho q C_p \frac{\partial T_p}{\partial z} + 2\pi r_p h_p \left(T_p - T_{sea}\right) = -\frac{\partial}{\partial t}\left(\pi r_p^2 \rho C_p T_p\right) + Q_p = -\pi r_p^2 \rho C_p \frac{\partial T_p}{\partial t} + Q_p \quad \text{Eq (5-15)}$$

Control volume 2: Fluid in the return line

$$\rho q C_p \frac{\partial T_{rtl}}{\partial z} + 2\pi r_{rtl,ID} h_p \left(T_{trl} - T_{sea}\right) = -\frac{\partial}{\partial t}\left(\pi r_{rtl,ID}^2 \rho C_p T_{rtl}\right) + Q_{rtl} = -\pi r_{rtl,ID}^2 \rho C_p \frac{\partial T_{rtl}}{\partial t} + Q_{rtl}$$

Eq (5-16)

The well system below the mudline

Control volume 1: Fluid in the drill pipe

$$\rho q C_p \frac{\partial T_p}{\partial z} + 2\pi r_p h_p \left(T_p - T_w\right) = -\frac{\partial}{\partial t}\left(\pi r_p^2 \rho C_p T_p\right) + Q_p = -\pi r_p^2 \rho C_p \frac{\partial T_p}{\partial t} + Q_p \quad \text{Eq (5-17)}$$

Control volume 2: Drillpipe Wall

$$0 = \left(r_a^2 - r_p^2\right)\frac{\partial q}{\partial z} + 2 r_a h_a \left(T_a - T_w\right) + 2 r_p h_p \left(T_p - T_w\right) + \left(r_a^2 - r_p^2\right)\rho_w C_{p,w} \frac{\partial T_w}{\partial t} \quad \text{Eq (5-18)}$$

where $q = -k \dfrac{\partial T_w}{\partial z}$

Control volume 3: Fluid in the annulus

$$Q_a = \rho q C_p \frac{\partial T_a}{\partial z} + 2\pi r_a h_a \left(T_w - T_a\right) + 2\pi r_o h_a \left(T_f - T_a\right) + \frac{\partial}{\partial t}\left(\pi\left(r_o^2 - r_a^2\right)\rho C_p T_a\right) \quad \text{Eq (5-19)}$$

Control volume 4: Near-wellbore Formation

For conduction in cylinder solid

$$\left[\frac{1}{r}\frac{\partial}{\partial r}\left(rk\frac{\partial T}{\partial r}\right) + \frac{\partial^2 T}{\partial z^2}\right] + H = \rho C_p \frac{\partial T}{\partial t} \quad \text{Eq (5-23)}$$

5.4.2 Implicit Finite difference Discretization

Fluid in the drill pipe or Fluid in the returnline

$$\rho q C_p \frac{T_{1,j}^{n+1} - T_{1,j-1}^{n+1}}{\Delta z_j} + 2\pi r_p h_p \left(T_{1,j}^{n+1} - T_{2,j}^{n+1}\right) = -\pi r_p^2 \rho C_p \frac{T_{1,j}^{n+1} - T_{1,j}^{n}}{\Delta t} + Q_p \quad \text{Eq (5-20)}$$

Drillpipe wall or returnline wall

$$0 = \left(r_a^2 - r_p^2\right)\left(\frac{T_{2,j+1}^{n+1} - T_{2,j}^{n+1}}{\Delta z_{j+0.5}} - \frac{T_{2,j}^{n+1} - T_{2,j-1}^{n+1}}{\Delta z_{j-0.5}}\right) + 2r_a h_a\left(T_{3,j}^{n+1} - T_{2,j}^{n+1}\right)$$

$$+ 2r_p h_p\left(T_{1,j}^{n+1} - T_{2,j}^{n+1}\right) + \left(r_a^2 - r_p^2\right)\rho_w C_{pw}\frac{T_{2,j}^{n+1} - T_{2,j}^{n}}{\Delta t} \qquad \text{Eq (5-21)}$$

Fluid in the annulus

$$Q_a = \rho q C_p \frac{T_{3,j+1}^{n+1} - T_{3,j}^{n+1}}{\Delta z_j} + 2\pi r_a h_a\left(T_{2,j}^{n+1} - T_{3,j}^{n+1}\right)$$

$$+ 2\pi r_o h_o\left(T_{4,j}^{n+1} - T_{3,j}^{n+1}\right) + \pi\left(r_o^2 - r_a^2\right)\rho C_p \frac{T_{3,j}^{n+1} - T_{3,j}^{n}}{\Delta t} \qquad \text{Eq (5-22)}$$

The formation

$$\rho_f C_{pf}\frac{T_{i,j}^{n+1} - T_{i,j}^{n}}{\Delta t} = \left[\frac{T_{i,j+1}^{n+1} - 2T_{i,j}^{n+1} + T_{i,j-1}^{n+1}}{\left(\Delta z_j\right)^2}\right] + \frac{k_f}{r_i}\frac{1}{\Delta r_i}\left[T_{i+1,j}^{n+1} - T_{i,j}^{n+1}\right] + \frac{k_f}{\left(\Delta r_i\right)^2}\left[T_{i+1,j}^{n+1} - 2T_{i,j}^{n+1} + T_{i-1,j}^{n+1}\right]$$

Eq (5-23)

CHAPTER VI

RESULTS AND DISCUSSIONS

6.1 Results And Discussion For The Steady-state Heat Transfer

The results are based on the steady-state model of conventional riser drilling and riserless drilling. In addition to that, the visual basic program was developed to indicate the temperature profile for both cases. Figure 6-1, Figure 6-2, Figure 6-3 and Figure 6-4 indicate four tablets of the interface. The information of riser, return line size is shown in Figure 6-1.Figure 6-2 depicts the general well information such as well geometry, nozzle size and flow rate etc. Figure 6-3 depicts the mud properties and readings at 3 rpm, 100rpm, 300 rpm and 600 rpm respectively. Figure 6-4 provides information of heat flow such as inlet temperature, mud specific heat, geothermal gradient etc.

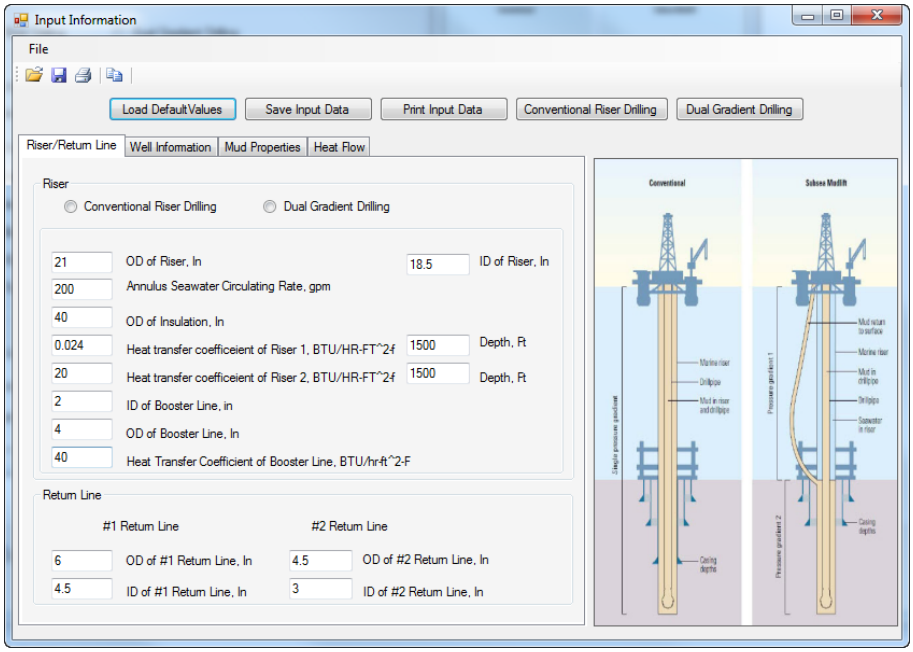

Figure 6-1 Riser/Return line tab of the data input interface

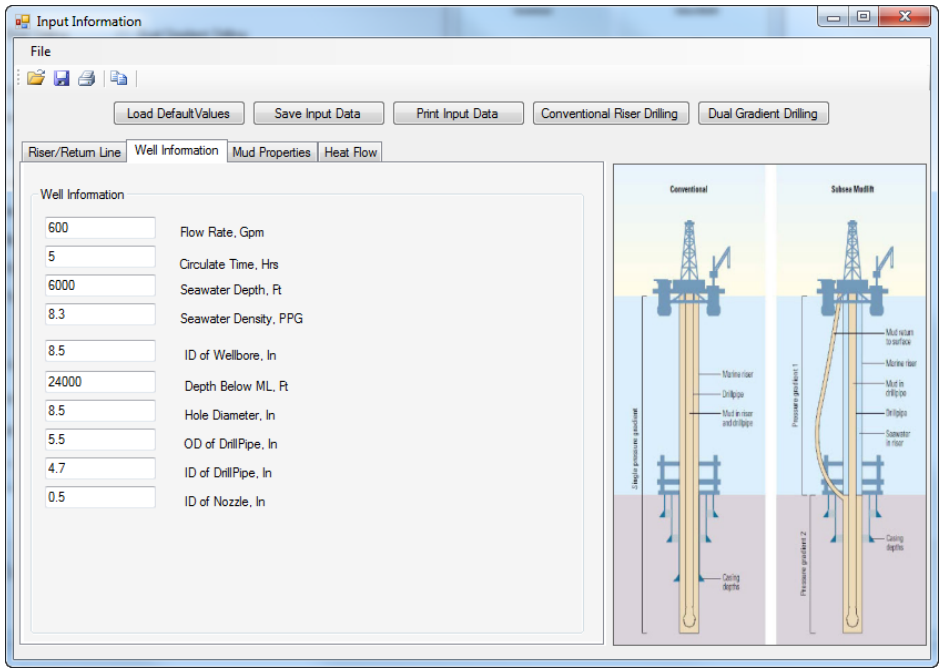

Figure 6-2 Well information tab of the data input interface

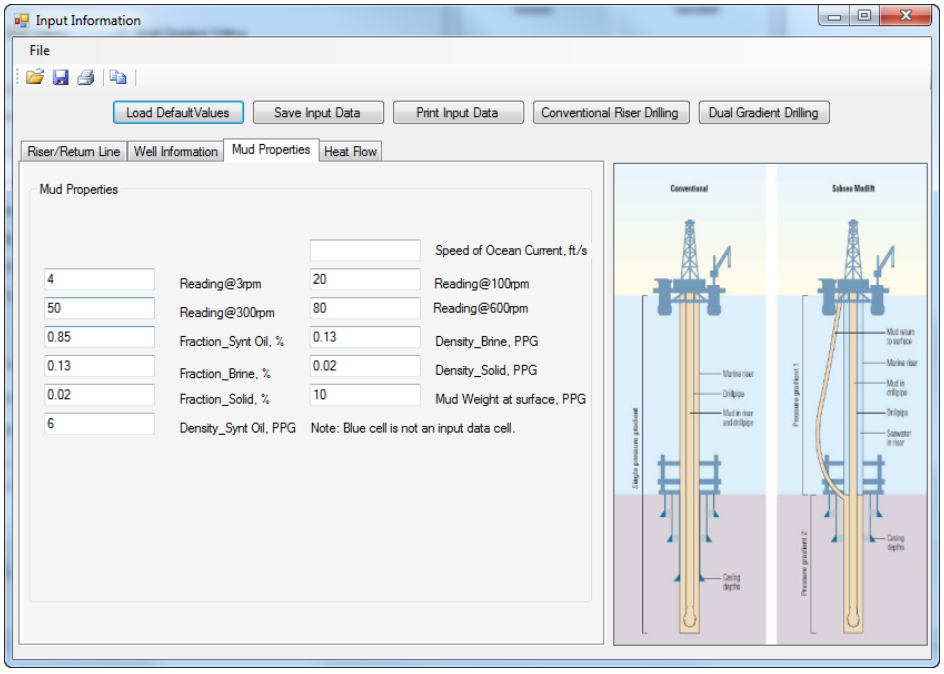

Figure 6-3 Mud properties tab of the data input interface

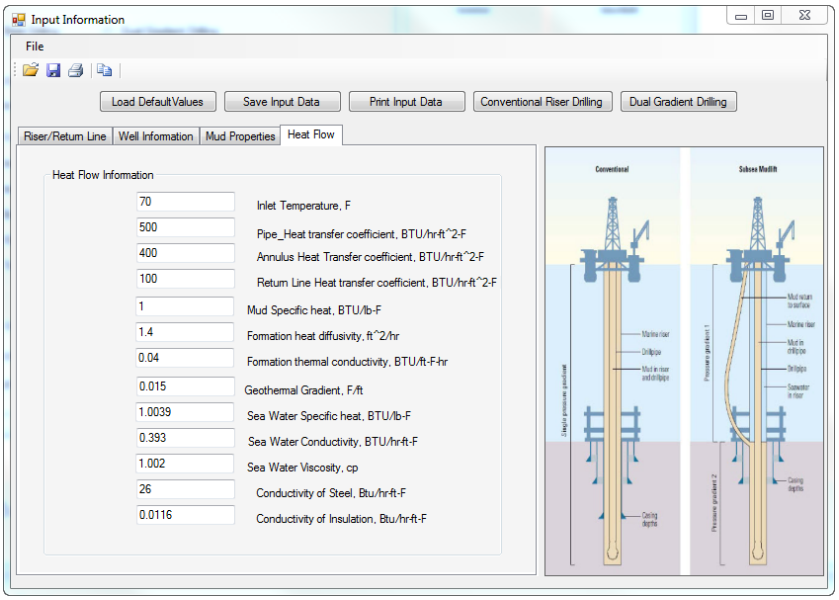

Figure 6-4 Thermal properties tab of the data input interface

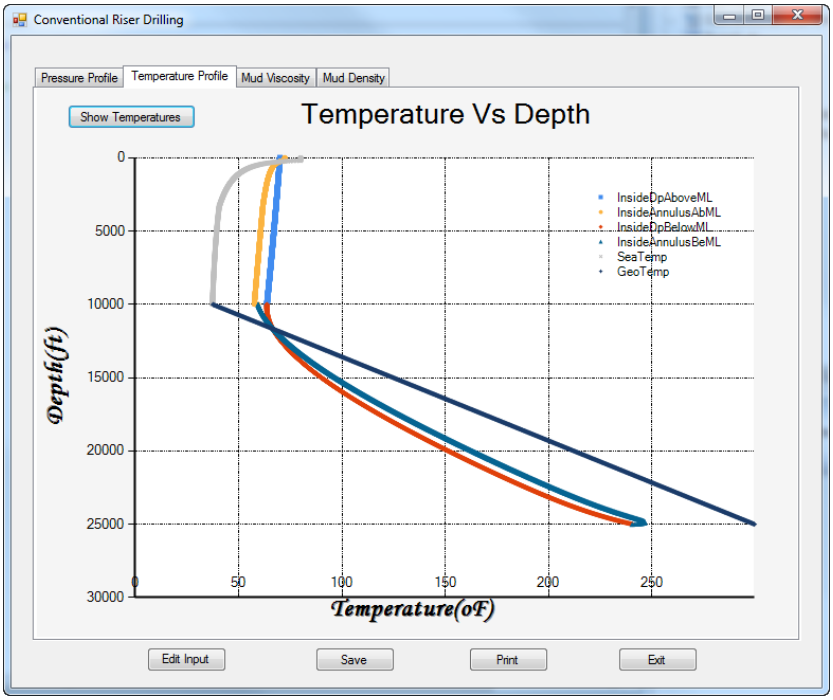

Figure 6-5 Temperature profile for conventional riser drilling @Q=2,000 gal/min, water depth=10,000ft, well depth=15,000 ft below the mudline

Table 6-1 Some parameters for Fig 6-5

Q=2000 gpm	Renold Numbers	Prandtl Number	Nussult Number	Heat Convection Coefficient (Btu/hr-ft2-oF)	Overall Heat Transfer Coefficient (Btu/hr-ft^2-^{o}F)
In the Drillpipe Below Mudline	33848	300	647	633	2.4
In the Drillpipe Above Mudline	33848	300	647	633	195
In the Annulus Below Mudline	19411	176	344	528	528
In the Annulus Above Mudline	1732		6.8	2.4	2
Maximum Temperature (^{o}F)	246.5 oF at 14840 ft beblow the mudline				
Bottom Tempearature (^{o}F)	240.5				

When the mud circulation flow rate for the conventional riser drilling is 2000 gpm, the flows in the drillpipe, annulus above the mudline, annulus below the mudline indicated in Table 6-1 are turbulent flow, laminar flow and turbulent flow respectively. With Prandtl number and Nussult number, the heat convection coefficients and overall heat transfer coefficients can be computed. The grey curve, the black blue line, the yellow curve, the light blue curve, the red curve and dark blue curve in the Figure 6-5 are the ocean temperatures, geothermal temperature, the fluid temperatures in annulus of riser, the fluid temperatures in the drillpipe above the seafloor, the temperatures in the drillpipe below the seafloor and the temperature in the annulus below the seafloor respectively.

The flow temperature at the inlet is 70^{o}F, with the water depth increasing, the flow temperature in the drillpipe decreases to 67.67 ^{o}F at the seafloor. Now the geothermal temperature is less than the temperature in the drillpipe, the temperature, the light blue curve and dark blue curve in the Figure 6-5, in the drillpipe continues decreasing until there isn't temperature difference at 500ft below the mudline, which is about 70 ^{o}F in the drillpipe and annulus. Below this point, the temperature in the drillpipe keeps lower than that in the annulus, the temperature difference is about 10 ^{o}F. The bottomhole

temperature is 240.5 ^{o}F while the maximum temperature exists in the annulus below the mudline, which is 246.5 ^{o}F at 14840 feet below the mudline. At the bit, the heat by the heat by the dynamic energy loss could lead to the temperature increase by 30 ^{o}F in this case. Based on that heat loss by the dynamic energy loss, we could change the nozzle size. From the Figure 6-5, the temperature cure in the annulus is always between the geothermal temperature and the temperature in the drillpipe for the conventional riser drilling. Due to the strong convection effect, the temperatures in the well are not linear, which also means the heat convection overwhelms. With the drilling mud is circulated back through annulus to the surface, the temperature in the annulus at the mudline achieves 59.4 ^{o}F. The temperature in the annulus keep increasing with the depth decreasing, at the surface, the outflow temperature in the annulus is 72^{o}F.

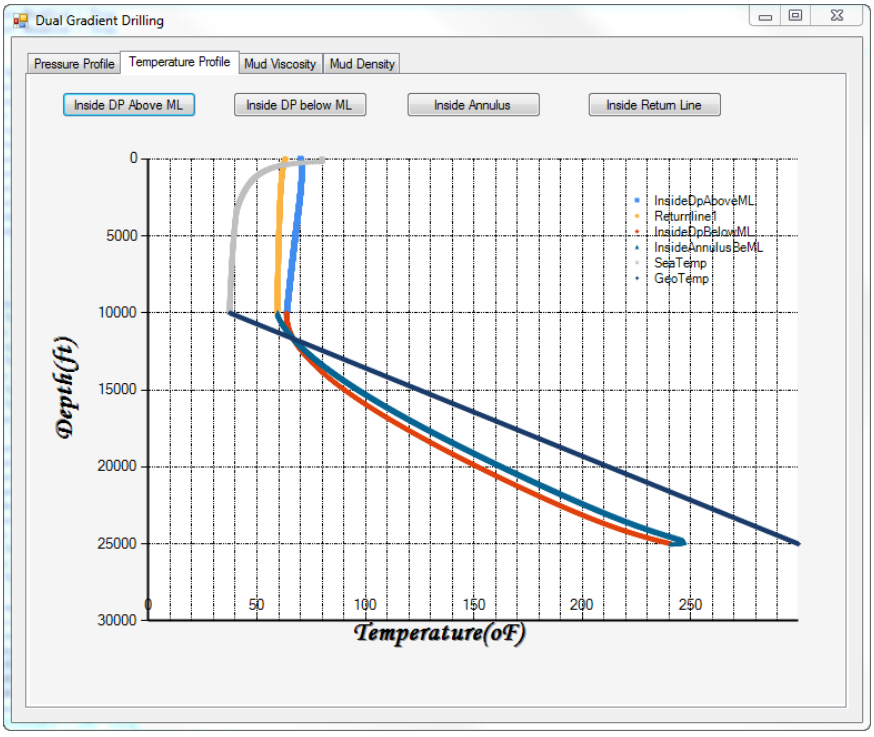

Figure 6-6 Temperature profile for riserless drilling @Q=2,000 gal/min, water depth=10,000ft, well depth=15,000 ft below the mudline

Table 6-2 Some parameters for Fig.6-6

Q=2000 gpm	Renold Numbers	Prandtl Number	Nussult Number	Heat Convection Coefficient (Btu/hr-ft2-oF)	Overall Heat Transfer Coefficient (Btu/hr-ft^2-^{o}F)
In the Drillpipe Below Mudline	33848	300	647	633	70.6
In the Drillpipe Above Mudline	33848	300	647	633	195
In the Annulus Below Mudline	19411	176	344	528	528
In the Return Line	36870	1288	1684	698	61.4
Maximum Temperature (^{o}F)	246.9 at 14850 ft beblow the mudline				
Bottom Tempearature (^{o}F)	240.9				

The grey curve, the black blue line, the yellow curve, the light blue curve, the red curve and dark blue curve in the Figure 6-6 are the ocean temperatures, geothermal temperature, the fluid temperatures in the returnline, the fluid temperatures in the drillpipe above the seafloor, the temperatures in the drillpipe below the seafloor and the temperature in the annulus below the seafloor respectively. Table 6-2 indicates the flow through the entire well system is turbulent flow. Table 6-3 contains hydraulic parameters for conventional riser drilling at 200 gpm flowrate. Table 6-4 lists hydraulic parameters for riserless drilling at 200 gpm flowrate. For the riserless drilling, the flow temperature at the inlet is 70 ^{o}F in Figure 6-6, with the water depth increasing, the flow temperature in the drillpipe decreases to 63.7 ^{o}F at the mudeline, which is 4 ^{o}F less than that for the conventional riser drilling. The temperatures in the drillpipe, annulus at the mudline are 63.7^{o}F, 59.5^{o}F, which indicates the sea water has obvious effect on the riserless drilling without thermal insulation than that on the conventional riserless drilling. The outflow temperature, yellow curve, in the returnline at the surface is 63^{o}F, which is obviously less than that in the conventional riser drilling in Figure 6-5.

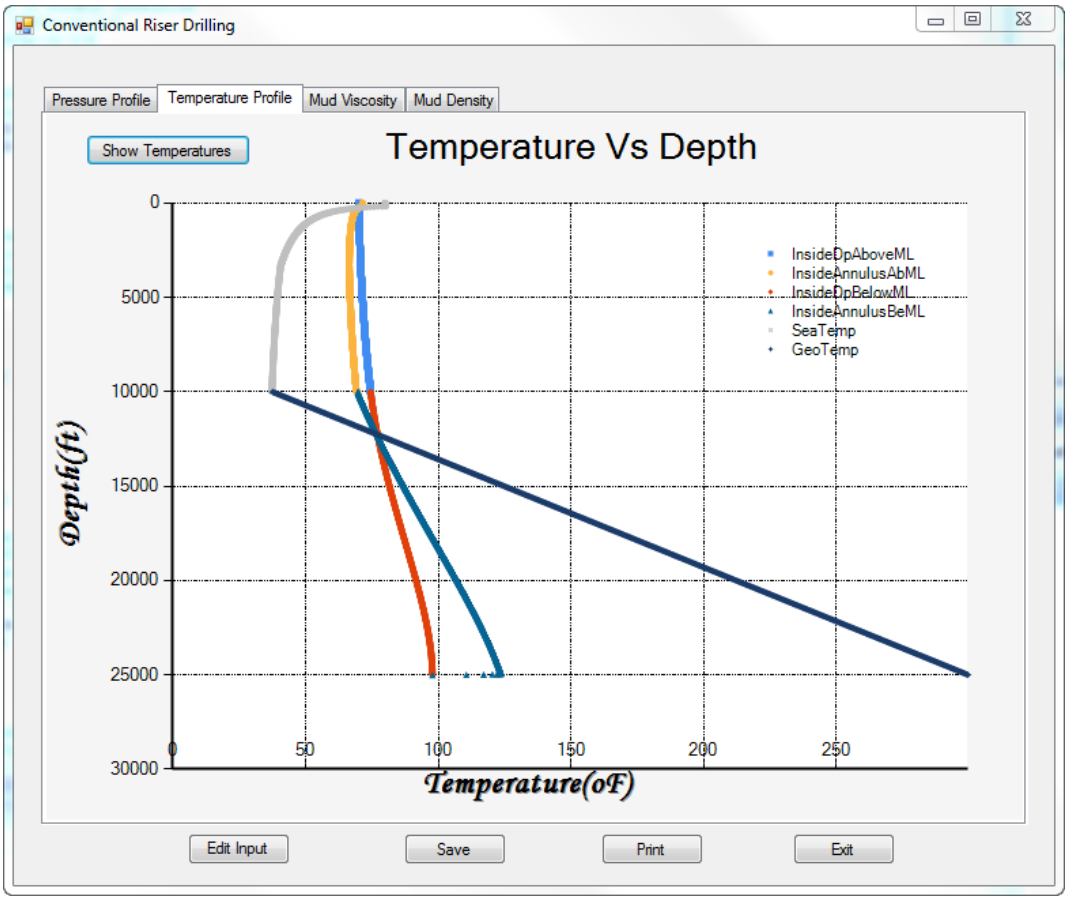

Figure 6-7 Temperature profile for conventional riser drilling @Q=200 gal/min, water depth=10000ft, well depth=15,000 ft below the mudline

Table 6-3 Some parameters for Fig.6-7

Q=200 gpm	Renold Numbers	Prandtl Number	Nussult Number	Heat Convection Coefficient (Btu/hr-ft2-oF)	Overall Heat Transfer Coefficient (Btu/hr-ft^2-^{o}F)
In the Drillpipe Below Mudline	1611	300	3.66	3.6	2.2
In the Drillpipe Above Mudline	1611	300	3.66	3.6	1.36
In the Annulus Below Mudline	50	176	5.4	8.3	8.3
In the Annulus Above Mudline	558		6.9	2.4	2
Maximum Temperature (^{o}F)	123.6 at 14890 ft beblow the mudline				
Bottom Tempearature (^{o}F)	97.8				

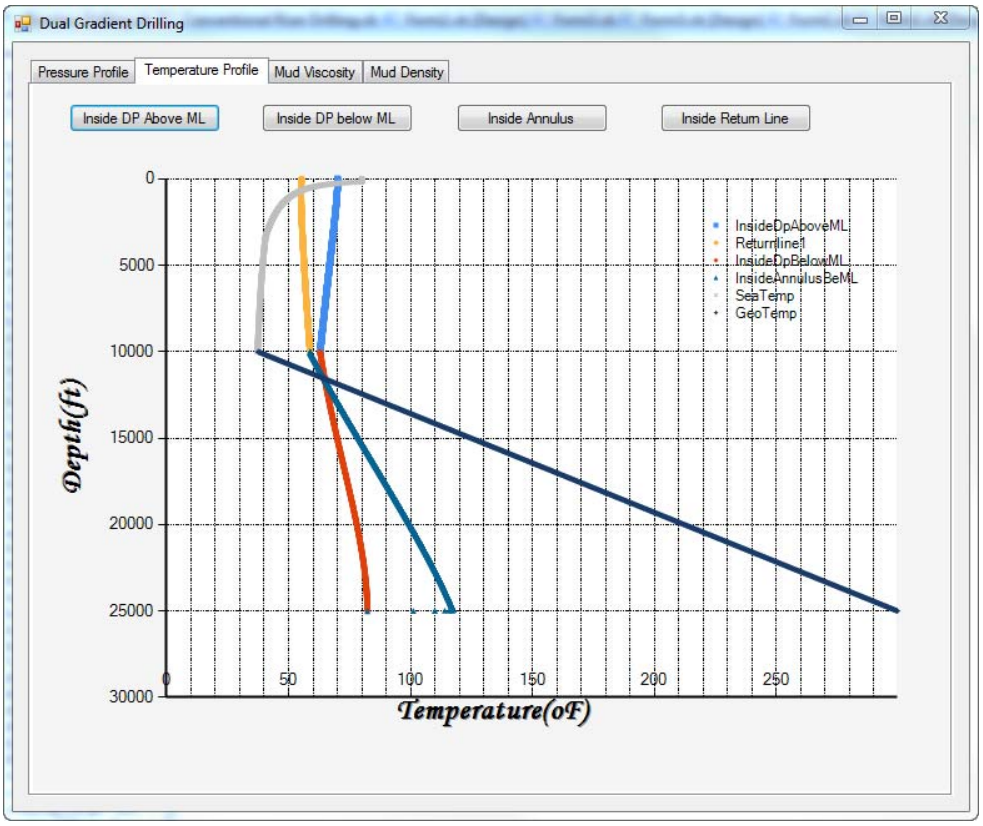

Figure 6-8 Temperature profile for riserless drilling @Q=200 gal/min, water depth=10000ft, well depth=15,000 ft below the mudline

Table 6-4 Some parameters for Fig.6-8

Q=200 gpm	Renold Numbers	Prandtl Number	Nussult Number	Heat Convection Coefficient (Btu/hr-ft2-oF)	Overall Heat Transfer Coefficient (Btu/hr-ft^2-^{o}F)
In the Drillpipe Below Mudline	1611		3.66	3.6	2.9
In the Drillpipe Above Mudline	1611		3.66	3.6	1.9
In the Annulus Below Mudline	1558		3.66	5.6	8.3
In the Return Line	1755		3.66	3.8	2.7
Maximum Temperature (^{o}F)	17.4 at 14890 ft beblow the mudline				
Bottom Tempearature (^{o}F)	82.3				

For the Figure 6-7 and Figure 6-8, the temperature follows similar trend but the temperature profile is approaching linear distribution, it is that the heat convection flow is getting weak by the laminar flow. Figure 6-9, Figure 6-10, Figure 6-11and Figure 6-12 could be explained in similar way.

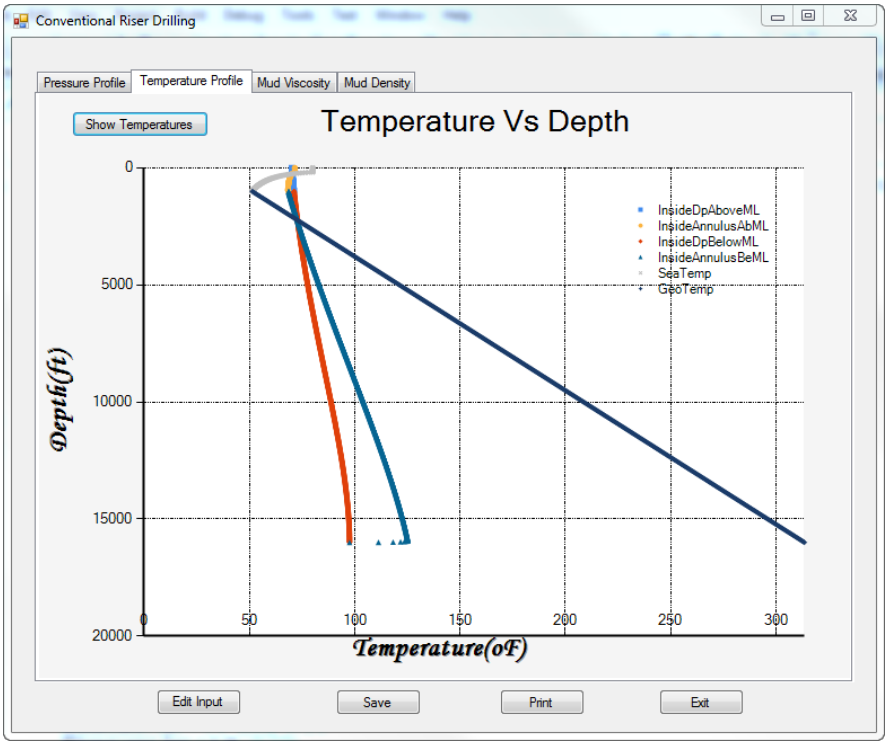

Figure 6-9 Temperature profile for conventional riser drilling @Q=200 gal/min, water depth=1000ft, well depth=15,000 ft below the mudline

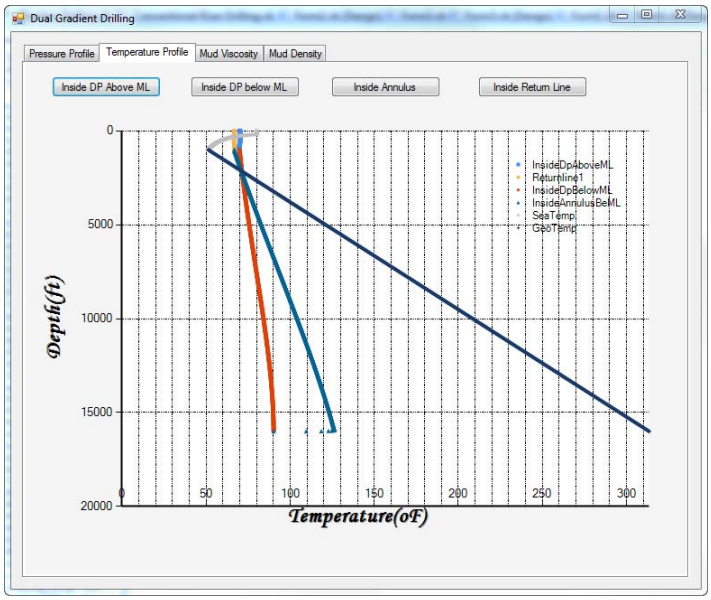

Figure 6-10 Temperature profile for riserless drilling @Q=200 gal/min, water depth=1000ft, well depth=15,000 ft below the mudline

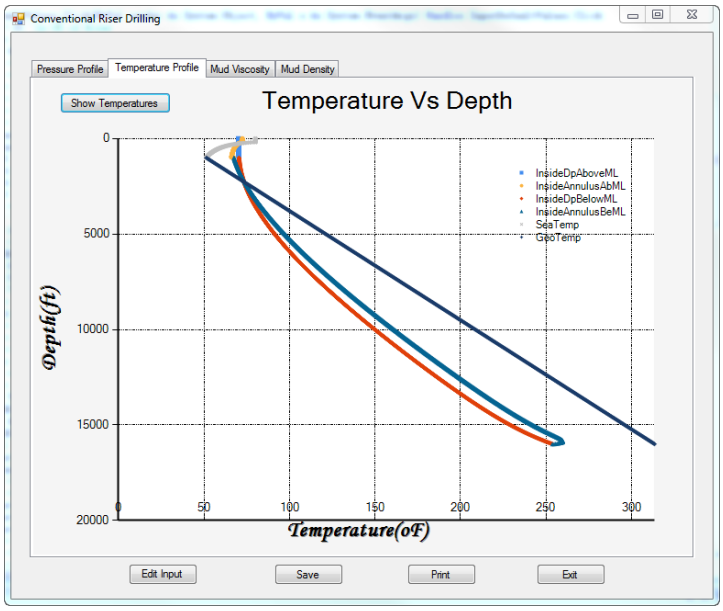

Figure 6-11 Temperature profile for conventional riser drilling @Q=2,000 gal/min, water depth=1000ft, well depth=15,000 ft below the mudline

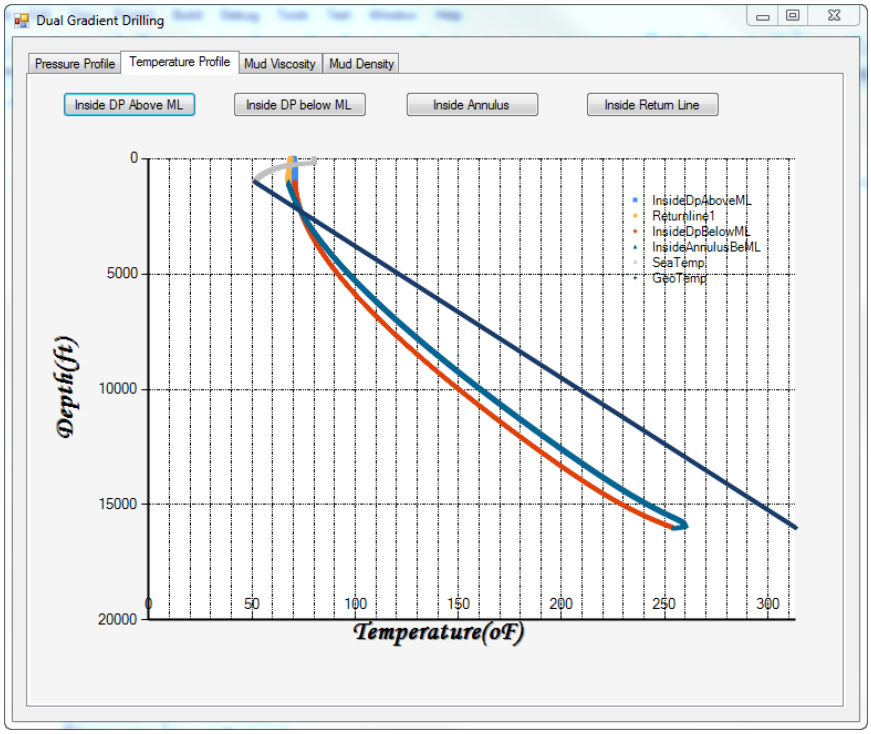

Figure 6-12 Temperature profile for riserless drilling @Q=2,000 gal/min, water depth=1000ft, well depth=15,000 ft below the mudline

6.2 Results And Discussions For The Transient Heat Transfer Of Riserless Drilling

For every well, the wellbore geometry is specified. The properties of drilling fluid such as viscosity, density, conductivity and heat capacity could be treated as constants. The circulating flow rates overwhelm the temperature distribution in the drillstring, annulus, returnline and formation so that we focus on the sensitivity analysis for different circulating rates. Table 6-5 shows the default parameters like wellbore geometries, properties of fluid and geothermal gradient. Table 6-6 shows the calculated hydraulic parameters based on Table 6-5.

Table 6-5 Default parameters

ρ_m=	10	ppg
Dsw=	10000	ft
Dw=	10000	ft
Delta Z=	40	ft
ID of Dp=	4.7	in
OD of Dp =	5.5	in
ID of Rl=	4.5	in
OD of Rl=	6	in
hedp=	61	Btu/hr-ft2-F
herl=	67	Btu/hr-ft2-F
Δt=	0.5	hrs
Wellbore Size=	8.5	in
ρ_f =	144	lb/ft3
k_{dp}=	26	Btu/hr-ft-F
k_f=	1.76	Btu/hr-ft-F
Δr =	1	ft
Gthermal Gradient=	0.0175	^{o}F/ft
Tinlet=	70	^{o}F/ft

Table 6-6 Some parameters for 5gpm

Q=5 gpm	Renold Numbers	Heat Convection Coefficient (Btu/hr-ft2-oF)
In the Drillpipe Below Mudline	12	3.58
In the Drillpipe Above Mudline	12	3.58
In the Annulus Below Mudline	1.9	5.6
In the Return Line	13.4	3.8

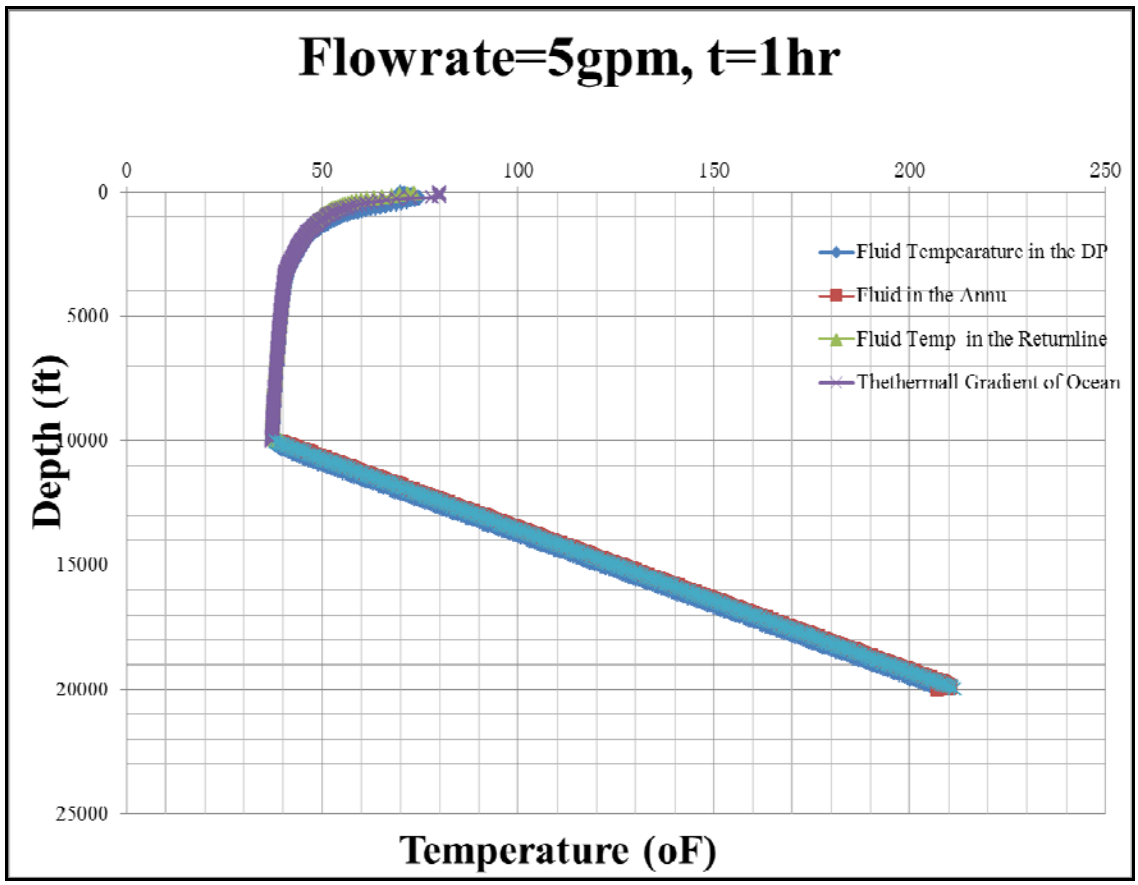

Figure 6-13 Temperature profile for 5gpm at t=1hr

The flow temperature at the inlet is 70°F, with the water depth increasing, the flow temperature in the drillpipe decreases to 37.36 °F at the mudline, which is 0.16 °F more than that of the sea water. The calculated temperature profiles of fluid in the drillpipe above the seafloor, in the drillpipe below the seafloor, in the annulus and in the returnline in Figure 6-13 overlap the ocean temperature profile and geothermal temperature profile, which means they are almost as same at initial time step based on the initial conditions. Figure 6-14, Figure 6-15, Figure 6-16 and Figure 6-17 also indicate same conclusions. There is minor temperature difference, which is due to the weak convection heat transfer by the low circulating flow rate. At 168 hours in Figure 6-

16, the maximum temperature, 201.1 ^{o}F, takes place at 19,600 feet deep. If the circulate is 2.5 gpm and the circulation time is 168 hours, the fluid temperature difference between the drillpipe and annulus could be as low as 3 ^{o}F.

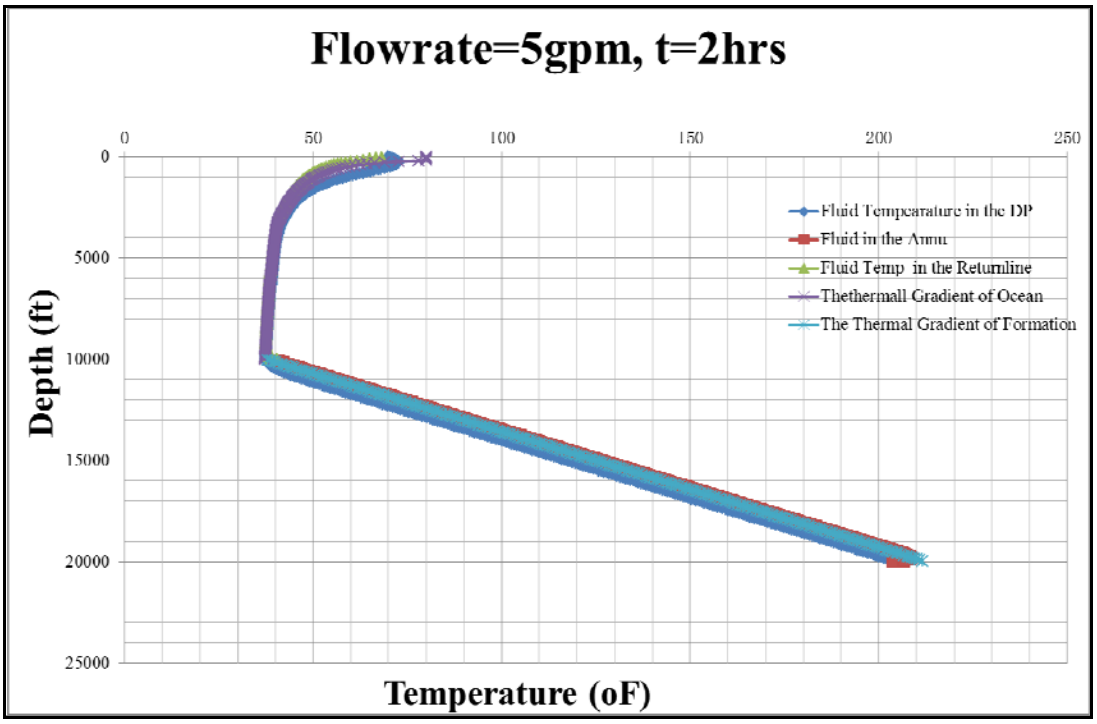

Figure 6-14 Temperature profile for 5gpm at t=2hr

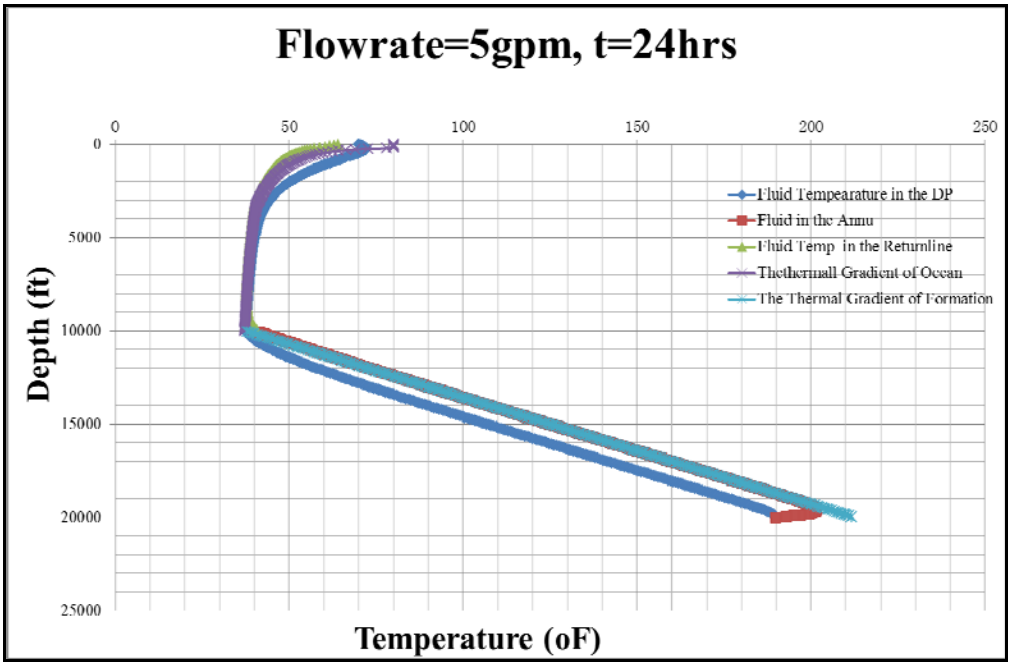

Figure 6-15 Temperature profile for 5gpm at t=24hrs

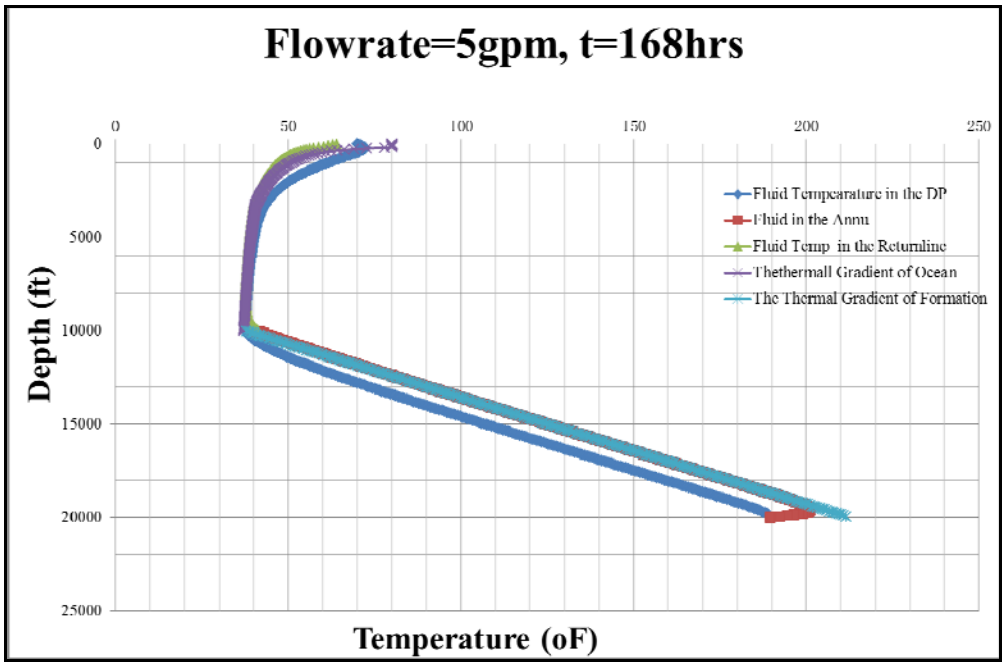

Figure 6-16 Temperature profile for 5gpm at t=168hrs

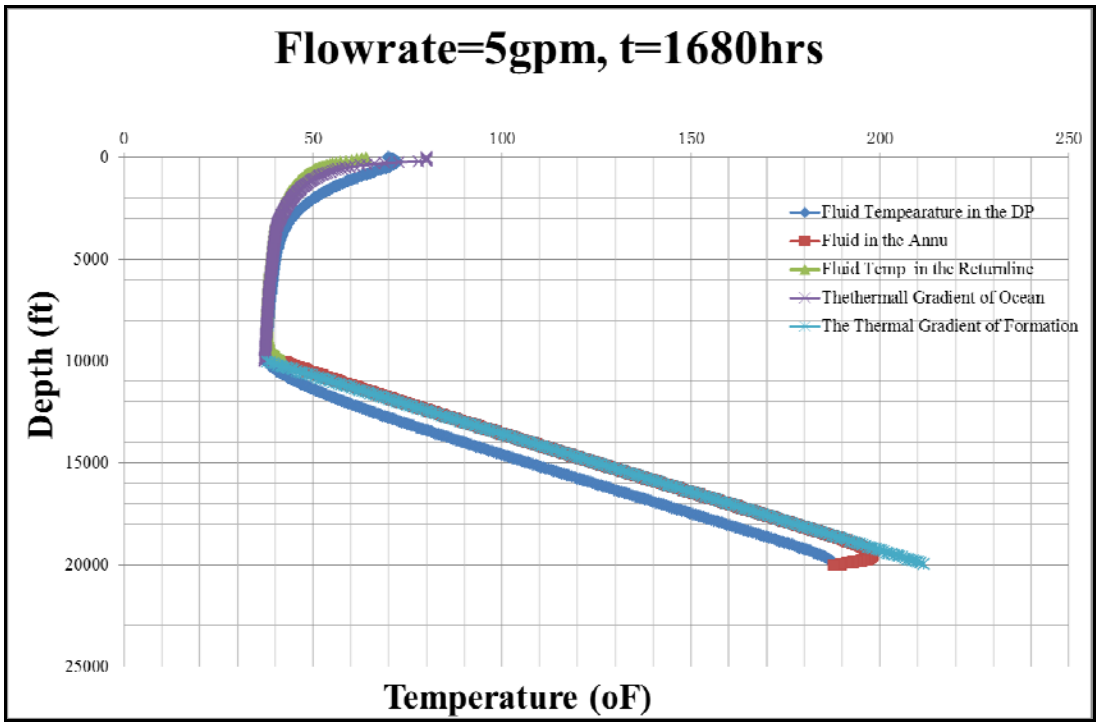

Figure 6-17 Temperature profile for 5gpm at t=1680hrs

Since the "new" flow pushes the previous drilling fluid downward, the temperature of drilling fluid is a little less than that of geothermal temperature at the same depth due to "weak" convection heat transfer diffusion. The corresponding temperature in the annulus is about 5 ^{o}F higher than the geothermal temperature, which is at the bottom of wellbore, the drilling fluid temperature achieves the maximum, which is 188.85 ^{o}F, 20 ^{o}F less than that of geothermal temperature. As a matter of fact, the weak convection heat transfer both in the drillpipe and annulus leads that the previous temperature profile is pushed upward or downward, which also indicate the "new" drilling fluid is displacing the "old" one.

Table 6-7 Some parameters for 200gpm

Q=200 gpm	Renold Numbers	Heat Convection Coefficient (Btu/hr-ft2-oF)
In the Drillpipe Below Mudline	1611	3.58
In the Drillpipe Above Mudline	1611	3.58
In the Annulus Below Mudline	559	5.6
In the Return Line	1755	3.8

Table 6-7 shows the hydraulic parameters at the 200 gpm flowrate. Figure 6-18 though Figure 6-25 indicate the temperature profiles at 0.1 hour, 1 hour, 2 hours, 8 hours, 24 hours, 168 hours and 1680 hours respectively.

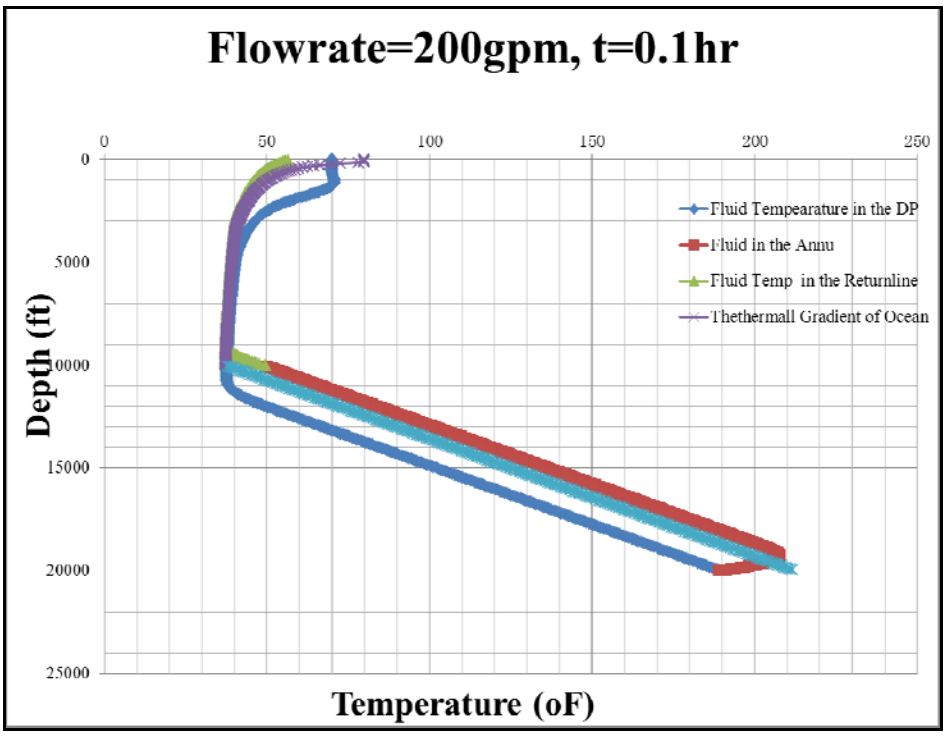

Figure 6-18 Temperature profile for 200gpm at t=0.1 hr

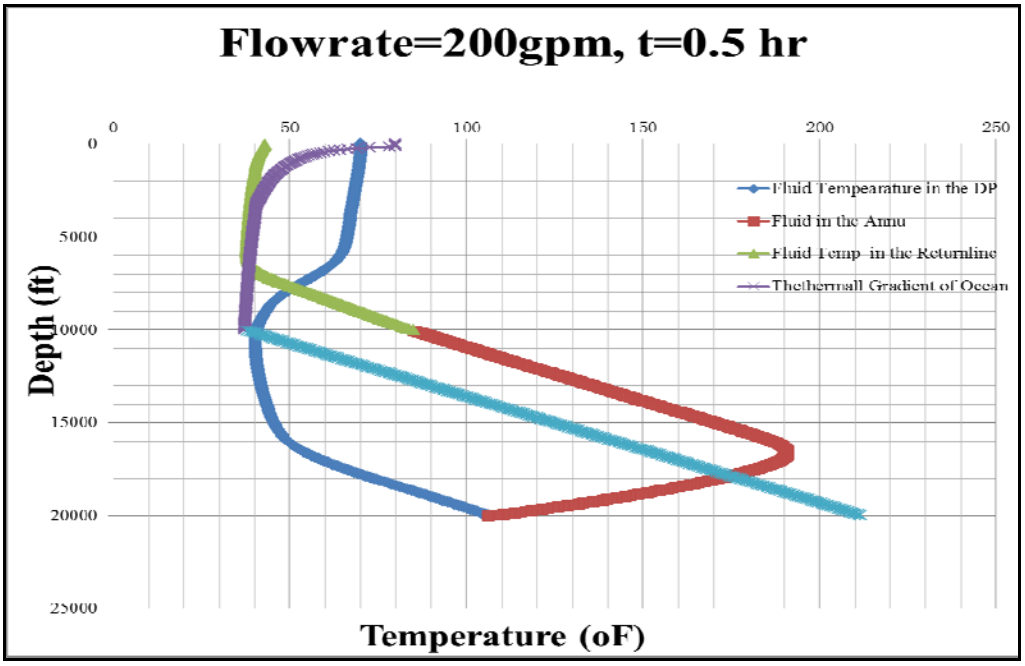

Figure 6-19 Temperature profile for 200gpm at t=0.5 hr

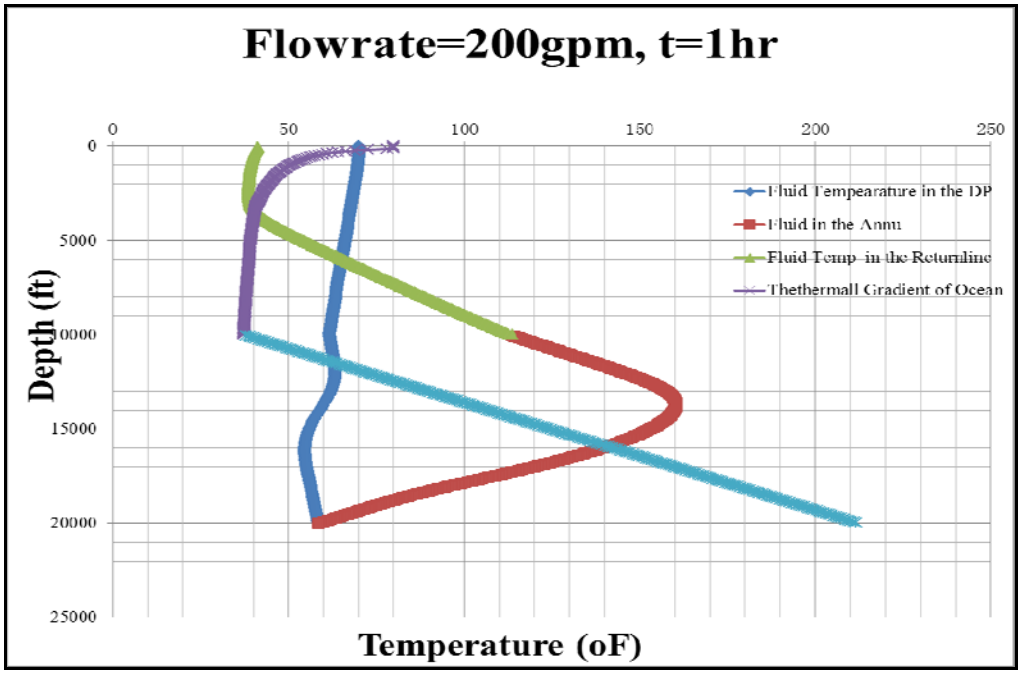

Figure 6-20 Temperature profile for 200gpm at t=1 hr

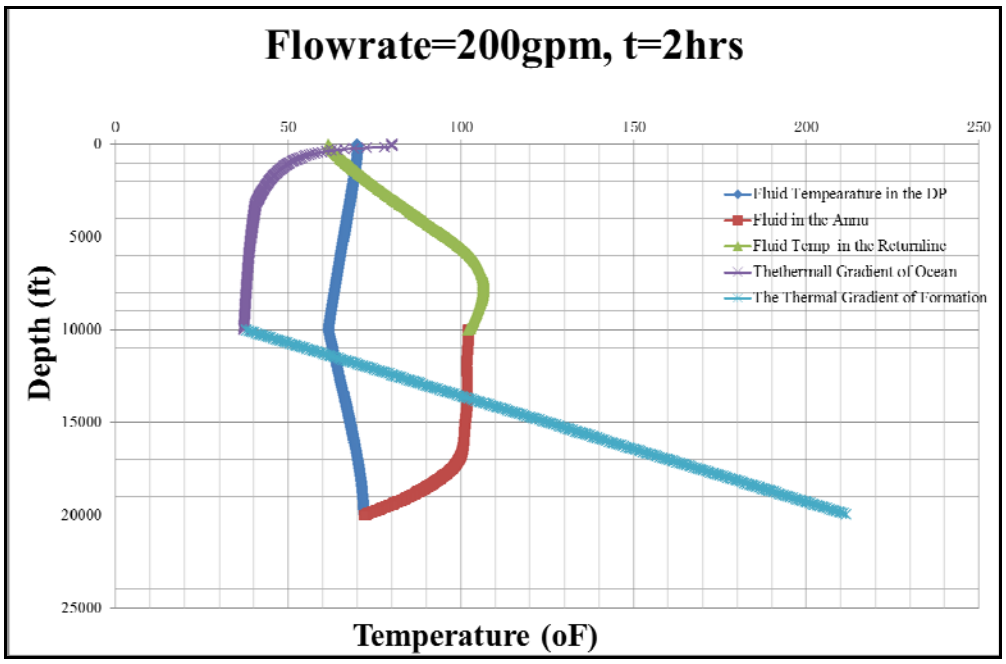

Figure 6-21 Temperature profile for 200gpm at t=2 hrs

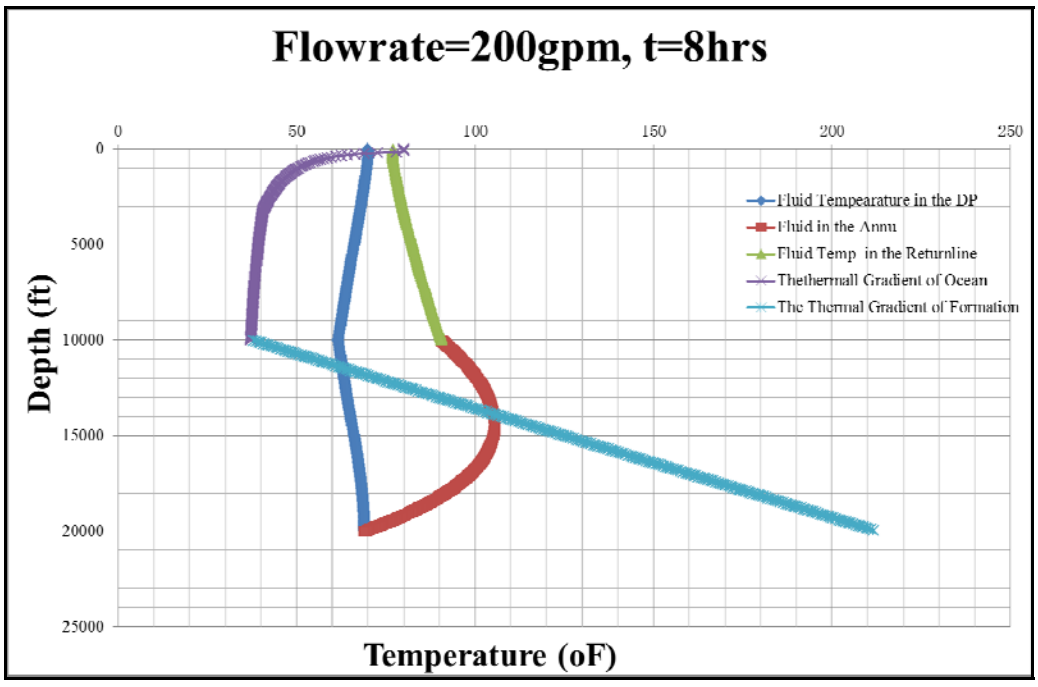

Figure 6-22 Temperature profile for 200gpm at t=8 hrs

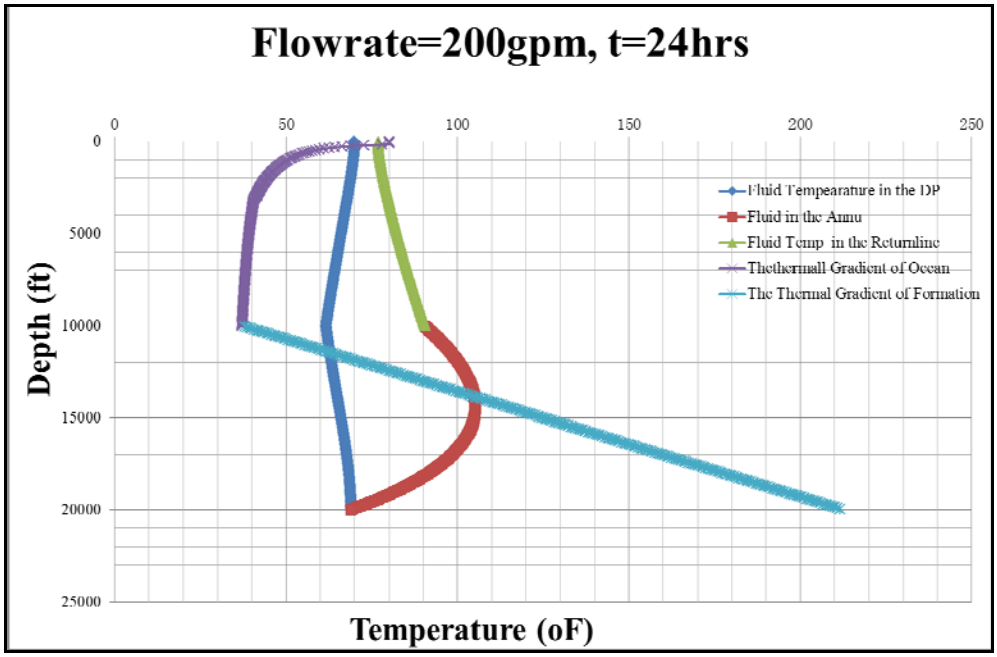

Figure 6-23 Temperature profile for 200gpm at t=24 hrs

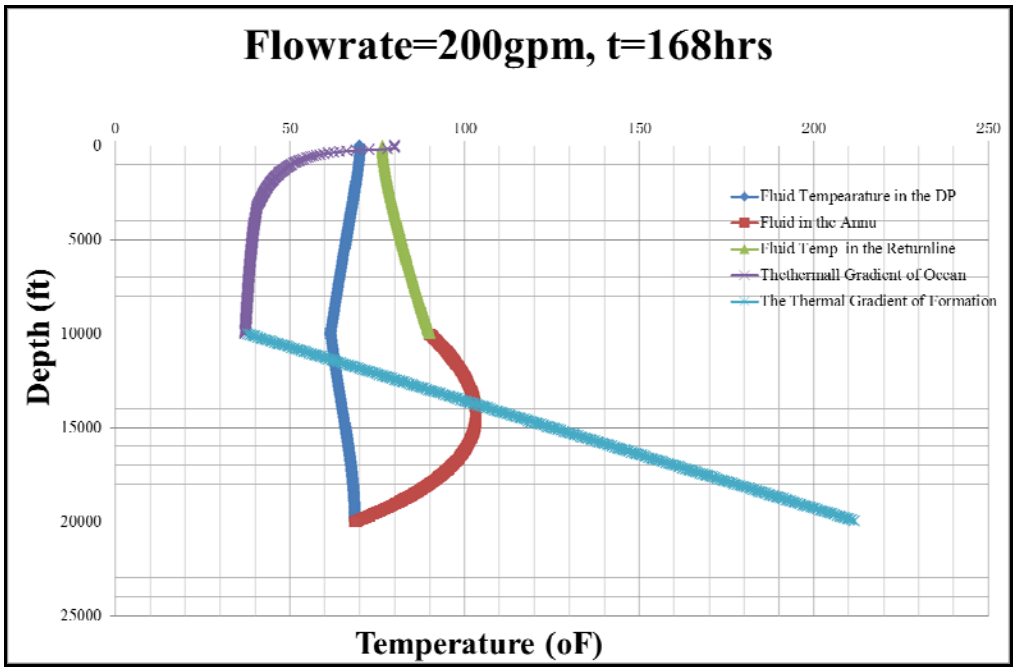

Figure 6-24 Temperature profile for 200gpm at t=168 hrs

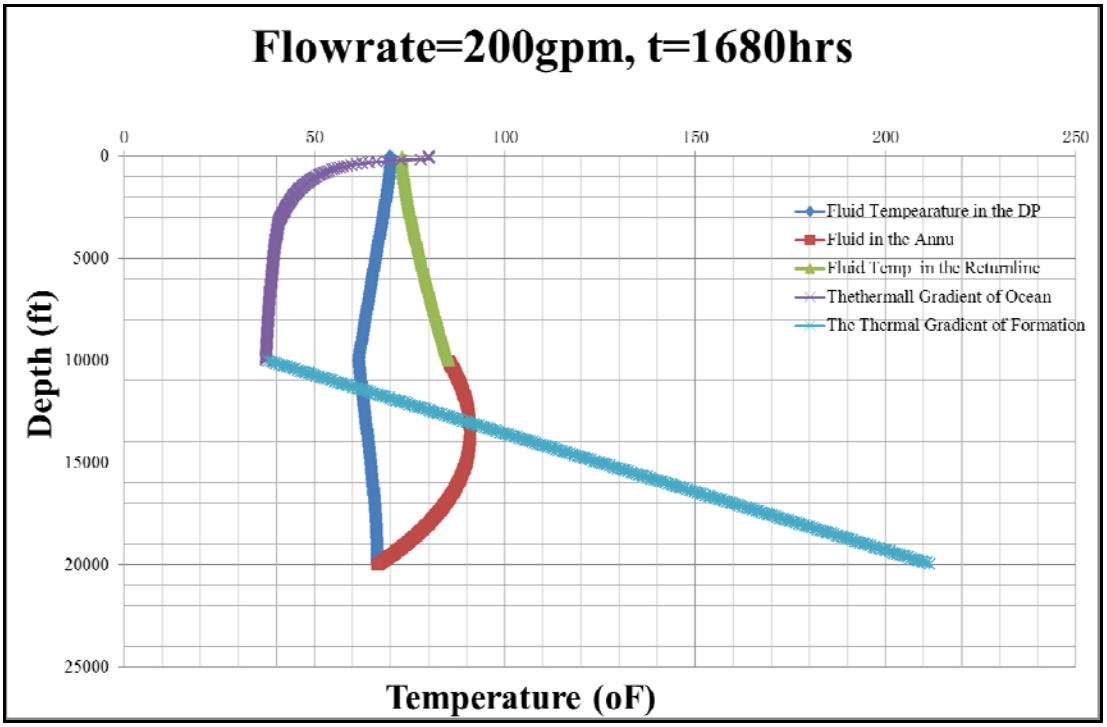

Figure 6-25 Temperature profile for 200gpm at t=1680 hrs

Table 6-8 Some parameters for 400gpm

Q=400 gpm	Renold Numbers	Heat Convection Coefficient (Btu/hr-ft2-oF)
In the Drillpipe Below Mudline	4030	137.2
In the Drillpipe Above Mudline	4030	137.2
In the Annulus Below Mudline	1626	5.6
In the Return Line	4390	151.3

Table 6-8 shows the hydraulic parameters at the 400 gpm flowrate. Figure 6-26 though Figure 6-31 indicate the temperature profiles at 0.05 hour, 2 hours, 8 hours, 24 hours, 168 hours and 1680 hours respectively.

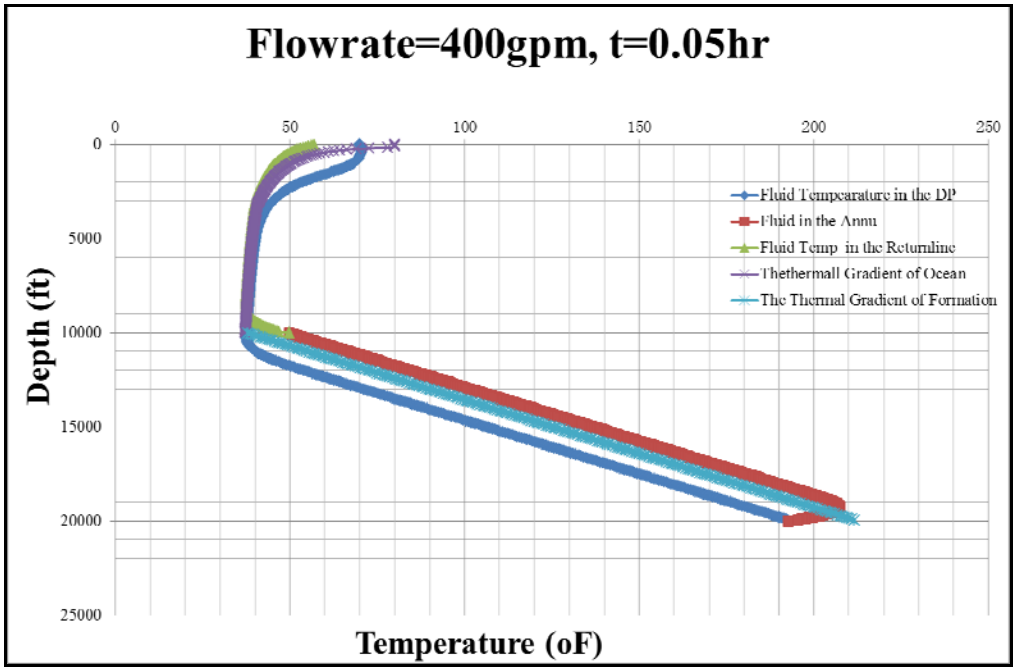

Figure 6-26 Temperature profile for 400gpm at t=0.05 hr

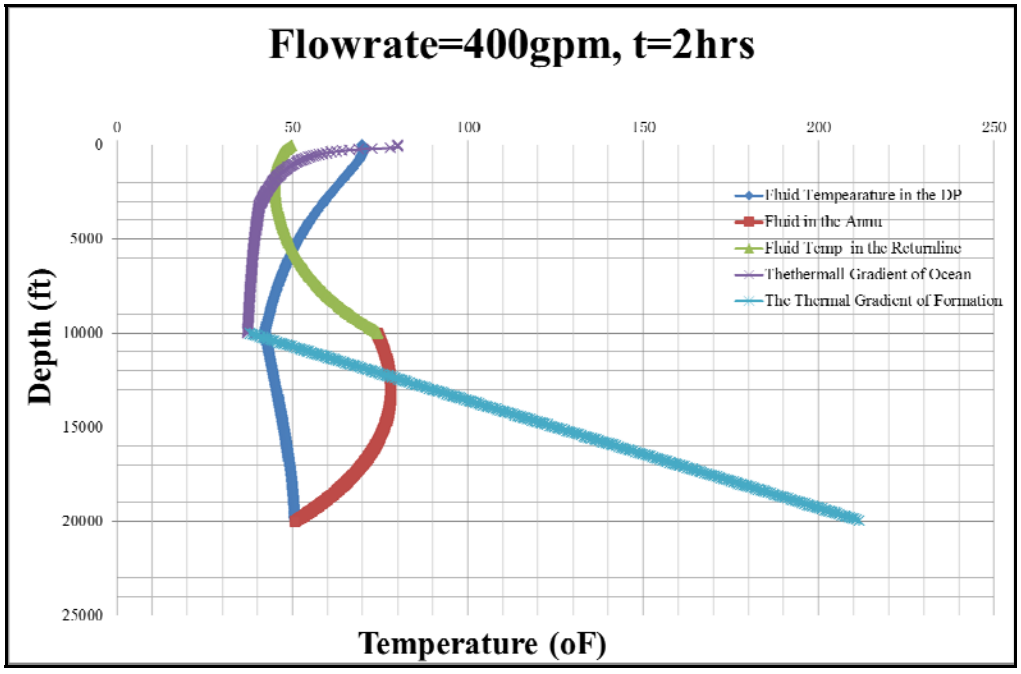

Figure 6-27 Temperature profile for 400gpm at t=2 hrs

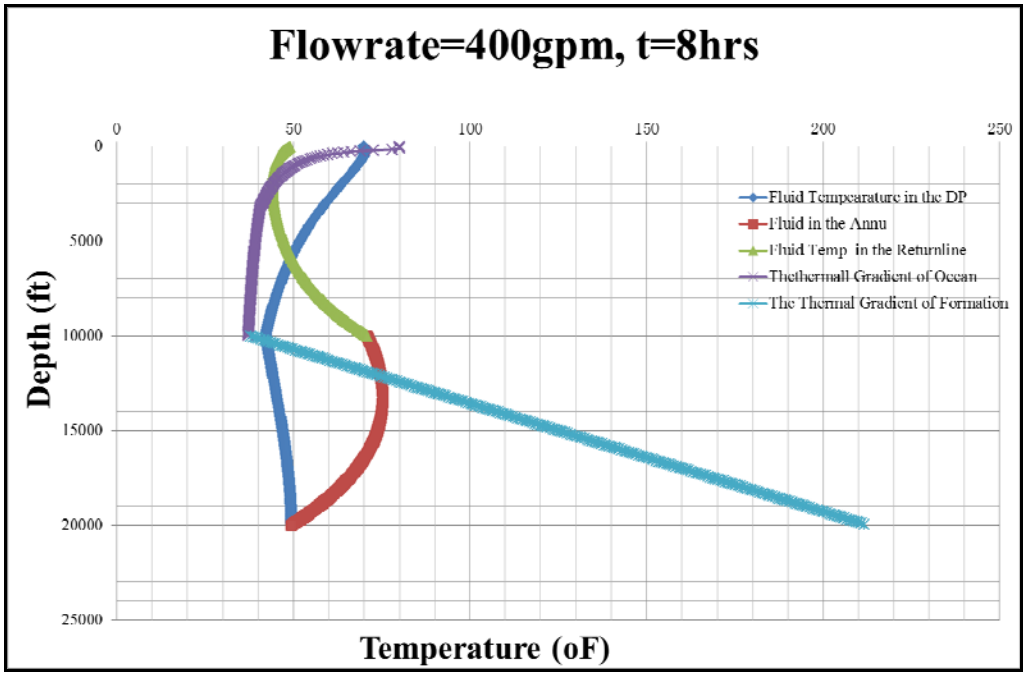

Figure 6-28 Temperature profile for 400gpm at t=8 hrs

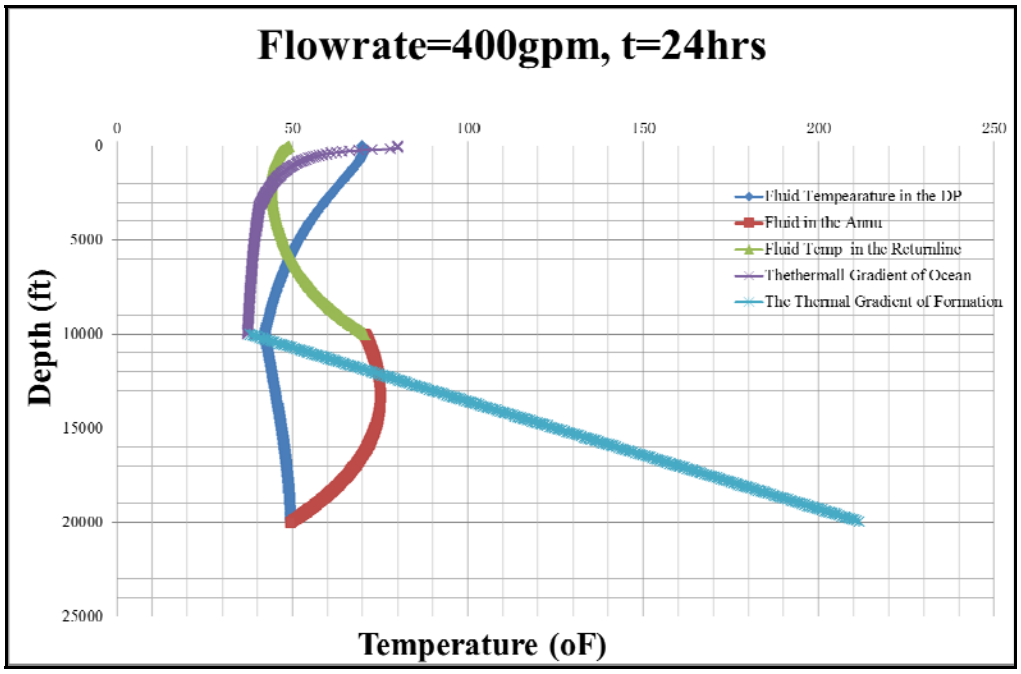

Figure 6-29 Temperature profile for 400gpm at t=24 hrs

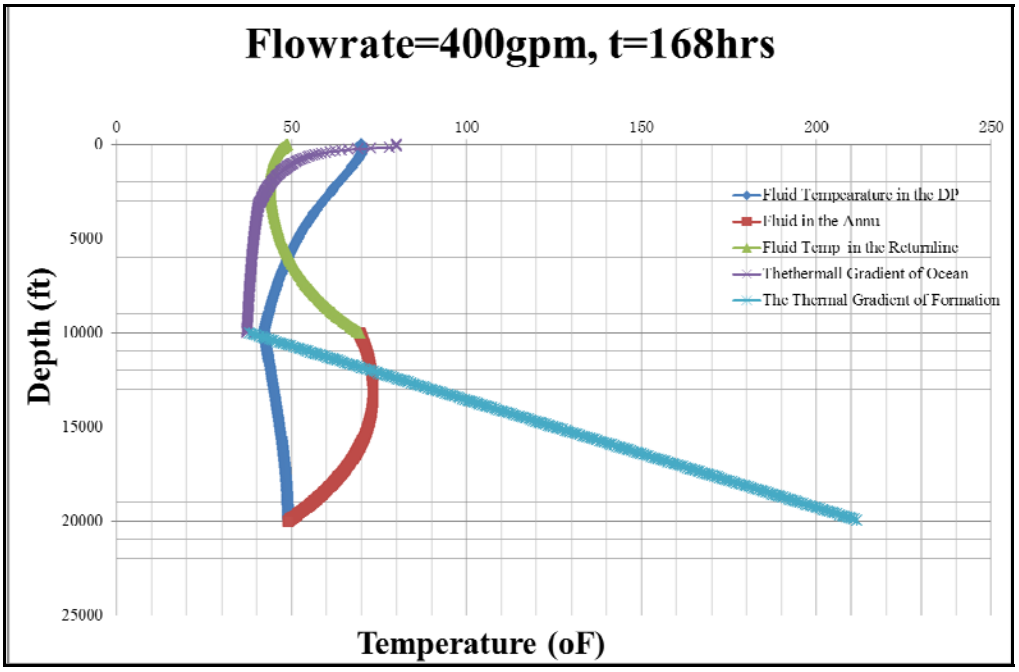

Figure 6-30 Temperature profile for 400gpm at t=168 hrs

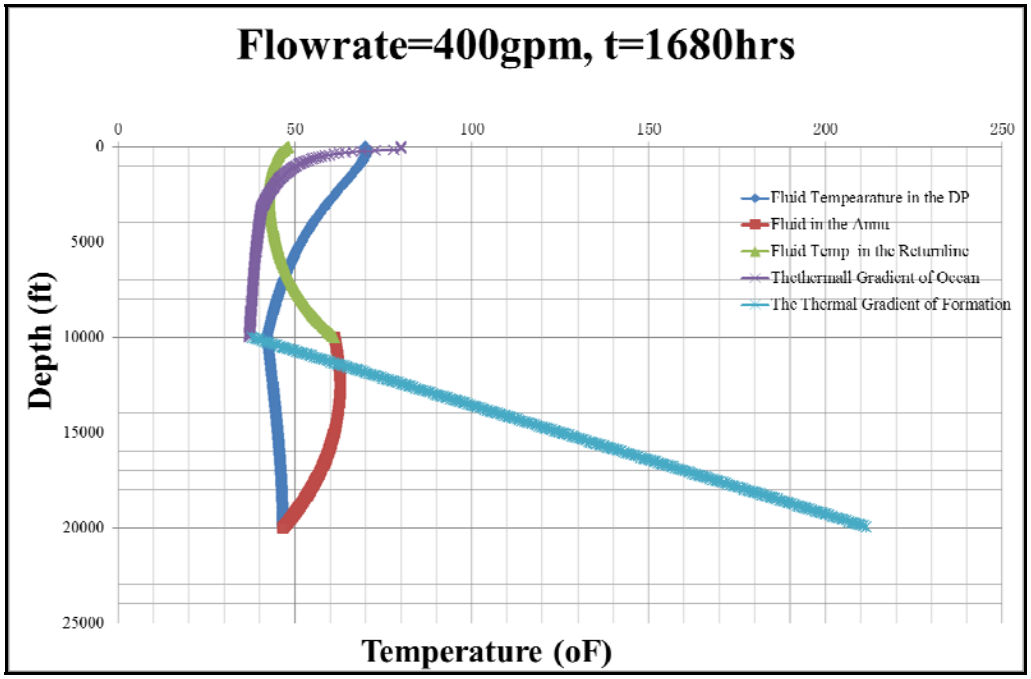

Figure 6-31 Temperature profile for 400gpm at t=1680 hrs

Table 6-9 Some parameters for 600gpm

Q=600 gpm	Renold Numbers	Heat Convection Coefficient (Btu/hr-ft2-oF)
In the Drillpipe Below Mudline	6889	201.7
In the Drillpipe Above Mudline	6889	201.7
In the Annulus Below Mudline	3370	120.6
In the Return Line	7504	222.5

Table 6-9 shows the hydraulic parameters at the 600 gpm flowrate. Figure 6-32 though Figure 6-37 indicate the temperature profiles at 2 hours, 4 hours, 8 hours, 24 hours, 168 hours and 1680 hours respectively.

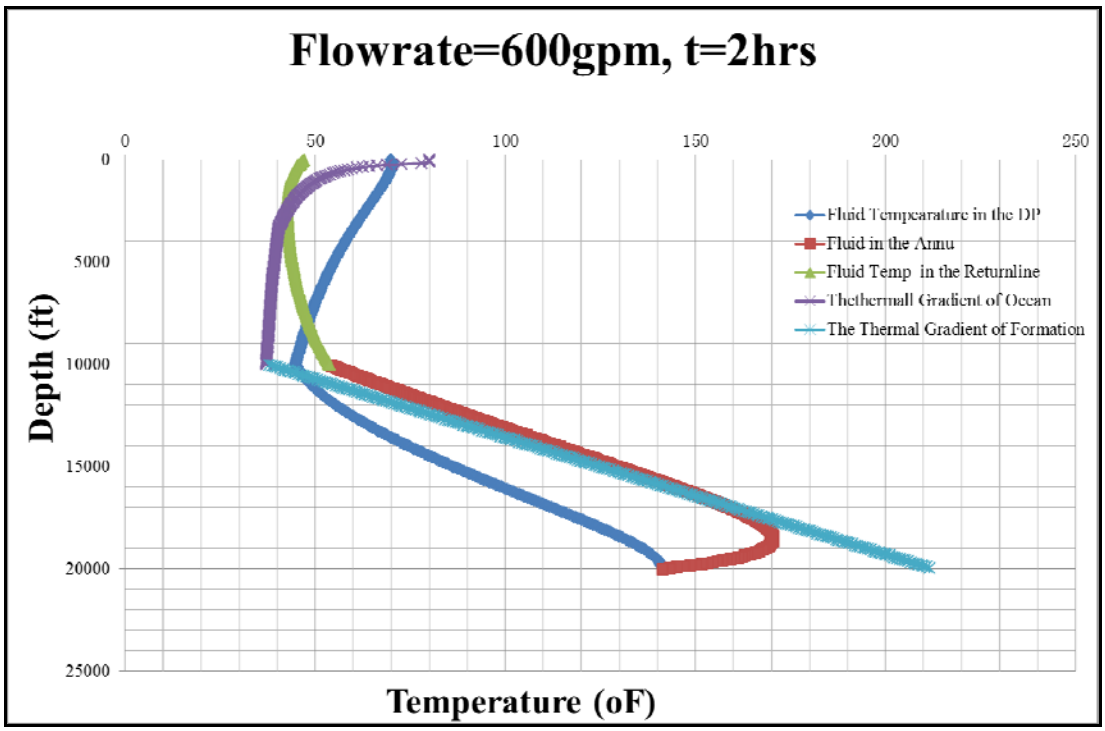

Figure 6-32 Temperature profile for 600gpm at t=2 hrs

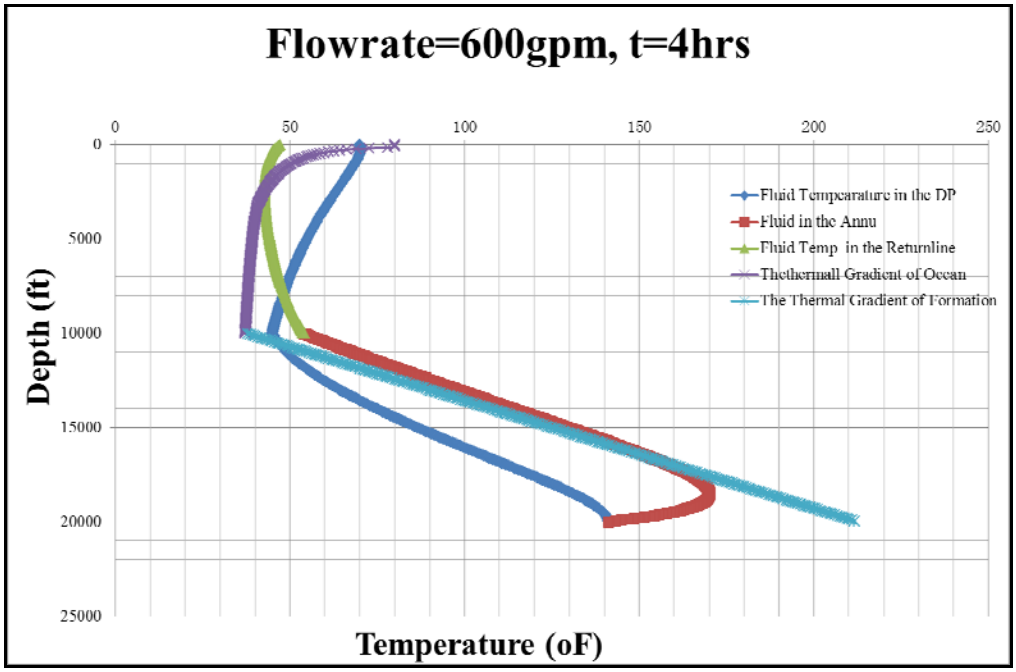

Figure 6-33 Temperature profile for 600gpm at t=4 hrs

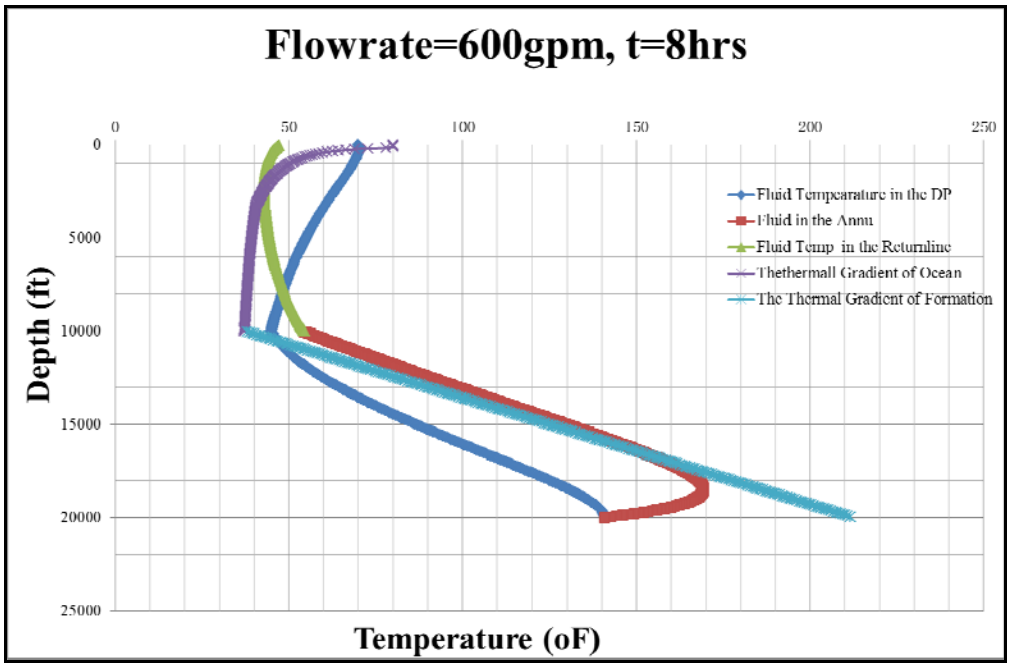

Figure 6-34 Temperature profile for 600gpm at t=8 hrs

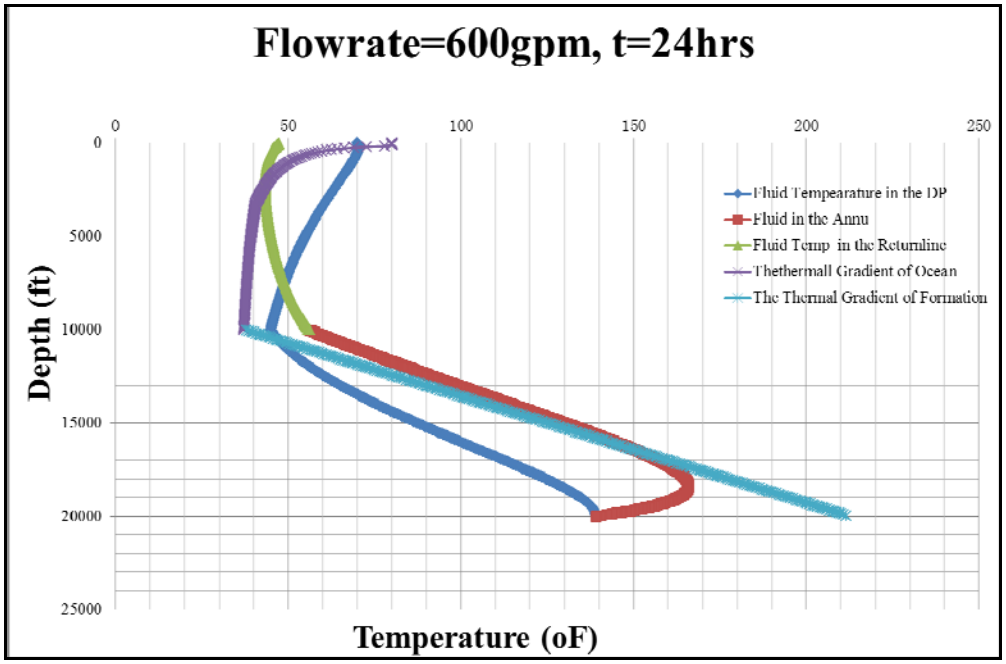

Figure 6-35 Temperature profile for 600gpm at t=24 hrs

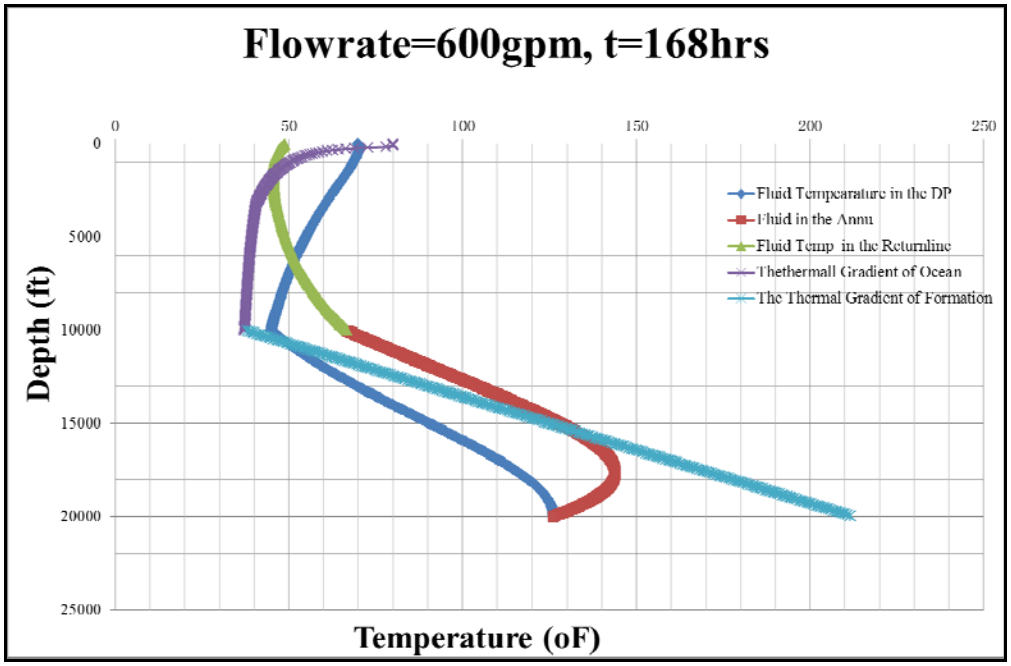

Figure 6-36 Temperature profile for 600gpm at t=168 hrs

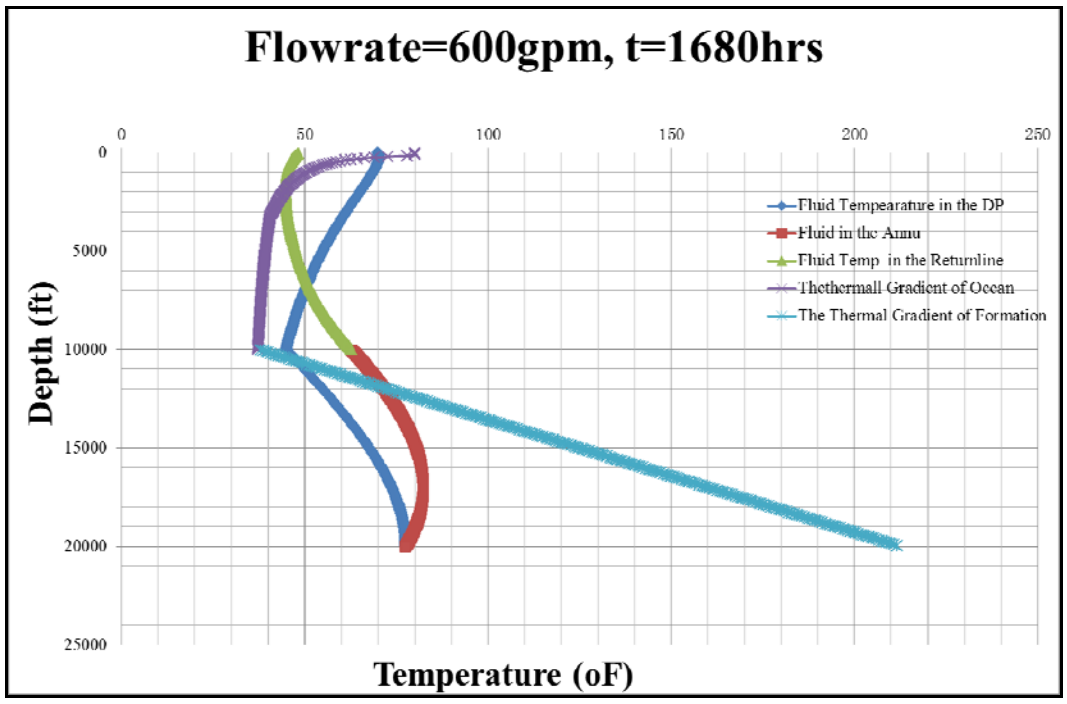

Figure 6-37 Temperature profile for 600gpm at t=1680 hrs

Table 6-10 Some parameters for 1000gpm

Q=1000 gpm	Renold Numbers	Heat Convection Coefficient (Btu/hr-ft2-oF)
In the Drillpipe Below Mudline	13536	327.8
In the Drillpipe Above Mudline	13536	327.8
In the Annulus Below Mudline	6672	225.6
In the Return Line	14744	361.5

Table 6-10 shows the hydraulic parameters at the 1000 gpm flowrate. Figure 6-38 though Figure 6-43 indicate the temperature profiles at 2 hours, 4 hours, 8 hours, 24 hours, 168 hours and 1680 hours respectively.

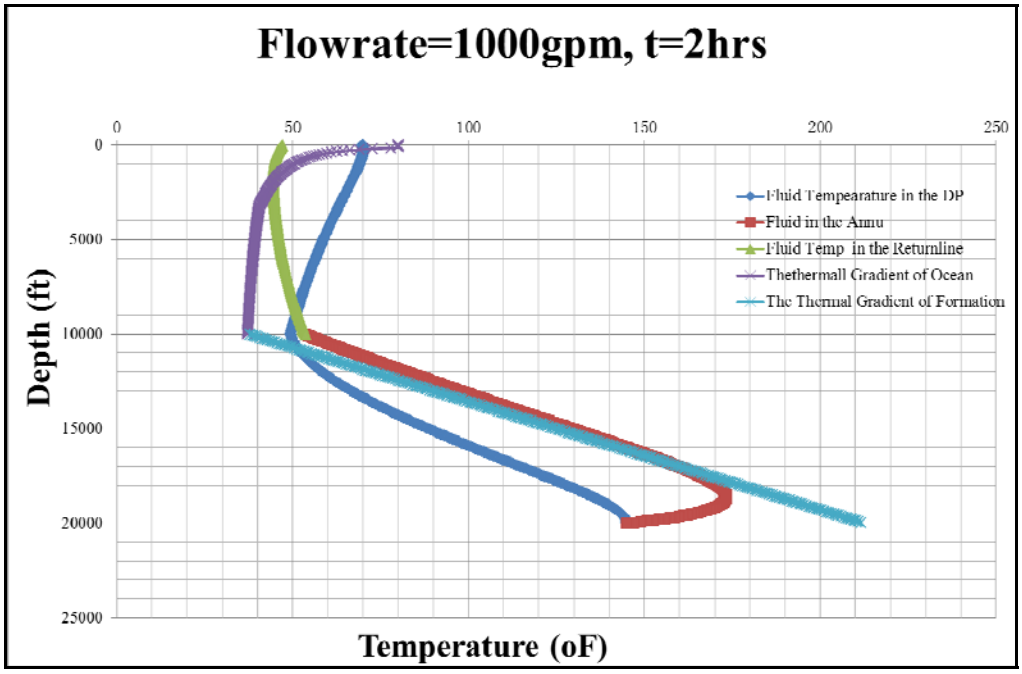

Figure 6-38 Temperature profile for 1000gpm at t=2 hrs

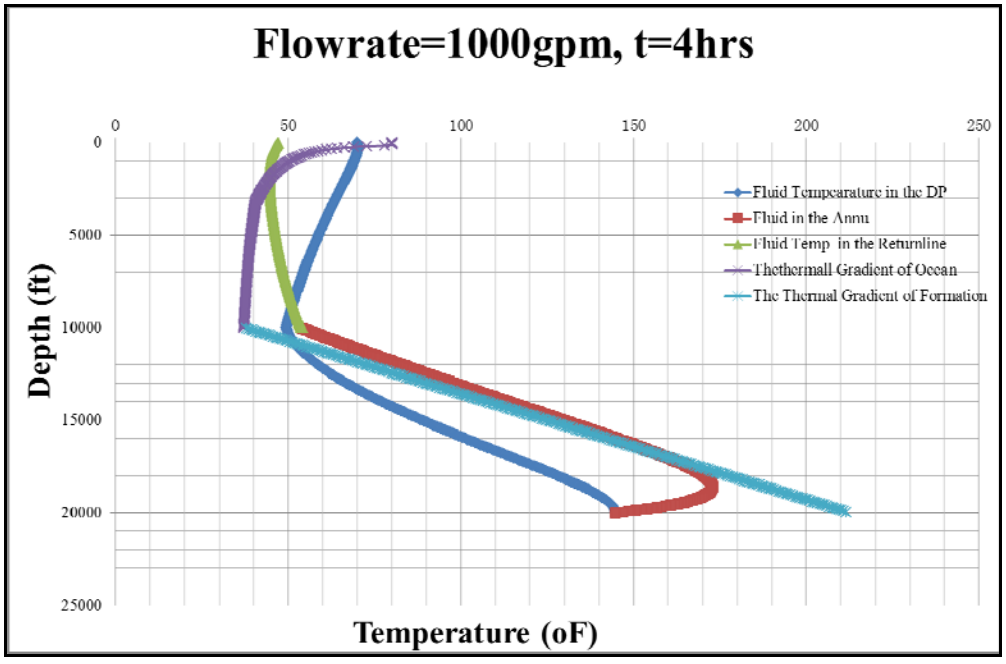

Figure 6-39 Temperature profile for 1000gpm at t=4 hrs

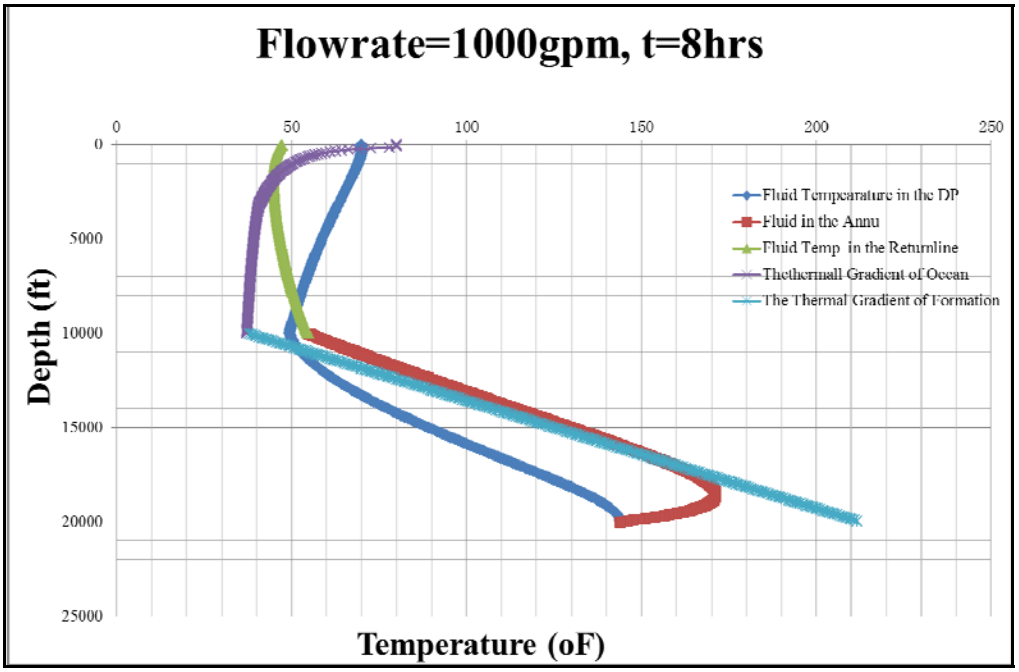

Figure 6-40 Temperature profile for 1000gpm at t=8 hrs

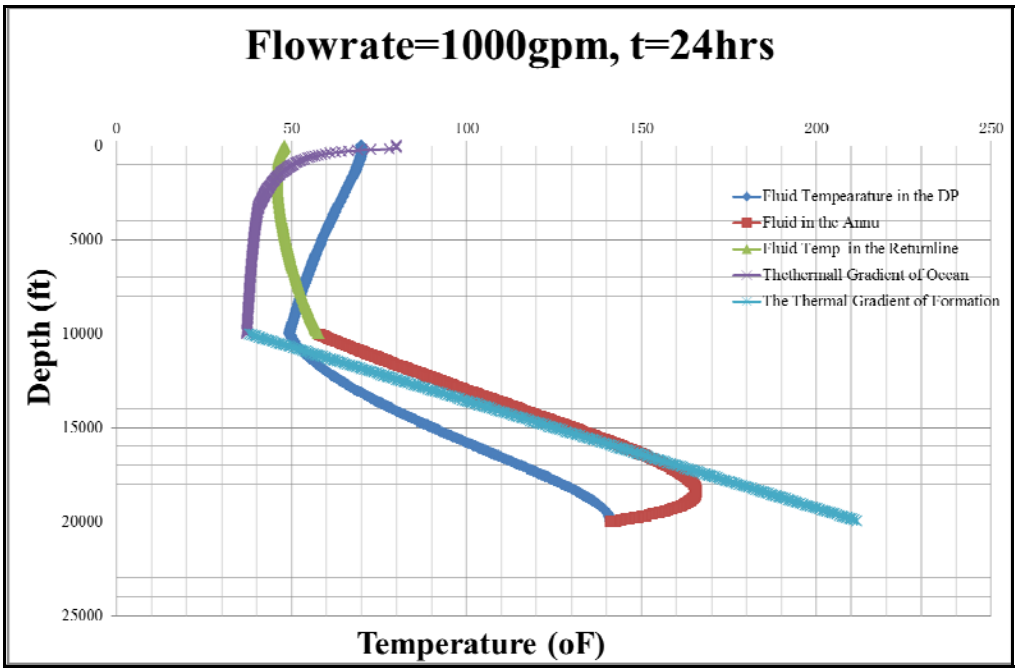

Figure 6-41 Temperature profile for 1000gpm at t=24 hrs

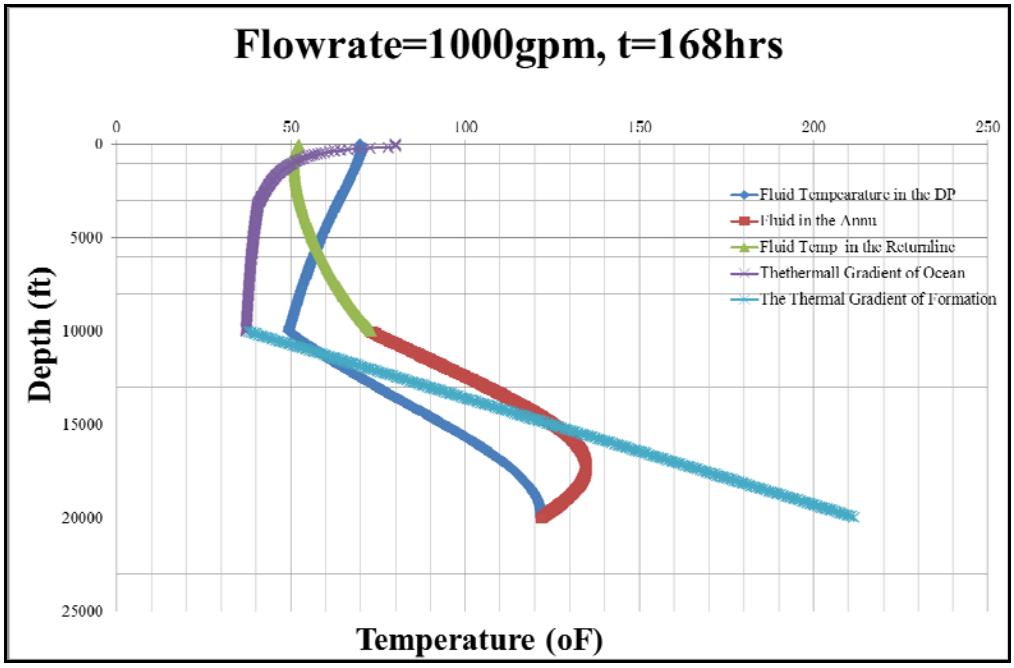

Figure 6-42 Temperature profile for 1000gpm at t=168 hrs

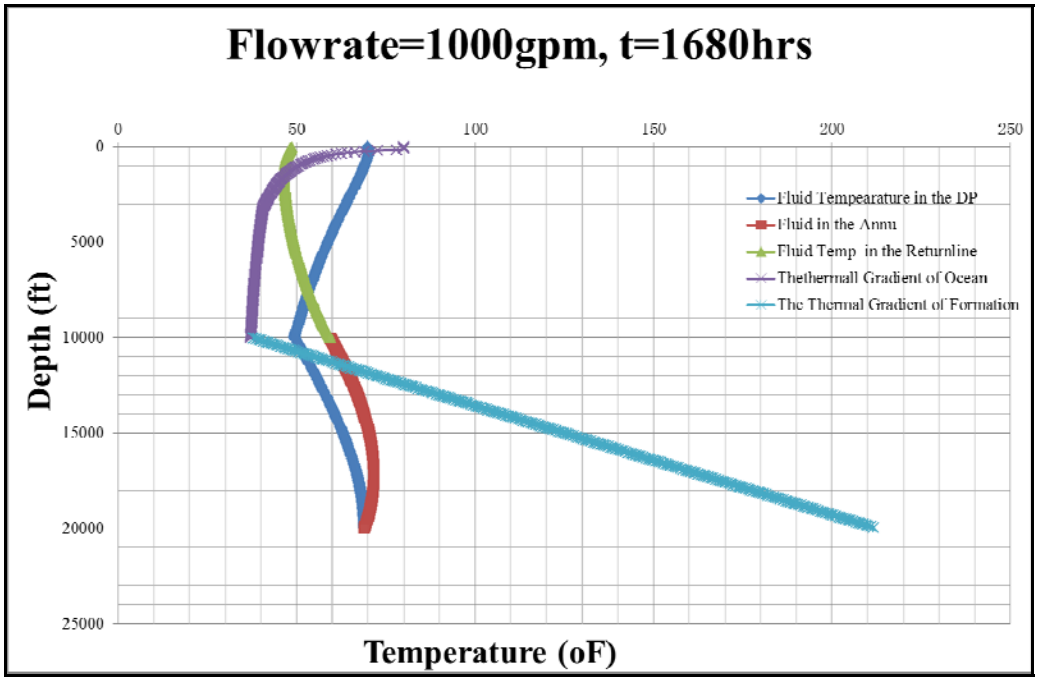

Figure 6-43Temperature profile for 1000gpm at t=1680 hrs

Table 6-11 Some parameters for 1200gpm

Q=1200 gpm	Renold Numbers	Heat Convection Coefficient (Btu/hr-ft2-oF)
In the Drillpipe Below Mudline	17226	389.8
In the Drillpipe Above Mudline	17226	389.8
In the Annulus Below Mudline	8836	282.2
In the Return Line	18764	429.9

Table 6-11 shows the hydraulic parameters at the 1200 gpm flowrate. Figure 6-44 though Figure 6-49 indicate the temperature profiles at 1 hour, 4 hours, 8 hours, 24 hours, 168 hours and 1680 hours respectively.

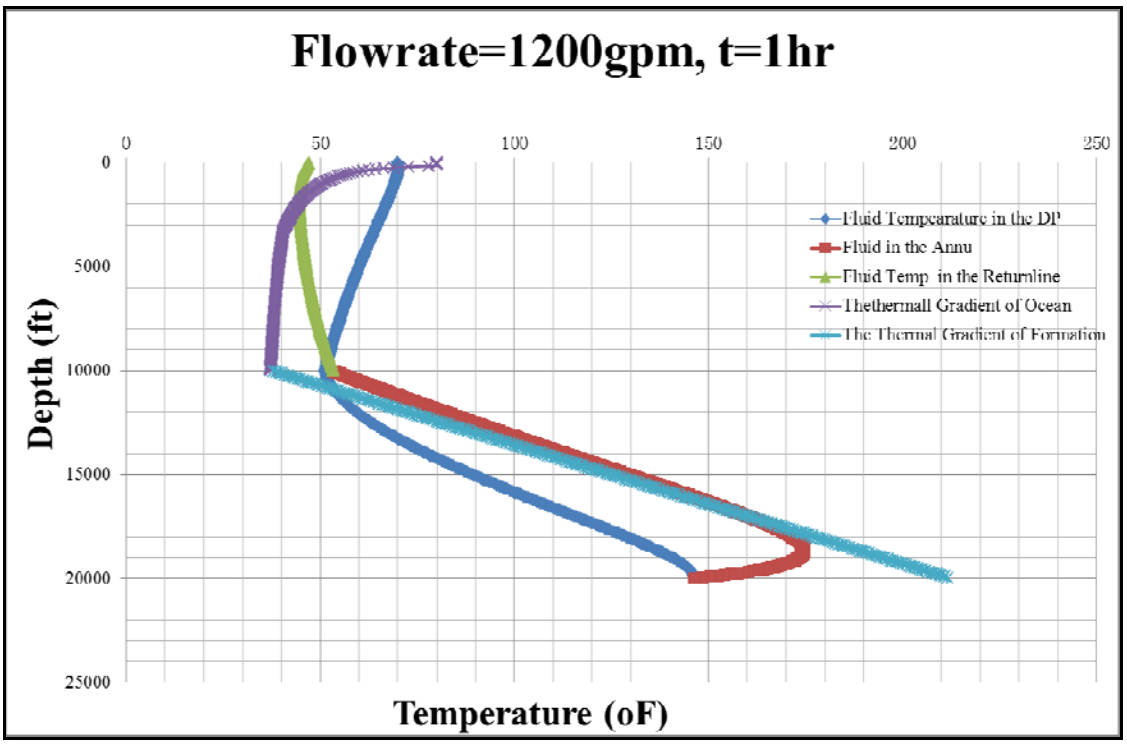

Figure 6-44 Temperature profile for 1200gpm at t=1 hr

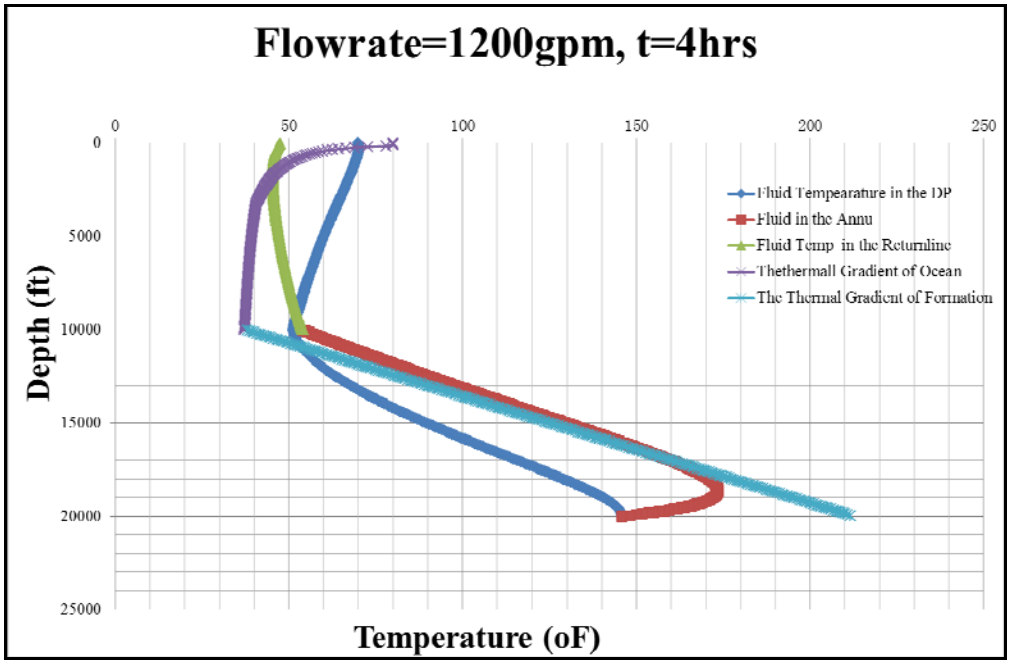

Figure 6-45 Temperature profile for 1200gpm at t=4 hrs

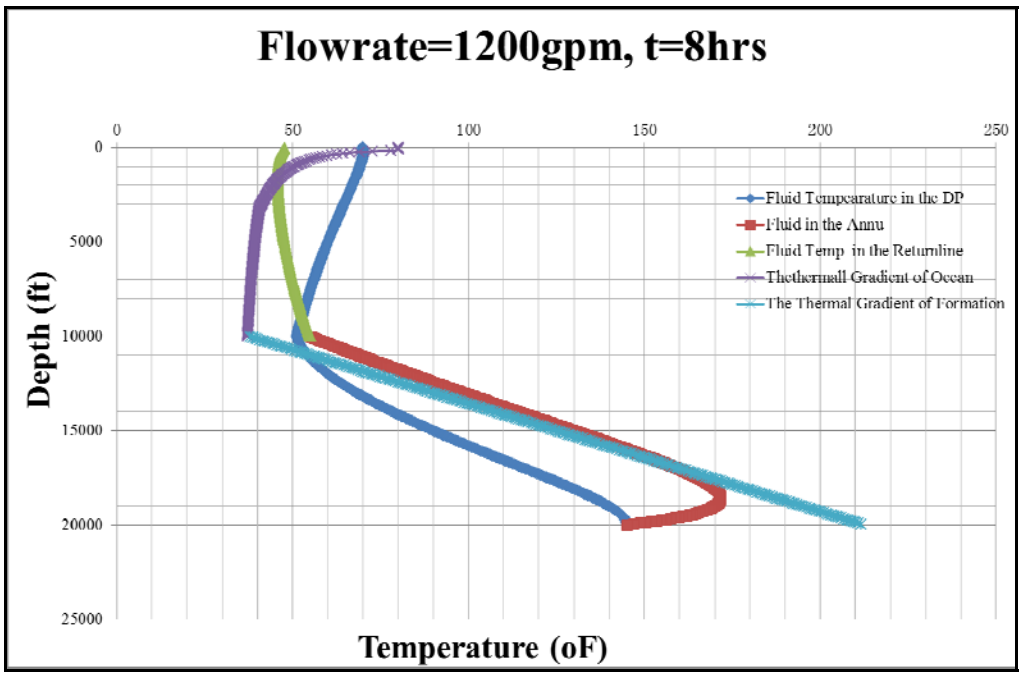

Figure 6-46 Temperature profile for 1200gpm at t=8 hrs

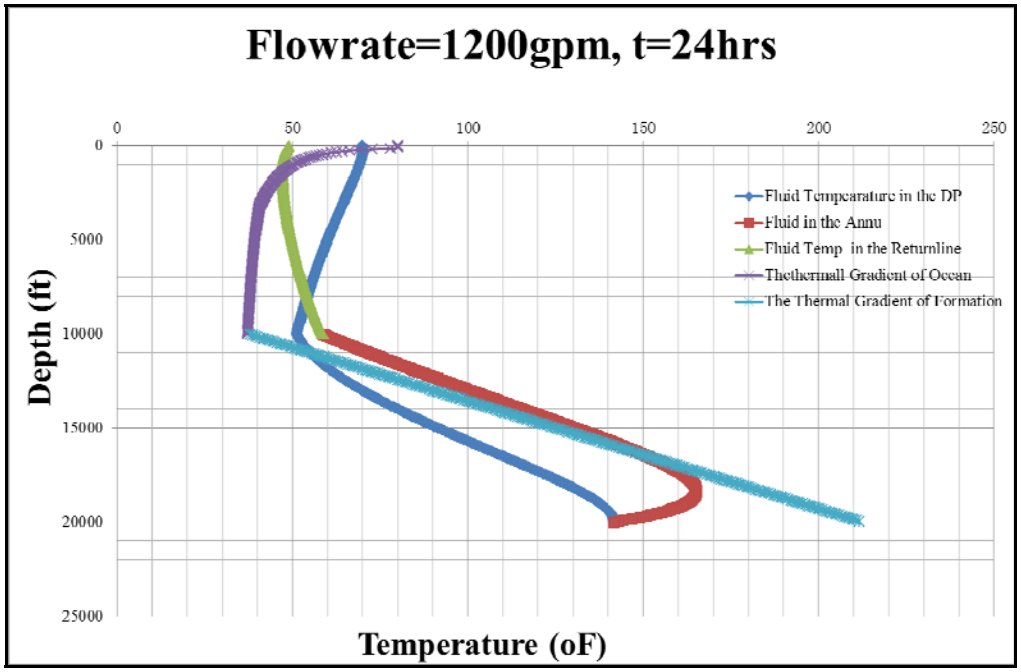

Figure 6-47 Temperature profile for 1200gpm at t=24 hrs

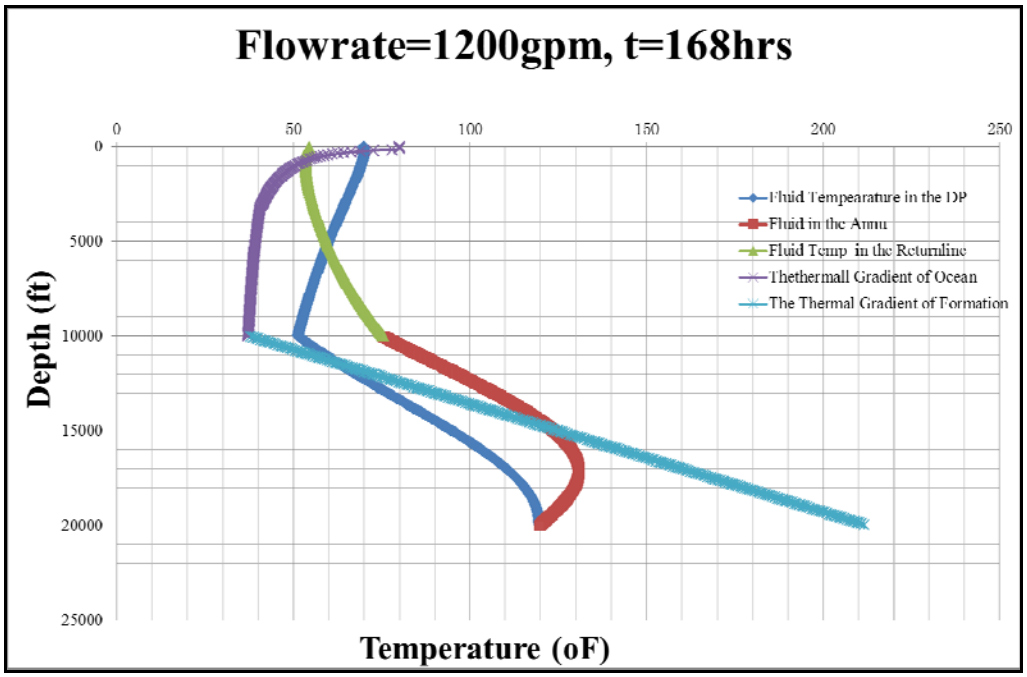

Figure 6-48 Temperature profile for 1200gpm at t=168 hrs

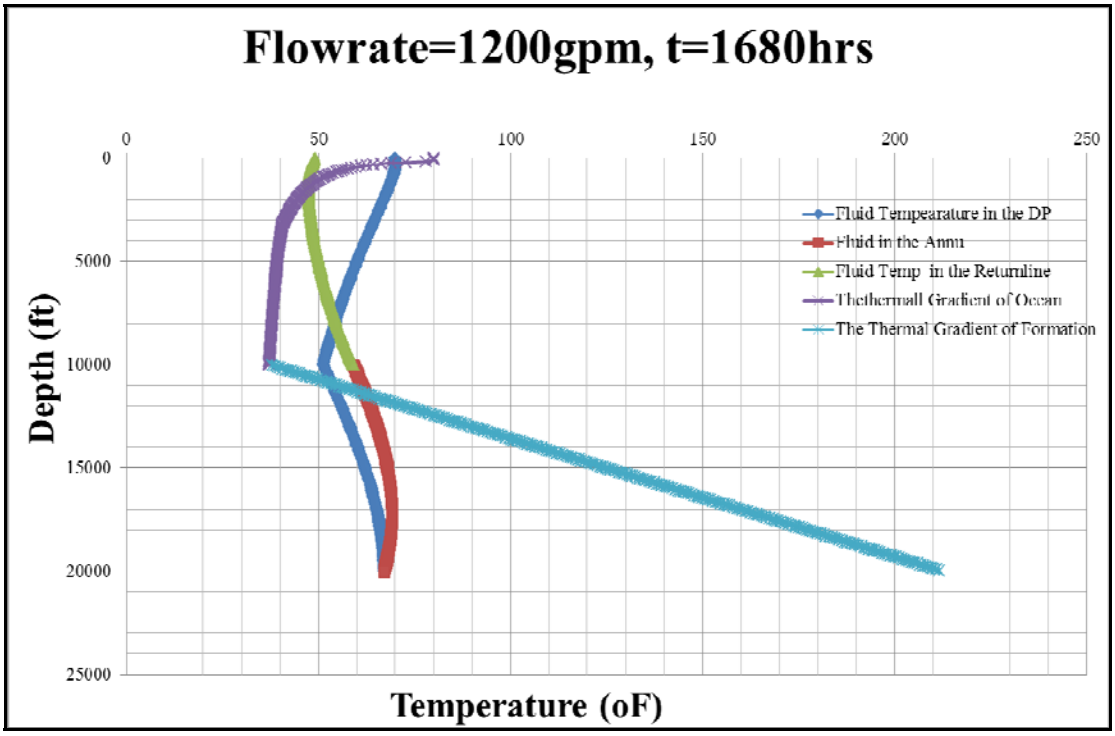

Figure 6-49 Temperature profile for 1200gpm at t=1680 hrs

Table 6-12 Some parameters for 1600gpm

Q=1600 gpm	Renold Numbers	Heat Convection Coefficient (Btu/hr-ft2-oF)
In the Drillpipe Below Mudline	25200	512.4
In the Drillpipe Above Mudline	25200	512.4
In the Annulus Below Mudline	13764	401.65
In the Return Line	27550	565.1

Table 6-12 shows the hydraulic parameters at the 1600 gpm flowrate. Figure 6-50 though Figure 6-55 indicate the temperature profiles at 1 hour, 4 hours, 8 hours, 24 hours, 168 hours and 1680 hours respectively.

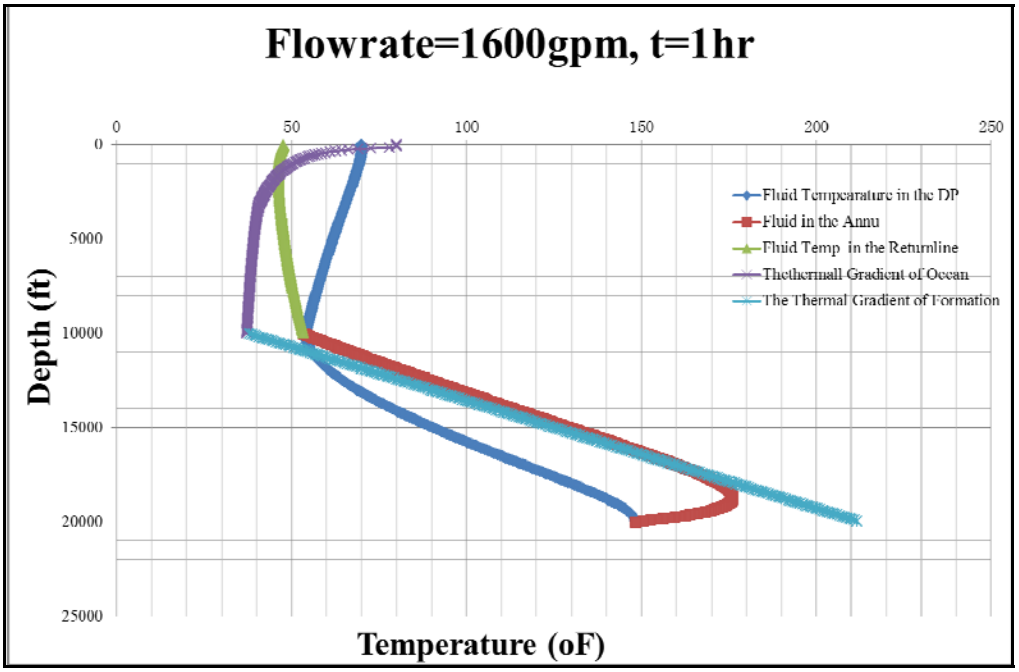

Figure 6-50 Temperature profile for 1600gpm at t=1 hr

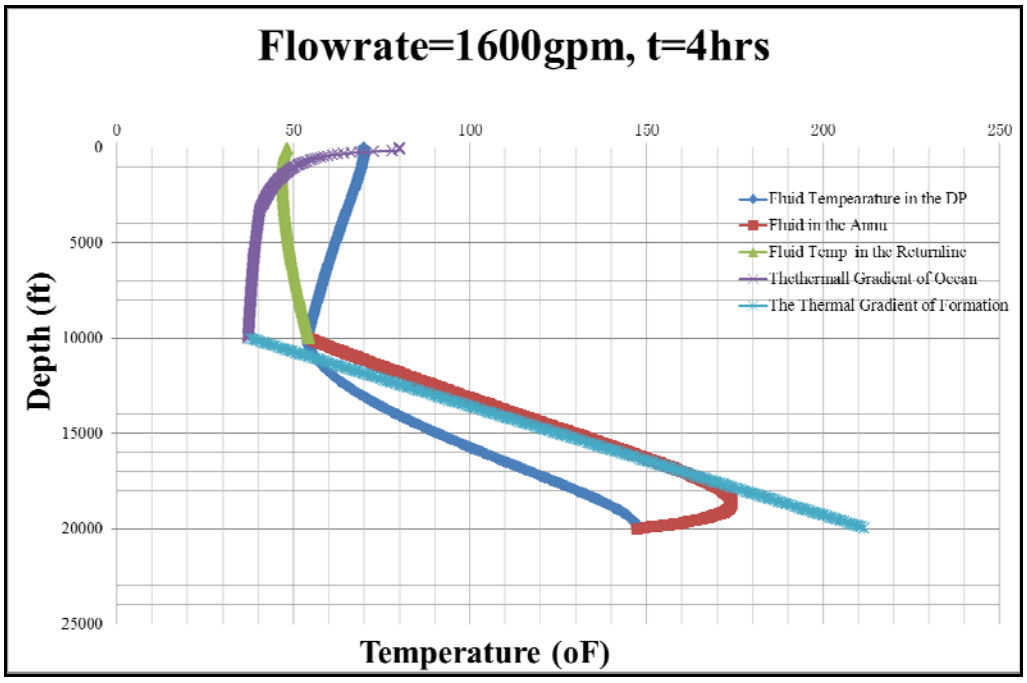

Figure 6-51 Temperature profile for 1600gpm at t=4 hrs

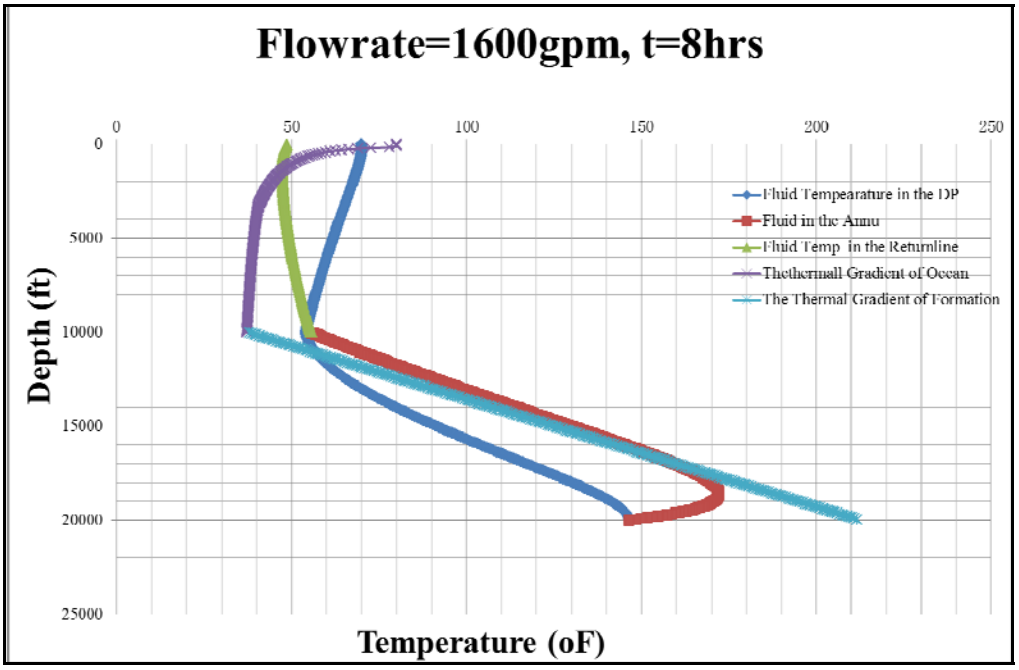

Figure 6-52 Temperature profile for 1600gpm at t=8 hrs

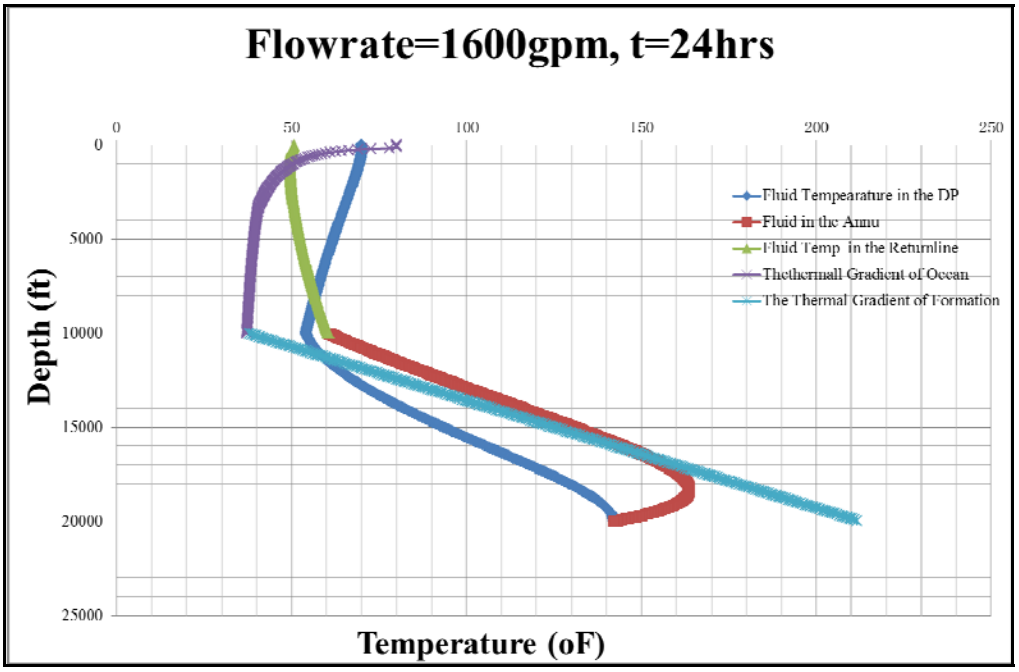

Figure 6-53 Temperature profile for 1600gpm at t=24 hrs

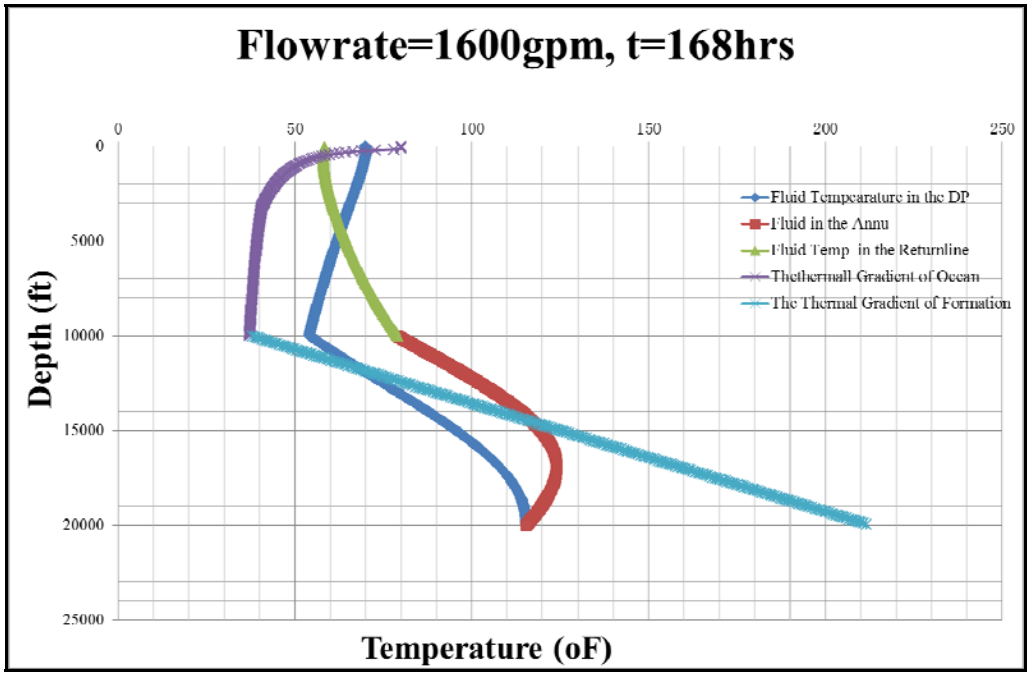

Figure 6-54 Temperature profile for 1600gpm at t=168 hrs

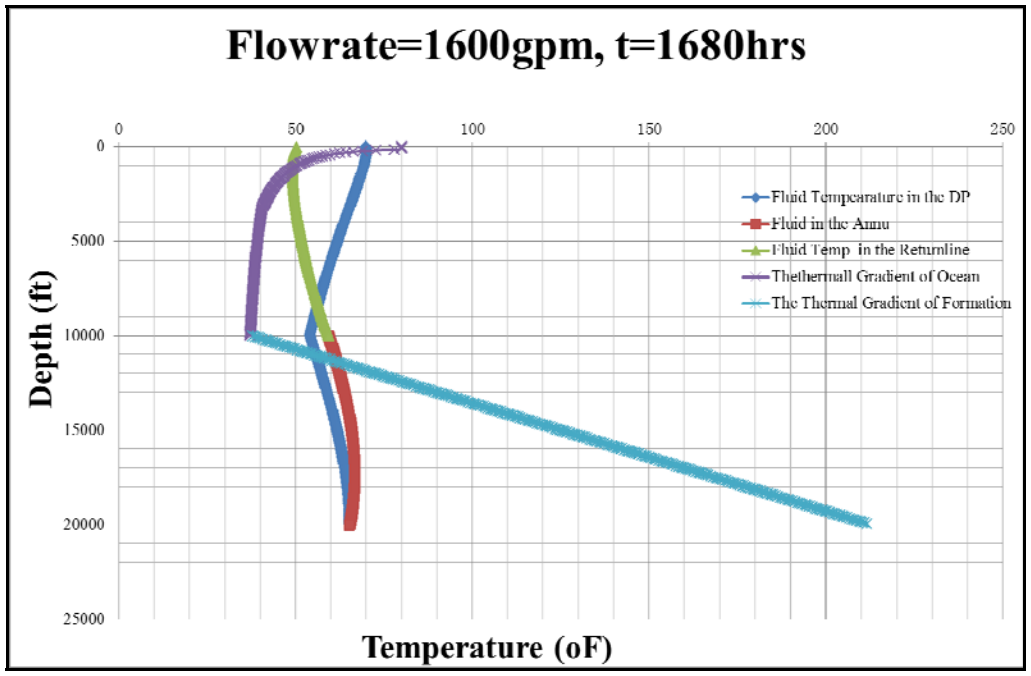

Figure 6-55 Temperature profile for 1600gpm at t=1680 hrs

Table 6-13 Some parameters for 2000gpm

Q=2000 gpm	Renold Numbers	Heat Convection Coefficient (Btu/hr-ft2-oF)
In the Drillpipe Below Mudline	33848	633.45
In the Drillpipe Above Mudline	33848	633.45
In the Annulus Below Mudline	19412	528.15
In the Return Line	36871	698.6

Table 6-13 shows the hydraulic parameters at the 2000 gpm flowrate. Figure 6-56 though Figure 6-61 indicate the temperature profiles at 0.01 hour, 4 hours, 8 hours, 24 hours, 168 hours and 1680 hours respectively.

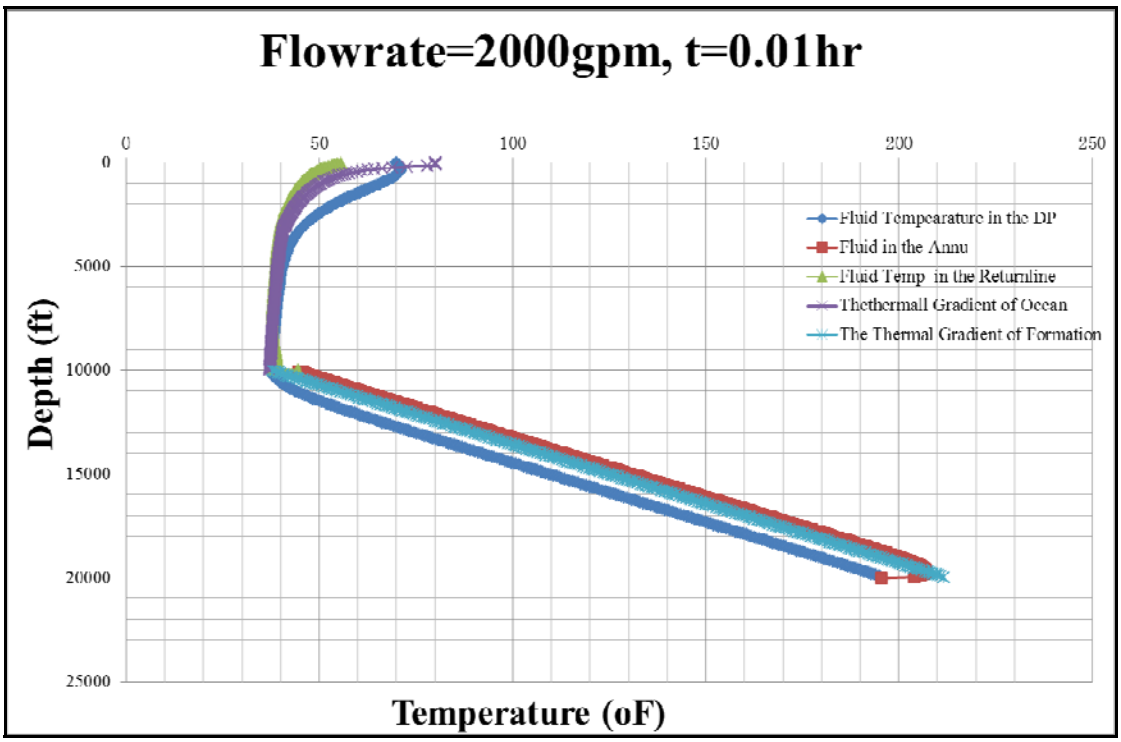

Figure 6-56 Temperature profile for 2000gpm at t=0.01 hr

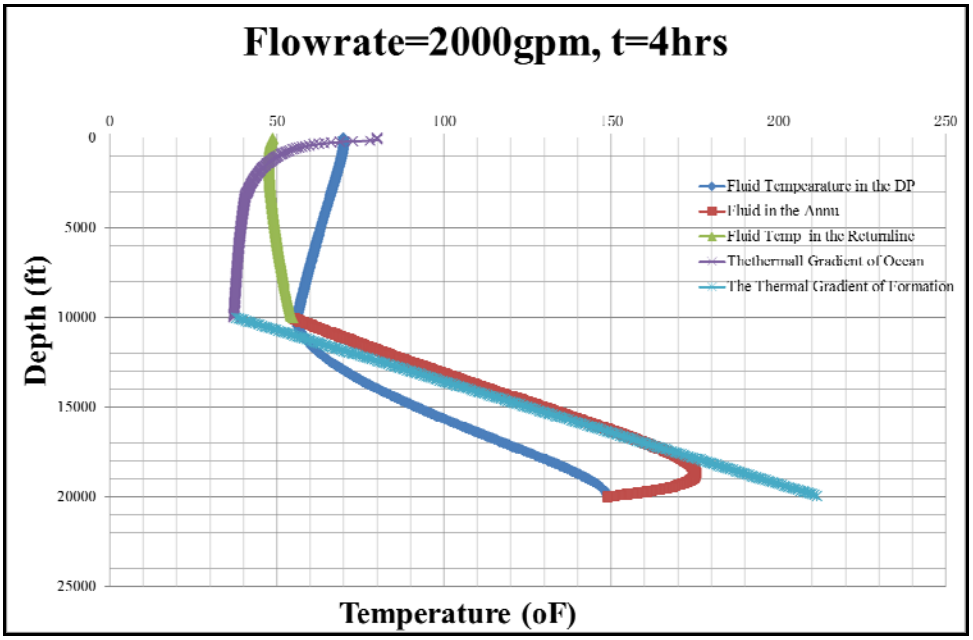

Figure 6-57 Temperature profile for 2000gpm at t=4 hrs

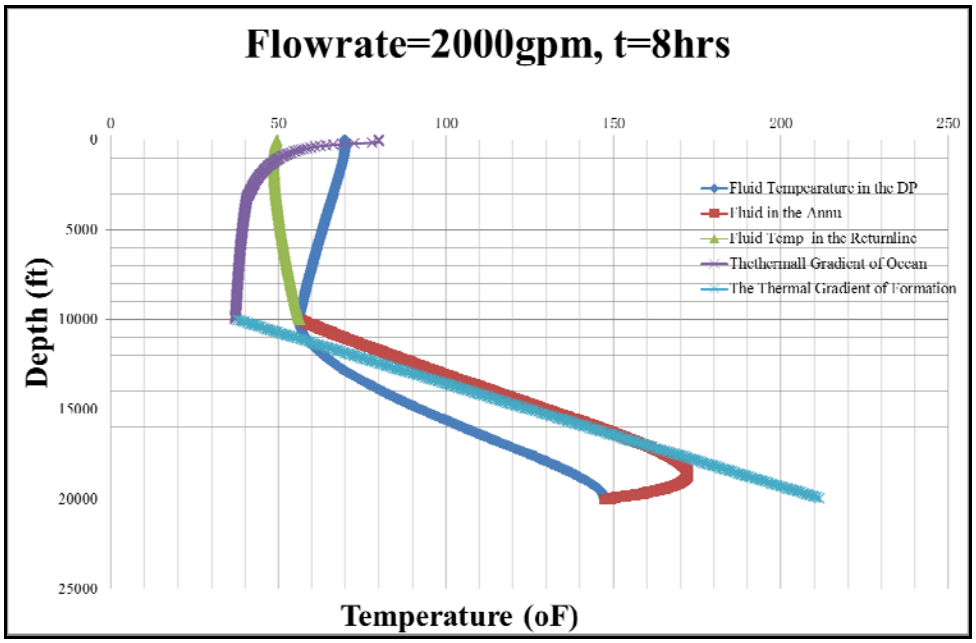

Figure 6-58 Temperature profile for 2000gpm at t=8 hrs

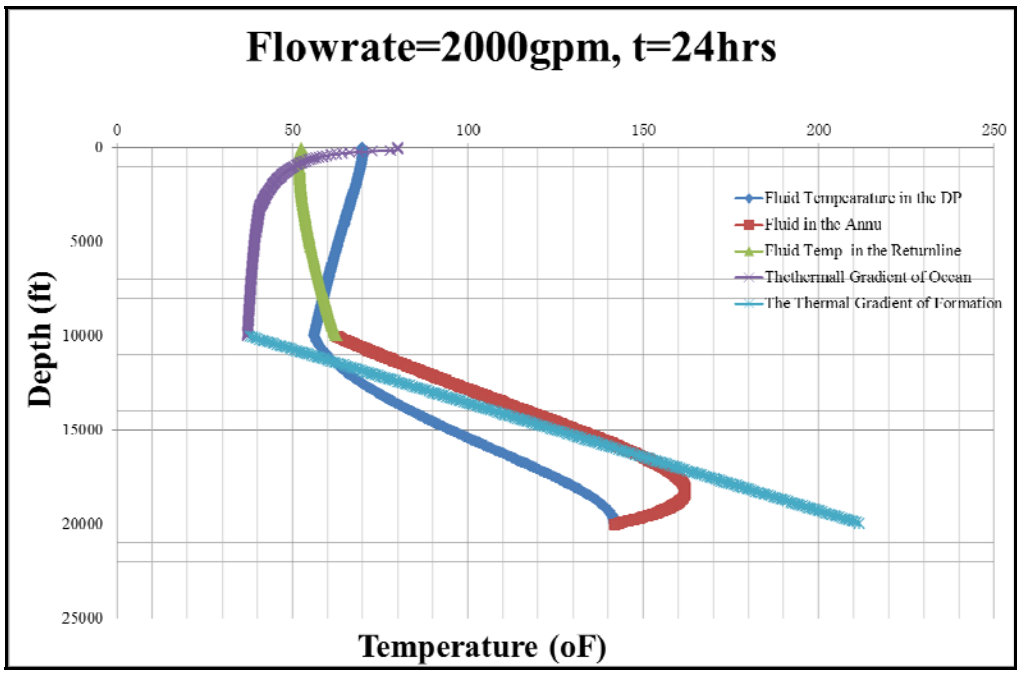

Figure 6-59 Temperature profile for 2000gpm at t=24 hrs

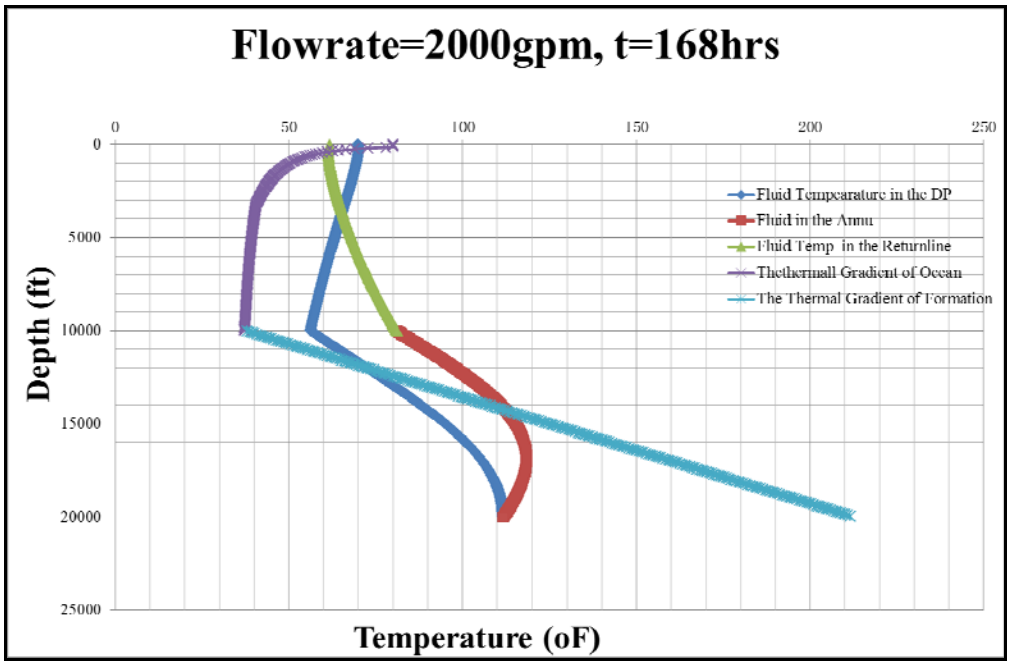

Figure 6-60 Temperature profile for 2000gpm at t=168 hrs

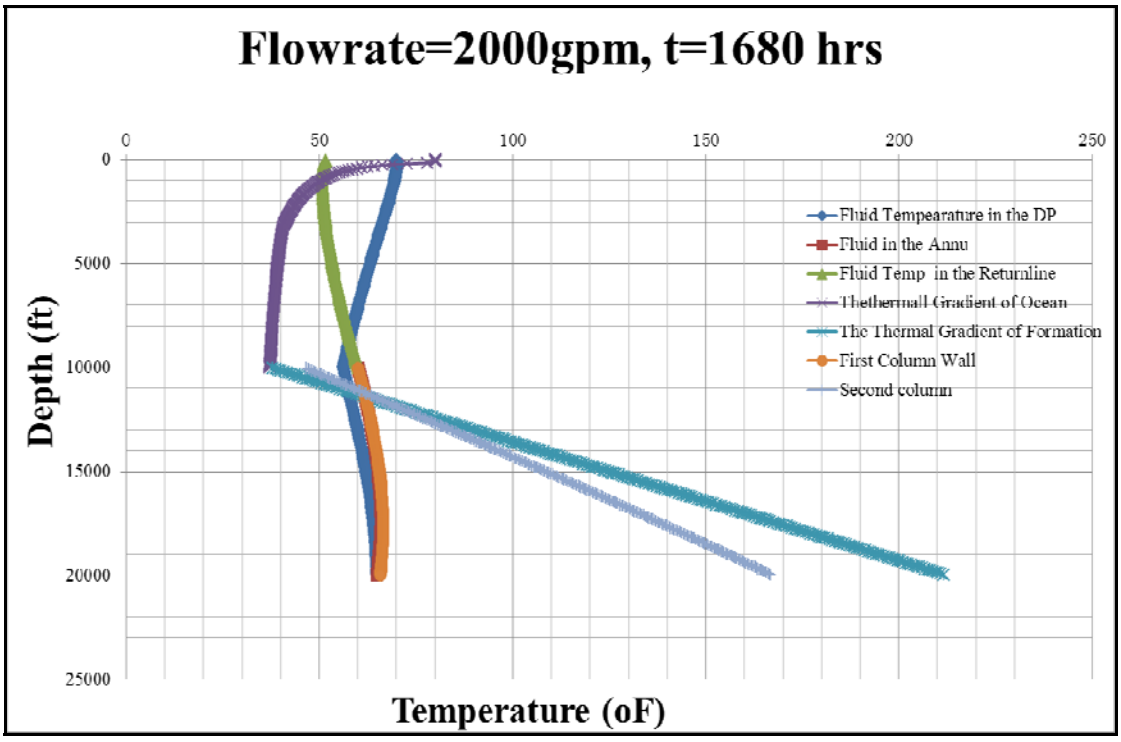

Figure 6-61 Temperature profile for 2000gpm at t=1680 hrs

CHAPTER VII

CONCLUSIONS AND RECOMMENDATIONS

7.1 Conclusions

Upon the study we finished, following conclusions were made:

I. At specific wellbore geometry, the flow rate is the most important factor to affect the temperature distribution in the system.
II. Steady-state heat transfer can not indicate the dynamic temperature change versus time.
III. The boundary conditions in steady-state heat transfer are oversimplified.
IV. The drilling fluid in transient heat transfer of wellbore actually is cooling down the formation if there is not heat influx into the boundary.
V. At low circulating flow rate, the temperature profile in transient heat transfer of riserless drilling matches that in steady-state heat transfer of riserless drilling.

7.2 Recommendations

Further study should focus on:

I. Calibrate the circulating mud density with temperature to figure out how the temperature affects the circulating pressure in the well system.
II. Considering the case that there is fluid influx into the well.
III. Considering the effects of penetration rate on the temperature profile.

IV. Integrating the transient heat transfer modeling for conventional riser drilling and the dual gradient drilling with riser.

NOMENCLATURE

Symbol	Description
A	area
Ax	cross-sectional area of heat flow
ce	earth heat capacity
cflt	heat capacity of tubing fluid
cp	centipoise
Cp	heat capacity
^{o}C	Celsius temperature
d	difference
D	total vertical well depth
f	friction factor
ft	foot or feet
F	force
^{o}F	degree Fahrenheit
g_G	geothermal gradient
h	flow enthalpy or convection heat transfer coefficient
in	inch
k	conduction heat transfer coefficient
*k*e	conductivity of earth
*k*p	Primary wellbore parameter
*k*a	Annulus wellbore parameter
$\bar{k}$	Product of ka , kp

^{o}K	Kelvin temperature
L	Total well depth
$\dot{m}$	Mass flow rate of circulation
m	meter or number of nodes
Nu	Nussult Number
n	number of nodes
p	pressure
Pr	Prandtl number
q	heat transfer rate per depth
qa	convective heat flow in annulus
qF	heat flow from formation to annulus fluid
qta	heat flow from annulus to tubing fluid
r	distance from center of circle, tube, or pipe
rc, rw	wellbore radius
Re	Renold Number
s	second
sec	second
t	time
*t*D	dimensionless circulation time
T	temperature
Ta	temperature of annular fluid
Tei	initial earth temperature
Tes	surface earth temperature
TD	dimensionless temperature
Tt	temperature of tubing

Twb	temperature at wellbore/formation interface
$\tilde{T}$	Geothermal temperature at slope discontinuity
u	velocity
U	overall heat transfer coefficient
Upa	overall heat transfer coefficient between primary and annulus fluids
Ua5	overall heat transfer coefficient between annulus fluid and outermost casing
Ueff	Effective heat transfer coefficient due to soil
V	volume
^{w}	mass flow rate of fluid
Ztmax	depth at which maximum temperature occurs
Z	Axial coordinate
Z*	Normalized well depth, z/L
$\hat{z}$	Depth of bilinear slope discontinuity
Z_0	Normalized depth of slope discontinuity, $\hat{z}$ /L

Greek

Symbol	Description
α	Heat transfer parameter
α_∞	Soil thermal diffusivity
ε	Emissivity
θ	Normalized temperature, T/Tln
$\Delta\theta_o$	Normalized outlet temperature
$\Delta\theta_{bh}$	Normalized bottom-hole temperature
θ_∞	Geothermal temperature distribution
K	Biot number

λ	Fourier number
μ	Viscosity
υ	kinetic viscosity
π	a mathematical constant whose value is the ratio of any circle's circumference to its diameter
ρ	density
ρ_e	earth density
ρ_f	fluid density or formation density
τ	shear stress
Δ	indicates difference

Subscripts

Symbol	Description
a	Annulus
bf	Formation at bottom-hole depth
bf	Bottom-hole
g	Geothermal slope
ins	Insulation
in	Inlet
λ	outlet
p	Primary
p	drillpipe or dillstring
s	Formation at surface
1	Near-surface gradient
2	Secondary gradient

REFERENCES

Aadnøy, B.S. 1999. Optimization of mud temperature and fluid models in offshore applications. Offshore Europe Oil and Gas Exhibition and Conference. Aberdeen, United Kingdom, 7 September.

API Recommended Practice 13D. 1995. Recommended Practice on the Rheology and Hydraulics of Oil-Well Drilling Fluids. Dallas, TX, American Petroleum Institute.

Ascencio-Cendejas, F., Reyes, O., and Nass, M.A. 2006. Thermal Design of Wells Producing Highly Viscous Oils in Offshore Fields in the Gulf of Mexico. First International Oil Conference and Exhibition in Mexico. Cancun, Mexico, 31 August.

Banks, D. 2008. An Introduction to Thermalgeology: Ground Source Heating and Cooling, London, Blackwell.

Bartlett, L.E. 1967. Effect of Temperature on the Flow Properties of Drilling Fluids. Annual Fall Meeting of the *Society of Petroleum Engineers of* AIME. Houston, TX, 1-4 October.

Bland, R.G., Mullen, G.A., Gonzalez, Y.N., Harvey, F.E., and Pless, M. 2006. HPHT Drilling Fluid Challenges. IADC/SPE Asia Pacific Drilling Technology Conference and Exhibition. Bangkok, Thailand, 11 November.

Brown, T.S., Clapham, J., Clapham, J., Danielson, T.J., Harris, R.G., and Erickson, D.D. 1996. Application of a Transient Heat Transfer Model for Bundled, Multiphase Pipelines. SPE Annual Technical Conference and Exhibition. Denver, Colorado, 6 Oct.

Calvert, D.G., and Griffin, T.J. 1998. Determination of Temperatures for Cementing in Wells Drilled in Deep Water. IADC/SPE Drilling Conference. Dallas, Texas, 3 March.

Carlson, T., and Hemphill, T. 1994. Meeting the Challenges of Deepwater Gulf of Mexico Drilling With Non-Petroleum Ester-Based Drilling Fluids. International Petroleum Conference and Exhibition of Mexico. Veracruz, Mexico, 10 October.

Carney, L.L., and Meyer, R.L. 1976. A New Approach to High Temperature Drilling Fields. SPE Annual Fall Technical Conference and Exhibition. New Orleans, Louisiana, 3 October.

Cesaroni, R., and Repetti, U. 1993. Solved Problems of High-Density and High-Temperature Drilling Fluid in an Environmentally Sensitive Area. SPE/IADC Drilling Conference. Amsterdam, Netherlands, 2 Feburary.

Chakrabarti, S.K. 2005. Handbook of Offshore Engineering. Vol I. Offshore Structure Analysis. Amsterdam, ELSEVIER.

Chen, Z., and Novotny, R.J. 2003. Accurate Prediction Wellbore Transient Temperature Profile Under Multiple Temperature Gradients: Finite Difference Approach and Case History. SPE Annual Technical Conference and Exhibition. Denver, Colorado, 5 October.

Chin, Y.D., Perera, R., Prescott, C.N., and Cain, R.E. 2000. Thermal Performance of an Insulated Multiple Flowline Bundle Using Active Heating. SPE International Petroleum Conference and Exhibition in Mexico. Villahermosa, Mexico, 1 Feburary.

Cline, D.D. 1981. A Thermal Analysis of Pseudo-steady Circulating Wellbores, Sandia National Laboratories Report SAND 81-0241, Sandia National Laboratories, Albuquerque, New Mexico.

Davison, M., Clary, S., Saasen, A., Allouche, M., Bodin, D., and Nhuyen, V-A 1999. Rheology ofVarious Drilling Fluid Systems Under Deepwater Drilling Conditions and the Importance of Accurate Predictions of Downhole Fluid Hydraulics. SPE Annual Technical Conference and Exhibition. Houston, TX, 3-6 October.

Demirdal, B., Miska, S.Z., Takach, N.E., and Cunha, J.C.S. 2007. Drilling Fluids Rheological and Volumetric Characterization Under Downhole Conditions. Latin American & Caribbean Petroleum Engineering Conference. Buenos Aires, Argentina, 15 April.

Dirker, J., and Meyer, J.P. 2002. Heat Transfer Coefficients in Concentric Annuli. *Journal of Heat Transfer* **124**(6): 1200-1203.

Duret, E., Lebreton, E., Heintze, E., Henriot, V., and Saint-Marcoux, J.F. 2000. Pipeline Bundles Model Implemented Into a Multiphase Flow Model. SPE Annual Technical Conference and Exhibition. Dallas, Texas, 1 October.

Durrant, A.J., and Thambynayagam, R.K.M. 1986. Wellbore Heat Transmission and Pressure Drop for Steam/Water Injection and Geothermal Production: A Simple Solution Technique. *SPE Reservoir Engineering* **1**(2): 148-162.

Edwardson, M.J., Girner, H.M., Parkison, H.R., Williams, C.D., Matthews, C.S. 1962. Calculation of Formation Temperature Disturbances Caused by Mud Circulation. *SPE Journal of Petroleum Technology* **14**(4): 416-426.

Finger, J.T., Jacobson, R.D., and Champness, A.T. 2002. Development and Testing of Insulated Drillpipe. *SPE Drilling & Completion* **17**(2): 132-136.

Fleyfel, F., Hernandez, O.Sturgis, R., and Meng, W. 2004. Evaluation of Pipeline Configurations with Active Heating for Export of Waxy Crude Oil. SPE Annual Technical Conference and Exhibition. Houston, Texas, 26 September.

Galate, J.W., and Mitchell, R.F. 1986. Behavior of Oil Muds During Drilling Operations. *SPE Drilling Engineering* **1**(2): 97-106.

Glassley, W.E., 2010. Geothermal Energy: Renewable Energy and the Environment. Renewable Energy and the Env. London, CRC Press.

Hasan, A.R., and Kabir, C.S. 1996. A Mechanistic Model for Computing Fluid Temperature Profiles in Gas-Lift Wells. *SPE Production & Operations* **11**(3): 179-185.

Hoberock, L.L., and Stanbery, S.R. 1981. Pressure Dynamics in Wells During Gas Kicks: Part 1 - Component Models and Results. *SPE Journal of Petroleum Technology* **33**(8): 1357-1366.

Holmes, C.S., and Swift, S.C. 1970. Calculation of Circulating Mud Temperatures. *SPE Journal of Petroleum Technology* **22**(6): 670-674.

Isambourg, P., Anfinsen, B.T., and Marken, C. 1996. Volumetric Behavior of Drilling Muds at High Pressure and High Temperature. European Petroleum Conference. Milan, Italy, 22 October.

Izgec, B., Hasan, A.R, Lin, D., and Kabir, C.S. 2010. Flow-Rate Estimation From Wellhead-Pressure and -Temperature Data. *SPE Production & Operations* **25**(1): 31-39.

Kaarstad, E., Aadnoy, B.S., and Fjelde, T. 2009. A Study of Temperature Dependent Friction in Wellbore Fluids. SPE/IADC Drilling Conference and Exhibition. Amsterdam, The Netherlands, 17 March.

Kabir, C.S., Hasan, A.R., Kouba, G.E., and Ameen, M. 1996. Determining Circulating Fluid Temperature in Drilling, Workover, and Well Control Operations. *SPE Drilling & Completion* **11**(2): 74-79.

Karstad, E., and Aadnoy, B.S. 1998. Density Behavior of Drilling Fluids During High Pressure High Temperature Drilling Operations. IADC/SPE Asia Pacific Drilling Technology. Jakarta, Indonesia, 7 September.

Kashikar, S.V., and Arnold, F.C. 1991. Determination of Formation Temperature From Flow Tests: A New Solution. SPE Production Operations Symposium. Oklahoma City, Oklahoma,7 April.

Kutasov, I.M. 1999. Applied Geothermics for Petroleum Engineers. Developments in Petroleum Science. Amsterdam, Elsevier Science.

Lima, H.R. 1998. A dynamic model of well hydraulics in deepwater riserless drilling operations using synthetic-based drilling fluids. Petroleum Engineering. College Station, Texas A&M University. Ph.D.

Maglione, R., Gallino, G., Giovanni, R., Raffaele, R., and Rolv, R. 1996. A Drilling Well as Viscometer: Studying the Effects of Well Pressure and Temperature on the Rheology of the Drilling Fluids. European Petroleum Conference. Milan, Italy, 22 October.

Marshall, T.R., and Lie, O.H. 1992. A Thermal Transient Model of Circulating Wells: 1. Model Development. European Petroleum Computer Conference. Stavanger, Norway, 24 May.

McMordie Jr., W.C., Bland, R.G., and Hauser, J.M. 1982. Effect of Temperature and Pressure on the Density of Drilling Fluids. SPE Annual Technical Conference and Exhibition. New Orleans, Louisiana, 26 September.

Mehta, A.P., Zabaras, G.J., Schoppa, W., and Peters, D.J. 2004. Unlocking Deepwater Heavy Oil Reserves: A Flow Assurance Perspective. Offshore Technology Conference. Houston, Texas, 3-6 May.

Mitchell, R.F., and Wedelich III , H.F. 1989. Prediction of Downhole Temperatures Can Be Key for Optimal Wellbore Design. SPE Production Operations Symposium. Oklahoma City, Oklahoma, 13 March.

Moussa, M.M., and Al-Marhoun, M.A. 1985. Dynamic Measurement of Drilling Fluid Rheology at Elevated Temperature and Pressure. Middle East Oil Technical Conference and Exhibition. Bahrain, 11 March.

Osisanya, S.O., and Harris, O.O. 2005. Evaluation of Equivalent Circulating Density of Drilling Fluids Under High Pressure/High Temperature Conditions. SPE Annual Technical Conference and Exhibition. Dallas, Texas, 9 October.

Osman, E.A., and Aggour, M.A. 2003. Determination of Drilling Mud Density Change with Pressure and Temperature Made Simple and Accurate by ANN. Middle East Oil Show. Bahrain, 9 June.

Oster, C.A., and Scheffler, W.A. 1976. Well-Hole Temperature Distribution In The Presence Of Aquifers, Joint Petroleum Mechanical Engineering and Pressure Vessels and Piping Conference, Mexico City, Mexico, 19-24 September.

Ozisik., M.N. 1977. Basic Heat Transfer. New York, McGraw-Hill.

Peters, E.J., Chenevert, M.E., and Zhang, C. 1990. A Model for Predicting the Density of Oil-Base Muds at High Pressures and Temperatures. *SPE Drilling Engineering* **5**(2): 141-148.

Piber, M., Prohaska, M., Hublik, G., and Thonhauser, G. 2006. Time-Dependent Behavior of Drilling Fluids Under Cyclic Temperature and Pressure Loads. SPE Annual Technical Conference and Exhibition. San Antonio, Texas, 24 September.

Pruess, K. 2002. Mathematical ModelingOf Fluid Flow And Heat Transfer In Geothermal Systems: An Introduction In Five Lectures, Lawrence Berkeley National Laboratory Report LBNL-51295, Lawrence Berkeley National Laboratory, Reykjavík, .

Ramey JR., H.J. 1962. Wellbore Heat Transmission. *SPE Journal of Petroleum Technology* **14**(4): 427-435.

Raymond, L.R. 1969. Temperature Distribution in a Circulating Drilling Fluid. *SPE Journal of Petroleum Technology* **21**(3): 333-341.

Sagar, R., Doty, D.R., and Schmidt, Z. 1991. Predicting Temperature Profiles in a Flowing Well. *SPE Production Engineering* **6**(4): 441-448.

Schoeppel, R.J., and Bennett, R.E. 1971. Numerical Simulation of Borehole and Formation Temperature Distributions While Drilling to Total Depth Total Depth. Fall Meeting of the *Society of Petroleum Engineers of* AIME. New Orleans, Louisiana, 3 October.

Sorelle, R.R., Jardiolin, R.A., Buckley, P., and Barrios, J.R. 1982. Mathematical Field Model Predicts Downhole Density Changes In Static Drilling Fluids. SPE Annual Technical Conference and Exhibition. New Orleans, Louisiana, 26 September.

Stiles, D., and Trigg, M.J. 2007. Mathematical Temperature Simulators for Drilling Deepwater HTHP Wells: Comparisons, Applications and Limitations. SPE/IADC Drilling Conference. Amsterdam, The Netherlands, 20 Feburary.

Tahmourpour, F., and Quinton, C.W. 2009. Saving Expensive Offshore Deepwater Rig Time by Modeling Accurate Subsea/Subsea Floor Temperature Modeling for Cementing Operations. SPE Annual Technical Conference and Exhibition. New Orleans, Louisiana, 4 October.

Vargo, R.F., Heathman, J.F., Kelingray, D.S., Ward, M.D., and Lummus, J.M. 2006. Improved Deepwater Cementing Practices Help Reduce Nonproductive Time. IADC/SPE Drilling Conference. Miami, Florida, USA, 21 Feburary.

Wang, H., and Su, Y. 2000. High Temperature & High Pressure (HTHP) Mud P-V-T Behavior and Its Effect on Wellbore Pressure Calculations. IADC/SPE Drilling Conference. New Orleans, Louisiana, 23 Feburary.

Ward, M., Granberry,V., Campos, G., Rausis, M., Sledz, M. et al. 2001. A Joint Industry Project to Assess Circulating Temperatures in Deepwater Wells. SPE Annual Technical Conference and Exhibition. New Orleans, Louisiana, 30 September.

Ward, M., Granberry,V., Campos, G., Rausis, M., Sledz, M. et al. 2003. A Joint Industry Project To Assess Circulating Temperatures in Deepwater Wells. *SPE Drilling & Completion* **18**(2): 133-137.

White, W., Zamora,W., and M. Svoboda, C.F. 1997. Downhole Measurements of Synthetic-Based Drilling Fluid in an Offshore Well Quantify Dynamic Pressure and Temperature Distributions. *SPE Drilling & Completion* **12**(3): 149-157.

Willhite, G.P., and Griston, S. 1987. Wellbore Refluxing in Steam Injection Wells. *SPE Journal of Petroleum Technology* **39**(3): 353-362.

Wooley, G.R. 1980. Computing Downhole Temperatures in Circulation, Injection, and Production Wells. *SPE Journal of Petroleum Technology* **32**(9): 1509-1522.

Zabaras, G.J. 1994. Physical Modelling Of Vertical Multiphase Flow: Prediction Of Pressure Gradients In Oil And Gas Wells. SPE Annual Technical Conference and Exhibition, Houston, Texas, 2-5 May.

Zabaras, G.J., and Zhang, J. 1997. Steady-state and Transient Thermal Performance of Subsea Hardware. Offshore Technology Conference, Houston, Texas, 5-8 May.

Zazovsky, A.F., Haddad, S., and Tertychnyi, V. 2005. Thermal History Reconstruction and Estimation of Formation Temperature Using Wireline Formation Tester Measurements. SPE Europec/EAGE Annual Conference. Madrid, Spain, 13 June.

Zhang, Y., and Duan, Y. 1998. High Temperature and High Pressure Well Drilling Practice in Ying-Qiong Area South China Sea. SPE International Oil and Gas Conference and Exhibition in China. Beijing, China, 2 November.

Zijsling, D.H. 1984. Analysis of Temperature Distribution and Performance of Polycrystalline Diamond Compact Bits Under Field Drilling Conditions. SPE Annual Technical Conference and Exhibition. Houston, Texas, 16 September.

Zilch, H.E., M.J., and Pye, D.S. 1991. The Evolution of Geothermal Drilling Fluid in the Imperial Valley. SPE Western Regional Meeting. Long Beach, California, 20 March.

APPENDIX A

This appendix is presented to derive the transient heat transfer model for the riserless drilling.

Thermal Analysis for Drilling System below the mudline based on the conservation of energy.

$$Q_{in} - Q_{out} = \Delta Q \qquad \text{Eq(A-1)}$$

The partial differential equations describing the energy balances within the system are derived. The heat source accumulated could be caused by hydraulic friction, bit rotation etc.

Fluid In The Drillpipe

$$Q_{in} = \left(\rho q C_p T_p \mid_z\right)\Delta t \qquad \text{Eq(A-2)}$$

$$Q_{out} = \left[\left(\rho q C_p T_p \mid_{z+\Delta z}^{t+\Delta t}\right) + hA\left(T_p \mid_z^t - T_w \mid_z^t\right)\right]\Delta t \qquad \text{Eq(A-3)}$$

$$\Delta Q = \left[\left(\pi r_p^2 \rho C_p T_p \mid_z^{t+\Delta t}\right) - \left(\pi r_p^2 \rho C_p T_p \mid_z^t\right)\right]\Delta z + Q_p \Delta t \Delta z \qquad \text{Eq(A-4)}$$

$$\left(\rho q C_p T_p \mid_z^t\right)\Delta t - \left[\left(\rho q C_p T_p \mid_{z+\Delta z}^{t+\Delta t}\right) + hA\left(T_p \mid_z^t - T_w \mid_z^t\right)\right]\Delta t = \left[\left(\pi r_p^2 \rho C_p T_p \mid_z^{t+\Delta t}\right) - \left(\pi r_p^2 \rho C_p T_p \mid_z^t\right)\right]\Delta z + Q_p \Delta t \Delta z$$

Eq(A-5)

$$\frac{\left(\rho q C_p T_p \mid_z^t\right) - \left[\left(\rho q C_p T_p \mid_{z+\Delta z}^{t+\Delta t}\right) + hA\left(T_p \mid_z^t - T_w \mid_z^t\right)\right]}{\Delta z} = \frac{\left[\left(\pi r_p^2 \rho C_p T_p \mid_z^{t+\Delta t}\right) - \left(\pi r_p^2 \rho C_p T_p \mid_z^t\right)\right]}{\Delta t} + Q_p$$

Eq(A-6)

Then we have the governing equation for the control volume in the drillpipe

$$\rho q C_p \frac{\partial T_p}{\partial z} + 2\pi r_p h_p \left(T_p - T_w\right) = -\frac{\partial}{\partial t}\left(\pi r_p^2 \rho C_p T_p\right) + Q_p = -\pi r_p^2 \rho C_p \frac{\partial T_p}{\partial t} + Q_p \qquad \text{Eq(A-7)}$$

If temperatures are evaluated at time level n+1, i.e., at time t+Δt, this results in a fully implicit equation, as follows:

$$\rho q C_p \frac{T_{1,j}^{n+1} - T_{1,j-1}^{n+1}}{\Delta z_j} + 2\pi r_p h_p \left(T_{1,j}^{n+1} - T_{2,j}^{n+1}\right) = -\pi r_p^2 \rho C_p \frac{T_{1,j}^{n+1} - T_{1,j}^{n}}{\Delta t} + Q_p \quad \text{Eq(A-8)}$$

The subscript 1 indicates the drillstring and the i-th node in radial direction , the subscript j indicates the j-th node in the depth. In the same way, we could derive the governing equations and fully implicit finite equations for the control volumes of drillstring wall, the fluid in the annulus and the formation.

Drillpipe Wall

$$0 = \left(r_a^2 - r_p^2\right)\frac{\partial q}{\partial z} + 2r_a h_a \left(T_a - T_w\right) + 2r_p h_p \left(T_p - T_w\right) + \left(r_a^2 - r_p^2\right)\rho_w C_{p,w} \frac{\partial T_w}{\partial t} \quad \text{Eq(A-9)}$$

$$q = -k \frac{\partial T_w}{\partial z} \quad \text{Eq(A-10)}$$

If temperatures are evaluated at time level n+1, i.e., at time t+Δt, this results in a fully implicit equation, as follows:

$$\begin{aligned} 0 = {} & \left(r_a^2 - r_p^2\right)\left(\frac{T_{2,j+1}^{n+1} - T_{2,j}^{n+1}}{\Delta z_{j+0.5}} - \frac{T_{2,j}^{n+1} - T_{2,j-1}^{n+1}}{\Delta z_{j-0.5}}\right) + 2r_a h_a \left(T_{3,j}^{n+1} - T_{2,j}^{n+1}\right) \\ & + 2r_p h_p \left(T_{1,j}^{n+1} - T_{2,j}^{n+1}\right) + \left(r_a^2 - r_p^2\right)\rho_w C_{pw} \frac{T_{2,j}^{n+1} - T_{2,j}^{n}}{\Delta t} \end{aligned} \quad \text{Eq(A-11)}$$

Fluid In The Annulus

$$Q_a = \rho q C_p \frac{\partial T_a}{\partial z} + 2\pi r_a h_a \left(T_w - T_a\right) + 2\pi r_o h_a \left(T_f - T_a\right) + \frac{\partial}{\partial t}\left(\pi\left(r_o^2 - r_a^2\right)\rho C_p T_a\right) \quad \text{Eq(A-12)}$$

The implicit finite difference for Eq(A-12)

$$Q_a = \rho q C_p \frac{T_{3,j+1}^{n+1} - T_{3,j}^{n+1}}{\Delta z_j} + 2\pi r_a h_a \left(T_{2,j}^{n+1} - T_{3,j}^{n+1}\right)$$
$$+ 2\pi r_o h_o \left(T_{4,j}^{n+1} - T_{3,j}^{n+1}\right) - \pi\left(r_o^2 - r_a^2\right)\rho C_p \frac{T_{3,j}^{n+1} - T_{3,j}^{n}}{\Delta t} \quad \text{Eq(A-13)}$$

Formation

$$\left[\frac{1}{r}\frac{\partial}{\partial r}\left(rk\frac{\partial T}{\partial r}\right) + \frac{\partial^2 T}{\partial z^2}\right] = \rho C_p \frac{\partial T}{\partial t}$$

$$\rho_f C_{pf} \frac{T_{i,j}^{n+1} - T_{i,j}^{n}}{\Delta t} = \left[\frac{T_{i,j+1}^{n+1} - 2T_{i,j}^{n+1} + T_{i,j-1}^{n+1}}{\left(\Delta z_j\right)^2}\right] + \frac{k_f}{r_i}\frac{1}{\Delta r_i}\left[T_{i+1,j}^{n+1} - T_{i,j}^{n+1}\right] + \frac{k_f}{\left(\Delta r_i\right)^2}\left[T_{i+1,j}^{n+1} - 2T_{i,j}^{n+1} + T_{i-1,j}^{n+1}\right]$$

Eq(A-14)

Fluid In The Drillpipe

$$A_p = \left[\frac{\rho q C_p}{\Delta z_j} + \frac{\pi r_p^2 \rho C_p}{\Delta t} + \frac{2\pi r_p h_p}{\Delta t}\right] \quad \text{Eq(A-15)}$$

$$B_p = -\frac{\rho q C_p}{\Delta z_j}, \quad \text{Eq(A-16)}$$

$$C_p = -2\pi r_p h_p, \quad \text{Eq(A-17)}$$

$$D_p = -\frac{\pi r_p^2 \rho C_p}{\Delta t} \quad \text{Eq(A-18)}$$

$$A_P T_{1,j}^{n+1} + B_P T_{1,j-1}^{n+1} + C_P T_{2,j}^{n+1} + D_P T_{1,j}^{n} - Q_p = 0 \quad \text{Eq(A-19)}$$

For different grid, we get a series of fully implicit linear equations. Write these equations in Matrix form, we have

$$\begin{bmatrix} A_P & 0 & 0 & 0 & 0 & 0 \\ B_P & A_P & 0 & 0 & 0 & 0 \\ 0 & B_P & A_P & 0 & 0 & 0 \\ \dots & \dots & \dots & \dots & \dots & \dots \\ 0 & 0 & 0 & B_P & A_P & 0 \\ 0 & 0 & 0 & 0 & B_P & A_P \end{bmatrix} \begin{bmatrix} T_{1,1}^{n+1} \\ T_{1,2}^{n+1} \\ T_{1,3}^{n+1} \\ \dots \\ T_{1,j-1}^{n+1} \\ T_{1,j}^{n+1} \end{bmatrix} + C_P \begin{bmatrix} T_{2,1}^{n+1} \\ T_{2,2}^{n+1} \\ T_{2,3}^{n+1} \\ \dots \\ T_{2,j-1}^{n+1} \\ T_{2,j}^{n+1} \end{bmatrix} + D_P \begin{bmatrix} T_{2,1}^{n} \\ T_{2,2}^{n} \\ T_{2,3}^{n} \\ \dots \\ T_{2,j-1}^{n} \\ T_{2,j}^{n} \end{bmatrix} + \begin{bmatrix} B_P T_{1,0}^{n+1} - Q_p \\ -Q_p \\ -Q_p \\ \dots \\ -Q_p \\ -Q_p \end{bmatrix} = 0$$

Eq(A-20)

$T_{1,0}^{n+1}$ is one of the BCs (Boundary Conditions), which means the inlet temperature.

Where

$$\left[M_p\right]=\begin{bmatrix} A_P & 0 & 0 & 0 & 0 & 0 \\ B_P & A_P & 0 & 0 & 0 & 0 \\ 0 & B_P & A_P & 0 & 0 & 0 \\ \cdots & \cdots & \cdots & \cdots & \cdots & \cdots \\ 0 & 0 & 0 & B_P & A_P & 0 \\ 0 & 0 & 0 & 0 & B_P & A_P \end{bmatrix},\quad \left[T_1^{n+1}\right]=\begin{bmatrix} T_{1,1}^{n+1} \\ T_{1,2}^{n+1} \\ T_{1,3}^{n+1} \\ \cdots \\ T_{1,j-1}^{n+1} \\ T_{1,j}^{n+1} \end{bmatrix},\quad \left[T_2^{n+1}\right]=\begin{bmatrix} T_{2,1}^{n+1} \\ T_{2,2}^{n+1} \\ T_{2,3}^{n+1} \\ \cdots \\ T_{2,j-1}^{n+1} \\ T_{2,j}^{n+1} \end{bmatrix},$$

$$\left[T_2^{n}\right]=\begin{bmatrix} T_{2,1}^{n} \\ T_{2,2}^{n} \\ T_{2,3}^{n} \\ \cdots \\ T_{2,j-1}^{n} \\ T_{2,j}^{n} \end{bmatrix},\quad \left[Z_p\right]=\begin{bmatrix} B_P T_{1,0}^{n+1}-Q_p \\ -Q_p \\ -Q_p \\ \cdots \\ -Q_p \\ -Q_p \end{bmatrix}$$

In matrix format

$$\left[M_p\right]\left[T_1^{n+1}\right]+C_P\left[T_2^{n+1}\right]+D_P\left[T_2^{n}\right]+\left[Z_p\right]=0 \qquad \text{Eq(A-21)}$$

Drillpipe Wall

$$A_w=\frac{\left(r_a^2-r_p^2\right)}{\Delta z_j^2},$$

$$B_w=\frac{\left(r_a^2-r_p^2\right)\rho_w C_{pw}}{\Delta t}-2\frac{\left(r_a^2-r_p^2\right)}{\Delta z_j^2}-2r_a h_a-2r_p h_p,$$

$$C_w=\frac{\left(r_a^2-r_p^2\right)}{\Delta z_j^2}, D_w=2r_a h_a$$

$$E_w=2r_p h_p,$$

$$F_w=-\frac{\left(r_a^2-r_p^2\right)\rho_w C_{pw}}{\Delta t}$$

Recasting in the matrix format, we have

$$\begin{bmatrix} B_w & A_w & 0 & 0 & 0 & 0 \\ C_w & B_w & A_w & 0 & 0 & 0 \\ 0 & C_w & B_w & A_w & 0 & 0 \\ \cdots & \cdots & \cdots & \cdots & \cdots & \cdots \\ 0 & 0 & 0 & C_w & B_w & A_w \\ 0 & 0 & 0 & 0 & C_w & B_w \end{bmatrix} \begin{bmatrix} T_{2,1}^{n+1} \\ T_{2,2}^{n+1} \\ T_{2,3}^{n+1} \\ \cdots \\ T_{2,j-1}^{n+1} \\ T_{2,j}^{n+1} \end{bmatrix} + D_w \begin{bmatrix} T_{3,1}^{n+1} \\ T_{3,2}^{n+1} \\ T_{3,3}^{n+1} \\ \cdots \\ T_{3,j-1}^{n+1} \\ T_{3,j}^{n+1} \end{bmatrix} + E_w \begin{bmatrix} T_{1,1}^{n+1} \\ T_{1,2}^{n+1} \\ T_{1,3}^{n+1} \\ \cdots \\ T_{1,j-1}^{n+1} \\ T_{1,j}^{n+1} \end{bmatrix} + F_w \begin{bmatrix} T_{2,1}^{n} \\ T_{2,2}^{n} \\ T_{2,3}^{n} \\ \cdots \\ T_{2,j-1}^{n} \\ T_{2,j}^{n} \end{bmatrix} + \begin{bmatrix} C_w T_{2,0}^{n+1} \\ 0 \\ 0 \\ \cdots \\ 0 \\ 0 \end{bmatrix} = 0$$

Eq(A-22)

where

$$[M_w] = \begin{bmatrix} B_w & A_w & 0 & 0 & 0 & 0 \\ C_w & B_w & A_w & 0 & 0 & 0 \\ 0 & C_w & B_w & A_w & 0 & 0 \\ \cdots & \cdots & \cdots & \cdots & \cdots & \cdots \\ 0 & 0 & 0 & C_w & B_w & A_w \\ 0 & 0 & 0 & 0 & C_w & B_w \end{bmatrix}, \quad [T_1^{n+1}] = \begin{bmatrix} T_{1,1}^{n+1} \\ T_{1,2}^{n+1} \\ T_{1,3}^{n+1} \\ \cdots \\ T_{1,j-1}^{n+1} \\ T_{1,j}^{n+1} \end{bmatrix}, \quad [T_2^{n+1}] = \begin{bmatrix} T_{2,1}^{n+1} \\ T_{2,2}^{n+1} \\ T_{2,3}^{n+1} \\ \cdots \\ T_{2,j-1}^{n+1} \\ T_{2,j}^{n+1} \end{bmatrix},$$

$$[T_2^n] = \begin{bmatrix} T_{2,1}^{n} \\ T_{2,2}^{n} \\ T_{2,3}^{n} \\ \cdots \\ T_{2,j-1}^{n} \\ T_{2,j}^{n} \end{bmatrix}, \quad [T_3^{n+1}] = \begin{bmatrix} T_{3,1}^{n+1} \\ T_{3,2}^{n+1} \\ T_{3,3}^{n+1} \\ \cdots \\ T_{3,j-1}^{n+1} \\ T_{3,j}^{n+1} \end{bmatrix} [Z_w] = \begin{bmatrix} C_w T_{2,0}^{n+1} \\ 0 \\ 0 \\ \cdots \\ 0 \\ 0 \end{bmatrix}$$

Recasting in the matrix format, we have

$$[M_w][T_2^{n+1}] + D_w[T_3^{n+1}] + E_w[T_1^{n+1}] + F_w[T_2^n] + [Z_w] = 0 \qquad \text{Eq(A-23)}$$

Fluid In The Annulus

$$A_a = \frac{\rho q C_p}{\Delta z_j},$$

$$B_a = \left[\frac{\pi\left(r_o^2 - r_a^2\right)\rho C_p}{\Delta t} - \frac{\rho q C_p}{\Delta z_j} - 2\pi r_a h_a - 2\pi r_o h_o \right],$$

$$D_a = 2\pi r_a h_a,$$

$$C_a = -\frac{\pi\left(r_o^2 - r_a^2\right)\rho C_p}{\Delta t},$$

$$E_a = 2\pi r_o h_o$$

Write these equations in Matrix form, we have

$$\begin{bmatrix} B_a & A_a & 0 & 0 & 0 & 0 \\ 0 & B_a & A_a & 0 & 0 & 0 \\ 0 & 0 & B_a & A_a & 0 & 0 \\ \cdots & \cdots & \cdots & \cdots & \cdots & \cdots \\ 0 & 0 & 0 & 0 & B_a & A_a \\ 0 & 0 & 0 & 0 & 0 & B_a \end{bmatrix} \begin{bmatrix} T_{3,1}^{n+1} \\ T_{3,2}^{n+1} \\ T_{3,3}^{n+1} \\ \cdots \\ T_{3,j-1}^{n+1} \\ T_{3,j}^{n+1} \end{bmatrix} + C_a \begin{bmatrix} T_{3,1}^{n} \\ T_{3,2}^{n} \\ T_{3,3}^{n} \\ \cdots \\ T_{3,j-1}^{n} \\ T_{3,j}^{n} \end{bmatrix} + D_a \begin{bmatrix} T_{2,1}^{n+1} \\ T_{2,2}^{n+1} \\ T_{2,3}^{n+1} \\ \cdots \\ T_{2,j-1}^{n+1} \\ T_{2,j}^{n+1} \end{bmatrix} + E_a \begin{bmatrix} T_{4,1}^{n+1} \\ T_{4,2}^{n+1} \\ T_{4,3}^{n+1} \\ \cdots \\ T_{4,j-1}^{n+1} \\ T_{4,j}^{n+1} \end{bmatrix} + \begin{bmatrix} -Q_a \\ -Q_a \\ -Q_a \\ \cdots \\ -Q_a \\ -Q_a \end{bmatrix} = 0$$

Eq(A-24)

where

$$[M_a] = \begin{bmatrix} B_a & A_a & 0 & 0 & 0 & 0 \\ 0 & B_a & A_a & 0 & 0 & 0 \\ 0 & 0 & B_a & A_a & 0 & 0 \\ \cdots & \cdots & \cdots & \cdots & \cdots & \cdots \\ 0 & 0 & 0 & 0 & B_a & A_a \\ 0 & 0 & 0 & 0 & 0 & B_a \end{bmatrix}, \quad \left[T_2^{n+1}\right] = \begin{bmatrix} T_{2,1}^{n+1} \\ T_{2,2}^{n+1} \\ T_{2,3}^{n+1} \\ \cdots \\ T_{2,j-1}^{n+1} \\ T_{2,j}^{n+1} \end{bmatrix}, \quad \left[T_3^{n}\right] = \begin{bmatrix} T_{3,1}^{n} \\ T_{3,2}^{n} \\ T_{3,3}^{n} \\ \cdots \\ T_{3,j-1}^{n} \\ T_{3,j}^{n} \end{bmatrix},$$

$$\left[T_3^{n+1}\right] = \begin{bmatrix} T_{3,1}^{n+1} \\ T_{3,2}^{n+1} \\ T_{3,3}^{n+1} \\ \cdots \\ T_{3,j-1}^{n+1} \\ T_{3,j}^{n+1} \end{bmatrix} \left[T_4^{n+1}\right] = \begin{bmatrix} T_{4,1}^{n+1} \\ T_{4,2}^{n+1} \\ T_{4,3}^{n+1} \\ \cdots \\ T_{4,j-1}^{n+1} \\ T_{4,j}^{n+1} \end{bmatrix}, \quad [Z_a] = \begin{bmatrix} -Q_a \\ -Q_a \\ -Q_a \\ \cdots \\ -Q_a \\ -Q_a \end{bmatrix}$$

$$[M_a]\left[T_3^{n+1}\right] + C_a\left[T_3^{n+1}\right] + D_a\left[T_2^{n+1}\right] + E_a\left[T_4^{n+1}\right] + [Z_a] = 0 \qquad \text{Eq(A-25)}$$

Near-wellbore conservation of Energy

$$2\pi\left(r_a+\frac{\Delta r}{2}\right)\frac{k}{\Delta r}T_{5,j}^{n+1}-\left[2\pi\left(r_a+\frac{\Delta r}{2}\right)\frac{k}{\Delta r}+2\pi rh_a+\frac{\rho\pi\left(2r\Delta r+(\Delta r)^2\right)}{\Delta t}C_p\right]T_{4,j}^{n+1}+2\pi r_a h_a T_{3,j}^{n+1}$$
$$+\frac{\rho\pi\left(2r\Delta r+(\Delta r)^2\right)}{\Delta t}C_p T_{4,j}^{n}=0$$

Eq(A-26)

$$2\pi\left(r_a+\frac{\Delta r}{2}\right)\frac{k}{\Delta r}T_{5,j}^{n+1}=\left[2\pi\left(r_a+\frac{\Delta r}{2}\right)\frac{k}{\Delta r}+2\pi rh_a+\frac{\rho\pi\left(2r_a\Delta r+(\Delta r)^2\right)}{\Delta t}C_p\right]T_{4,j}^{n+1}-2\pi r_a h_a T_{3,j}^{n+1}$$
$$-\frac{\rho\pi\left(2r_a\Delta r+(\Delta r)^2\right)}{\Delta t}C_p T_{4,j}^{n}$$

Eq(A-27)

where

$$A_{Bcs}=2\pi\left(r_a+\frac{\Delta r}{2}\right)\frac{k}{\Delta r}$$

$$B_{Bcs}=\left[2\pi\left(r_a+\frac{\Delta r}{2}\right)\frac{k}{\Delta r}+2\pi rh_a+\frac{\rho\pi\left(2r_a\Delta r+(\Delta r)^2\right)}{\Delta t}C_p\right]$$

$$C_{Bcs}=-2\pi r_a h_a$$

$$D_{Bcs}=-\frac{\rho\pi\left(2r_a\Delta r+(\Delta r)^2\right)}{\Delta t}C_p$$

$$A_{Bcs}T_{5,j}^{n+1}=B_{Bcs}T_{4,j}^{n+1}+C_{Bcs}T_{3,j}^{n+1}+D_{Bcs}T_{4,j}^{n}$$

$$A_{Bcs}\left[T_{5,*}^{n+1}\right]=B_{Bcs}\left[T_{4,*}^{n+1}\right]+C_{Bcs}\left[T_{3,*}^{n+1}\right]+D_{Bcs}\left[T_{4,*}^{n}\right] \qquad \text{Eq(A-28)}$$

$$\left[T_{5,*}^{n+1}\right]=\frac{B_{Bcs}}{A_{Bcs}}\left[T_{4,*}^{n+1}\right]+\frac{C_{Bcs}}{A_{Bcs}}\left[T_{3,*}^{n+1}\right]+\frac{D_{Bcs}}{A_{Bcs}}\left[T_{4,*}^{n}\right] \qquad \text{Eq(A-29)}$$

Formation

$$A_i=\left[\frac{\rho_f C_{pf}}{\Delta t}+\frac{2}{(\Delta z_j)^2}+\frac{k_f}{r_i}\frac{1}{\Delta r_i}+\frac{2k_f}{(\Delta r_i)^2}\right],$$

$$B = -\frac{\rho_f C_{pf}}{\Delta t},\ C = D = -\frac{1}{(\Delta z_j)^2},$$

$$E_i = -\left(\frac{k_f}{r_i}\frac{1}{\Delta r_i} + \frac{k_f}{(\Delta r_i)^2}\right),$$

$$G = \frac{k_f}{(\Delta r_i)^2}$$

Write these equations in Matrix form, we have

$$\begin{bmatrix} A_i & C & 0 & ... & 0 & 0 \\ D & A_i & C & ... & 0 & 0 \\ 0 & D & A_i & ... & 0 & 0 \\ ... & ... & ... & ... & ... & ... \\ 0 & 0 & 0 & ... & A_i & C \\ 0 & 0 & 0 & ... & D & A_i \end{bmatrix} \begin{bmatrix} T_{i,1}^{n+1} \\ T_{i,2}^{n+1} \\ T_{i,3}^{n+1} \\ ... \\ T_{i,j-1}^{n+1} \\ T_{i,j}^{n+1} \end{bmatrix} + B \begin{bmatrix} T_{i,1}^{n} \\ T_{i,2}^{n} \\ T_{i,3}^{n} \\ ... \\ T_{i,j-1}^{n} \\ T_{i,j}^{n} \end{bmatrix} + E_i \begin{bmatrix} T_{i+1,1}^{n+1} \\ T_{i+1,2}^{n+1} \\ T_{i+1,3}^{n+1} \\ ... \\ T_{i+1,j-1}^{n+1} \\ T_{i+1,j}^{n+1} \end{bmatrix} - G \begin{bmatrix} T_{i-1,1}^{n+1} \\ T_{i-1,2}^{n+1} \\ T_{i-1,3}^{n+1} \\ ... \\ T_{i-1,j-1}^{n+1} \\ T_{i-1,j}^{n+1} \end{bmatrix} + \begin{bmatrix} DT_{i,0}^{n+1} \\ 0 \\ 0 \\ 0 \\ 0 \\ CT_{i,j+1}^{n+1} \end{bmatrix} = 0$$

Eq(A-30)

Let i=5,6,7,….i, we have a series of matrix systems and write in block matrix system, we have

$$\begin{bmatrix} A_5 & C & 0 & ... & 0 & 0 \\ D & A_5 & C & ... & 0 & 0 \\ 0 & D & A_5 & ... & 0 & 0 \\ ... & ... & ... & ... & ... & ... \\ 0 & 0 & 0 & ... & A_5 & C \\ 0 & 0 & 0 & ... & D & A_5 \end{bmatrix} \begin{bmatrix} T_{5,1}^{n+1} \\ T_{5,2}^{n+1} \\ T_{5,3}^{n+1} \\ ... \\ T_{5,j-1}^{n+1} \\ T_{5,j}^{n+1} \end{bmatrix} + B \begin{bmatrix} T_{5,1}^{n} \\ T_{5,2}^{n} \\ T_{5,3}^{n} \\ ... \\ T_{5,j-1}^{n} \\ T_{5,j}^{n} \end{bmatrix} + E_5 \begin{bmatrix} T_{6,1}^{n+1} \\ T_{6,2}^{n+1} \\ T_{6,3}^{n+1} \\ ... \\ T_{6,j-1}^{n+1} \\ T_{6,j}^{n+1} \end{bmatrix} - G \begin{bmatrix} T_{4,1}^{n+1} \\ T_{4,2}^{n+1} \\ T_{4,3}^{n+1} \\ ... \\ T_{4,j-1}^{n+1} \\ T_{4,j}^{n+1} \end{bmatrix} + \begin{bmatrix} DT_{5,0}^{n+1} \\ 0 \\ 0 \\ 0 \\ 0 \\ CT_{5,j+1}^{n+1} \end{bmatrix} = 0$$

$$\begin{bmatrix} A_6 & C & 0 & \dots & 0 & 0 \\ D & A_6 & C & \dots & 0 & 0 \\ 0 & D & A_6 & \dots & 0 & 0 \\ \dots & \dots & \dots & \dots & \dots & \dots \\ 0 & 0 & 0 & \dots & A_6 & C \\ 0 & 0 & 0 & \dots & D & A_6 \end{bmatrix} \begin{bmatrix} T_{6,1}^{n+1} \\ T_{6,2}^{n+1} \\ T_{6,3}^{n+1} \\ \dots \\ T_{6,j-1}^{n+1} \\ T_{6,j}^{n+1} \end{bmatrix} + B \begin{bmatrix} T_{6,1}^{n} \\ T_{6,2}^{n} \\ T_{6,3}^{n} \\ \dots \\ T_{6,j-1}^{n} \\ T_{6,j}^{n} \end{bmatrix} + E_6 \begin{bmatrix} T_{7,1}^{n+1} \\ T_{7,2}^{n+1} \\ T_{7,3}^{n+1} \\ \dots \\ T_{7,j-1}^{n+1} \\ T_{7,j}^{n+1} \end{bmatrix} - G \begin{bmatrix} T_{5,1}^{n+1} \\ T_{5,2}^{n+1} \\ T_{5,3}^{n+1} \\ \dots \\ T_{5,j-1}^{n+1} \\ T_{5,j}^{n+1} \end{bmatrix} + \begin{bmatrix} DT_{6,0}^{n+1} \\ 0 \\ 0 \\ 0 \\ 0 \\ CT_{6,j+1}^{n+1} \end{bmatrix} = 0$$

$$\begin{bmatrix} A_7 & C & 0 & \dots & 0 & 0 \\ D & A_7 & C & \dots & 0 & 0 \\ 0 & D & A_7 & \dots & 0 & 0 \\ \dots & \dots & \dots & \dots & \dots & \dots \\ 0 & 0 & 0 & \dots & A_7 & C \\ 0 & 0 & 0 & \dots & D & A_7 \end{bmatrix} \begin{bmatrix} T_{7,1}^{n+1} \\ T_{7,2}^{n+1} \\ T_{7,3}^{n+1} \\ \dots \\ T_{7,j-1}^{n+1} \\ T_{7,j}^{n+1} \end{bmatrix} + B \begin{bmatrix} T_{7,1}^{n} \\ T_{7,2}^{n} \\ T_{7,3}^{n} \\ \dots \\ T_{7,j-1}^{n} \\ T_{7,j}^{n} \end{bmatrix} + E_7 \begin{bmatrix} T_{8,1}^{n+1} \\ T_{8,2}^{n+1} \\ T_{8,3}^{n+1} \\ \dots \\ T_{8,j-1}^{n+1} \\ T_{8,j}^{n+1} \end{bmatrix} - G \begin{bmatrix} T_{6,1}^{n+1} \\ T_{6,2}^{n+1} \\ T_{6,3}^{n+1} \\ \dots \\ T_{6,j-1}^{n+1} \\ T_{6,j}^{n+1} \end{bmatrix} + \begin{bmatrix} DT_{7,0}^{n+1} \\ 0 \\ 0 \\ 0 \\ 0 \\ 0 \end{bmatrix} = 0$$

....

$$\begin{bmatrix} A_i & C & 0 & \dots & 0 & 0 \\ D & A_i & C & \dots & 0 & 0 \\ 0 & D & A_i & \dots & 0 & 0 \\ \dots & \dots & \dots & \dots & \dots & \dots \\ 0 & 0 & 0 & \dots & A_i & C \\ 0 & 0 & 0 & \dots & D & A_i \end{bmatrix} \begin{bmatrix} T_{i,1}^{n+1} \\ T_{i,2}^{n+1} \\ T_{i,3}^{n+1} \\ \dots \\ T_{i,j-1}^{n+1} \\ T_{i,j}^{n+1} \end{bmatrix} + B \begin{bmatrix} T_{i,1}^{n} \\ T_{i,2}^{n} \\ T_{i,3}^{n} \\ \dots \\ T_{i,j-1}^{n} \\ T_{i,j}^{n} \end{bmatrix} + E_i \begin{bmatrix} T_{i+1,1}^{n+1} \\ T_{i+1,2}^{n+1} \\ T_{i+1,3}^{n+1} \\ \dots \\ T_{i+1,j-1}^{n+1} \\ T_{i+1,j}^{n+1} \end{bmatrix} - G \begin{bmatrix} T_{i-1,1}^{n+1} \\ T_{i-1,2}^{n+1} \\ T_{i-1,3}^{n+1} \\ \dots \\ T_{i-1,j-1}^{n+1} \\ T_{i-1,j}^{n+1} \end{bmatrix} + \begin{bmatrix} DT_{i,0}^{n+1} \\ 0 \\ 0 \\ 0 \\ 0 \\ CT_{i,j+1}^{n+1} \end{bmatrix} = 0$$

Let block matrix $S_i = \begin{bmatrix} A_i & C & 0 & ... & 0 & 0 \\ D & A_i & C & ... & 0 & 0 \\ 0 & D & A_i & ... & 0 & 0 \\ ... & ... & ... & ... & ... & ... \\ 0 & 0 & 0 & ... & A_i & C \\ 0 & 0 & 0 & ... & D & A_i \end{bmatrix}$, Column vector $T_{i,*}^{n+1} = \begin{bmatrix} T_{i,1}^{n+1} \\ T_{i,2}^{n+1} \\ T_{i,3}^{n+1} \\ ... \\ T_{i,j-1}^{n+1} \\ T_{i,j}^{n+1} \end{bmatrix}$,

$$T_{i,**}^{n+1} = \begin{bmatrix} DT_{i,0}^{n+1} \\ 0 \\ 0 \\ ... \\ 0 \\ CT_{i,j+1}^{n+1} \end{bmatrix}$$

$$\begin{bmatrix} S_5 & E_5 & 0 & ... & 0 & 0 \\ -G & S_6 & E_6 & ... & 0 & 0 \\ 0 & -G & S_7 & ... & 0 & 0 \\ ... & ... & ... & ... & ... & ... \\ 0 & 0 & 0 & ... & S_{i-1} & E_{i-1} \\ 0 & 0 & 0 & ... & -G & S_i \end{bmatrix} \begin{bmatrix} T_{5,*}^{n+1} \\ T_{6,*}^{n+1} \\ T_{7,*}^{n+1} \\ ... \\ T_{i-1,*}^{n+1} \\ T_{i,*}^{n+1} \end{bmatrix} + B \begin{bmatrix} T_{5,*}^{n} \\ T_{6,*}^{n} \\ T_{7,*}^{n} \\ ... \\ T_{i-1,*}^{n} \\ T_{i,*}^{n} \end{bmatrix} + \begin{bmatrix} T_{5,**}^{n+1} \\ T_{6,**}^{n+1} \\ T_{7,**}^{n+1} \\ ... \\ T_{i-1,**}^{n+1} \\ T_{i,**}^{n+1} \end{bmatrix} - G \begin{bmatrix} T_{4,*}^{n+1} \\ 0 \\ 0 \\ ... \\ 0 \\ 0 \end{bmatrix} + E_i \begin{bmatrix} 0 \\ 0 \\ 0 \\ ... \\ 0 \\ T_{i+1,*}^{n+1} \end{bmatrix} = 0$$

Eq(A-30)

Substituting Eq.(A-21), Eq.(A-23) into Eq.(A-25), we have

$$\begin{aligned} \left[T_{2,*}^{n+1}\right] &= \frac{-1}{C_p}\left\{\left[M_p\right]\left[T_{1,*}^{n+1}\right] + D_p\left[T_{1,*}^{n}\right] + \left[Z_p\right]\right\} \\ &= \frac{-1}{C_p}\left[M_p\right]\left[T_{1,*}^{n+1}\right] + \frac{-1}{C_p}D_p\left[T_{1,*}^{n}\right] + \frac{-1}{C_p}\left[Z_p\right] \end{aligned}$$

Eq.(A-31)

$$\left[T_{3,*}^{n+1}\right] = \frac{1}{D_w C_p}\left[M_w\right]\left[M_p\right]\left[T_{1,*}^{n+1}\right] - \frac{E_w}{D_w}\left[T_{1,*}^{n+1}\right] + \frac{D_p}{D_w C_p}\left[M_w\right]\left[T_{1,*}^{n}\right] + \frac{1}{D_w C_p}\left[M_w\right]\left[Z_p\right] - \frac{F_w}{D_w}\left[T_{2,*}^{n}\right] - \frac{1}{D_w}\left[Z_w\right]$$

Eq.(A-32)

$$\left[T_{4,*}^{n+1}\right] = \left\{\frac{-1}{E_a D_w C_p}\left[M_a\right]\left[M_w\right]\left[M_p\right] + \frac{E_w}{E_a D_w}\left[M_a\right] + \frac{D_a}{E_a C_p}\left[M_p\right]\right\}\left[T_{1,*}^{n+1}\right] + \left\{\frac{-D_p}{E_a D_w C_p}\left[M_a\right]\left[M_w\right] + \frac{D_a D_p}{E_a C_p}\right\}\left[T_{1,*}^{n}\right] + \frac{F_w}{E_a D_w}\left[M_a\right]\left[T_{2,*}^{n}\right] - \frac{C_a}{E_a}\left[T_{3,*}^{n}\right] - \frac{1}{E_a D_w C_p}\left[M_a\right]\left[M_w\right]\left[Z_p\right] + \frac{1}{E_a D_w}\left[M_a\right]\left[Z_w\right] + \frac{D_a}{E_a C_p}\left[Z_p\right] - \frac{1}{E_a}\left[Z_a\right]$$

Eq.(A-33)

$$\left[T_{5,*}^{n+1}\right]=\frac{B_{Bcs}}{A_{Bcs}}\left\{\frac{-1}{E_aD_wC_p}\left[M_a\right]\left[M_w\right]\left[M_p\right]+\frac{E_w}{E_aD_w}\left[M_a\right]+\frac{D_a}{E_aC_p}\left[M_p\right]\right\}\left[T_{1,*}^{n+1}\right]$$
$$+\frac{B_{Bcs}}{A_{Bcs}}\left\{\frac{-D_p}{E_aD_wC_p}\left[M_a\right]\left[M_w\right]+\frac{D_aD_p}{E_aC_p}\right\}\left[T_{1,*}^{n}\right]+\frac{B_{Bcs}}{A_{Bcs}}\frac{F_w}{E_aD_w}\left[M_a\right]\left[T_{2,*}^{n}\right]-\frac{B_{Bcs}}{A_{Bcs}}\frac{C_a}{E_a}\left[T_{3,*}^{n}\right]$$
$$-\frac{B_{Bcs}}{A_{Bcs}}\frac{1}{E_aD_wC_p}\left[M_a\right]\left[M_w\right]\left[Z_p\right]+\frac{B_{Bcs}}{A_{Bcs}}\frac{1}{E_aD_w}\left[M_a\right]\left[Z_w\right]+\frac{B_{Bcs}}{A_{Bcs}}\frac{D_a}{E_aC_p}\left[Z_p\right]-\frac{B_{Bcs}}{A_{Bcs}}\frac{1}{E_a}\left[Z_a\right]$$

$$+\frac{C_{Bcs}}{A_{Bcs}}\frac{1}{D_wC_p}\left[M_w\right]\left[M_p\right]\left[T_{1,*}^{n+1}\right]-\frac{C_{Bcs}}{A_{Bcs}}\frac{E_w}{D_w}\left[T_{1,*}^{n+1}\right]+\frac{C_{Bcs}}{A_{Bcs}}\frac{D_p}{D_wC_p}\left[M_w\right]\left[T_{1,*}^{n}\right]$$
$$+\frac{C_{Bcs}}{A_{Bcs}}\frac{1}{D_wC_p}\left[M_w\right]\left[Z_p\right]-\frac{C_{Bcs}}{A_{Bcs}}\frac{F_w}{D_w}\left[T_{2,*}^{n}\right]-\frac{C_{Bcs}}{A_{Bcs}}\frac{1}{D_w}\left[Z_w\right]+\frac{D_{Bcs}}{A_{Bcs}}\left[T_{4,*}^{n}\right]$$

$$=\frac{B_{Bcs}}{A_{Bcs}}\left\{\frac{-1}{E_aD_wC_p}\left[M_a\right]\left[M_w\right]\left[M_p\right]+\frac{E_w}{E_aD_w}\left[M_a\right]+\frac{D_a}{E_aC_p}\left[M_p\right]\right\}\left[T_{1,*}^{n+1}\right]$$
$$+\frac{C_{Bcs}}{A_{Bcs}}\frac{1}{D_wC_p}\left[M_w\right]\left[M_p\right]\left[T_{1,*}^{n+1}\right]-\frac{C_{Bcs}}{A_{Bcs}}\frac{E_w}{D_w}\left[T_{1,*}^{n+1}\right]$$
$$+\frac{B_{Bcs}}{A_{Bcs}}\left\{\frac{-D_p}{E_aD_wC_p}\left[M_a\right]\left[M_w\right]+\frac{D_aD_p}{E_aC_p}\right\}\left[T_{1,*}^{n}\right]+\frac{C_{Bcs}}{A_{Bcs}}\frac{D_p}{D_wC_p}\left[M_w\right]\left[T_{1,*}^{n}\right]$$
$$+\frac{B_{Bcs}}{A_{Bcs}}\frac{F_w}{E_aD_w}\left[M_a\right]\left[T_{2,*}^{n}\right]-\frac{C_{Bcs}}{A_{Bcs}}\frac{F_w}{D_w}\left[T_{2,*}^{n}\right]-\frac{B_{Bcs}}{A_{Bcs}}\frac{C_a}{E_a}\left[T_{3,*}^{n}\right]+\frac{D_{Bcs}}{A_{Bcs}}\left[T_{4,*}^{n}\right]$$
$$-\frac{B_{Bcs}}{A_{Bcs}}\frac{1}{E_aD_wC_p}\left[M_a\right]\left[M_w\right]\left[Z_p\right]+\frac{B_{Bcs}}{A_{Bcs}}\frac{1}{E_aD_w}\left[M_a\right]\left[Z_w\right]$$
$$+\frac{B_{Bcs}}{A_{Bcs}}\frac{D_a}{E_aC_p}\left[Z_p\right]-\frac{B_{Bcs}}{A_{Bcs}}\frac{1}{E_a}\left[Z_a\right]+\frac{C_{Bcs}}{A_{Bcs}}\frac{1}{D_wC_p}\left[M_w\right]\left[Z_p\right]-\frac{C_{Bcs}}{A_{Bcs}}\frac{1}{D_w}\left[Z_w\right]$$

Eq.(A-34)

Substituting Eq.(A-31), Eq.(A-32), Eq.(A-33) into Eq.(A-30), we have

$$
\begin{aligned}
[S_5]\Bigg\langle\;
&\frac{B_{Bcs}}{A_{Bcs}}\left\{\frac{-1}{E_a D_w C_p}[M_a][M_w][M_p]+\frac{E_w}{E_a D_w}[M_a]+\frac{D_a}{E_a C_p}[M_p]\right\}[T_{1,*}^{n+1}]\\
&+\frac{C_{Bcs}}{A_{Bcs}}\frac{1}{D_w C_p}[M_w][M_p][T_{1,*}^{n+1}]-\frac{C_{Bcs}}{A_{Bcs}}\frac{E_w}{D_w}[T_{1,*}^{n+1}]\\
&+\frac{B_{Bcs}}{A_{Bcs}}\left\{\frac{-D_p}{E_a D_w C_p}[M_a][M_w]+\frac{D_a D_p}{E_a C_p}\right\}[T_{1,*}^{n}]+\frac{C_{Bcs}}{A_{Bcs}}\frac{D_p}{D_w C_p}[M_w][T_{1,*}^{n}]\\
&+\frac{B_{Bcs}}{A_{Bcs}}\frac{F_w}{E_a D_w}[M_a][T_{2,*}^{n}]-\frac{C_{Bcs}}{A_{Bcs}}\frac{F_w}{D_w}[T_{2,*}^{n}]-\frac{B_{Bcs}}{A_{Bcs}}\frac{C_a}{E_a}[T_{3,*}^{n}]+\frac{D_{Bcs}}{A_{Bcs}}[T_{4,*}^{n}]\\
&-\frac{B_{Bcs}}{A_{Bcs}}\frac{1}{E_a D_w C_p}[M_a][M_w][Z_p]+\frac{B_{Bcs}}{A_{Bcs}}\frac{1}{E_a D_w}[M_a][Z_w]\\
&+\frac{B_{Bcs}}{A_{Bcs}}\frac{D_a}{E_a C_p}[Z_p]-\frac{B_{Bcs}}{A_{Bcs}}\frac{1}{E_a}[Z_a]+\frac{C_{Bcs}}{A_{Bcs}}\frac{1}{D_w C_p}[M_w][Z_p]-\frac{C_{Bcs}}{A_{Bcs}}\frac{1}{D_w}[Z_w]
\;\Bigg\rangle\\
+B[T_{5,*}^{n}]+E_5[T_{6,*}^{n+1}]-G\Bigg\langle\;
&\left\{\frac{-1}{E_a D_w C_p}[M_a][M_w][M_p]+\frac{E_w}{E_a D_w}[M_a]+\frac{D_a}{E_a C_p}[M_p]\right\}[T_{1,*}^{n+1}]\\
&+\left\{\frac{-D_p}{E_a D_w C_p}[M_a][M_w]+\frac{D_a D_p}{E_a C_p}\right\}[T_{1,*}^{n}]+\frac{F_w}{E_a D_w}[M_a][T_{2,*}^{n}]-\frac{C_a}{E_a}[T_{3,*}^{n}]\\
&-\frac{1}{E_a D_w C_p}[M_a][M_w][Z_p]+\frac{1}{E_a D_w}[M_a][Z_w]+\frac{D_a}{E_a C_p}[Z_p]-\frac{1}{E_a}[Z_a]
\;\Bigg\rangle\\
+[T_{5,**}^{n+1}]=0
\end{aligned}
$$

Eq.(A-35)

$$\left(\begin{array}{l}\dfrac{B_{Bcs}}{A_{Bcs}}[S_5]\left\{\dfrac{-1}{E_a D_w C_p}[M_a][M_w][M_p]+\dfrac{E_w}{E_a D_w}[M_a]+\dfrac{D_a}{E_a C_p}[M_p]\right\} \\ +\dfrac{C_{Bcs}}{A_{Bcs}}\dfrac{1}{D_w C_p}[S_5][M_w][M_p]-\dfrac{C_{Bcs}}{A_{Bcs}}\dfrac{E_w}{D_w}[S_5] \\ -G\left\{\dfrac{-1}{E_a D_w C_p}[M_a][M_w][M_p]+\dfrac{E_w}{E_a D_w}[M_a]+\dfrac{D_a}{E_a C_p}[M_p]\right\}\end{array}\right)[T_{1,*}^{n+1}]$$

$$+E_5[T_{6,*}^{n+1}]+\left(\begin{array}{l}\dfrac{B_{Bcs}}{A_{Bcs}}[S_5]\left\{\dfrac{-D_p}{E_a D_w C_p}[M_a][M_w]+\dfrac{D_a D_p}{E_a C_p}\right\}+\dfrac{C_{Bcs}}{A_{Bcs}}\dfrac{D_p}{D_w C_p}[S_5][M_w] \\ -G\left\{\dfrac{-D_p}{E_a D_w C_p}[M_a][M_w]+\dfrac{D_a D_p}{E_a C_p}\right\}\end{array}\right)[T_{1,*}^{n}]$$

$$+\left(\frac{B_{Bcs}}{A_{Bcs}}\frac{F_w}{E_a D_w}[S_5][M_a]-\frac{C_{Bcs}}{A_{Bcs}}\frac{F_w}{D_w}[S_5]-G\frac{F_w}{E_a D_w}[M_a][T_{2,*}^{n}]\right)[T_{2,*}^{n}]$$

$$+\left(-\frac{B_{Bcs}}{A_{Bcs}}\frac{C_a}{E_a}[S_5][T_{3,*}^{n}]+G\frac{C_a}{E_a}\right)[T_{3,*}^{n}]+\frac{D_{Bcs}}{A_{Bcs}}[S_5][T_{4,*}^{n}]+B[T_{5,*}^{n}]$$

$$-\frac{B_{Bcs}}{A_{Bcs}}\frac{1}{E_a D_w C_p}[S_5][M_a][M_w][Z_p]+\frac{B_{Bcs}}{A_{Bcs}}\frac{1}{E_a D_w}[S_5][M_a][Z_w]$$

$$+\frac{B_{Bcs}}{A_{Bcs}}\frac{D_a}{E_a C_p}[S_5][Z_p]-\frac{B_{Bcs}}{A_{Bcs}}\frac{1}{E_a}[S_5][Z_a]+\frac{C_{Bcs}}{A_{Bcs}}\frac{1}{D_w C_p}[S_5][M_w][Z_p]-\frac{C_{Bcs}}{A_{Bcs}}\frac{1}{D_w}[S_5][Z_w]$$

$$+G\frac{1}{E_a D_w C_p}[M_a][M_w][Z_p]-G\frac{1}{E_a D_w}[M_a][Z_w]-G\frac{D_a}{E_a C_p}[Z_p]+G\frac{1}{E_a}[Z_a]+[T_{5,**}^{n+1}]=0$$

Eq.(A-36)

Rewrite Eq(A-36)

$$[S_1][T_{1,*}^{n+1}]+E_5[T_{6,*}^{n+1}]+[S_{1A}][T_{1,*}^{n}]+[S_{1B}][T_{2,*}^{n}]+[S_{1C}][T_{3,*}^{n}]+[S_{1D}][T_{4,*}^{n}]+B[T_{5,*}^{n}]+[S_{1E}]=0$$

Eq(A-37)

where

$$[S_1]=\begin{pmatrix}\frac{B_{Bcs}}{A_{Bcs}}[S_5]\left\{\frac{-1}{E_aD_wC_p}[M_a][M_w][M_p]+\frac{E_w}{E_aD_w}[M_a]+\frac{D_a}{E_aC_p}[M_p]\right\}\\+\frac{C_{Bcs}}{A_{Bcs}}\frac{1}{D_wC_p}[S_5][M_w][M_p]-\frac{C_{Bcs}}{A_{Bcs}}\frac{E_w}{D_w}[S_5]\\-G\left\{\frac{-1}{E_aD_wC_p}[M_a][M_w][M_p]+\frac{E_w}{E_aD_w}[M_a]+\frac{D_a}{E_aC_p}[M_p]\right\}\end{pmatrix}$$

$$[S_{1A}]=\begin{pmatrix}\frac{B_{Bcs}}{A_{Bcs}}[S_5]\left\{\frac{-D_p}{E_aD_wC_p}[M_a][M_w]+\frac{D_aD_p}{E_aC_p}\right\}\\+\frac{C_{Bcs}}{A_{Bcs}}\frac{D_p}{D_wC_p}[S_5][M_w]-G\left\{\frac{-D_p}{E_aD_wC_p}[M_a][M_w]+\frac{D_aD_p}{E_aC_p}\right\}\end{pmatrix}$$

$$[S_{1B}]=\left(\frac{B_{Bcs}}{A_{Bcs}}\frac{F_w}{E_aD_w}[S_5][M_a]-\frac{C_{Bcs}}{A_{Bcs}}\frac{F_w}{D_w}[S_5]-G\frac{F_w}{E_aD_w}[M_a][T^n_{2,*}]\right)$$

$$[S_{1C}]=\left(-\frac{B_{Bcs}}{A_{Bcs}}\frac{C_a}{E_a}[S_5][T^n_{3,*}]+G\frac{C_a}{E_a}\right)$$

$$[S_{1D}]=\frac{D_{Bcs}}{A_{Bcs}}[S_5]$$

$$[S_{1E}]=-\frac{B_{Bcs}}{A_{Bcs}}\frac{1}{E_aD_wC_p}[S_5][M_a][M_w][Z_p]+\frac{B_{Bcs}}{A_{Bcs}}\frac{1}{E_aD_w}[S_5][M_a][Z_w]$$

$$+\frac{B_{Bcs}}{A_{Bcs}}\frac{D_a}{E_aC_p}[S_5][Z_p]-\frac{B_{Bcs}}{A_{Bcs}}\frac{1}{E_a}[S_5][Z_a]+\frac{C_{Bcs}}{A_{Bcs}}\frac{1}{D_wC_p}[S_5][M_w][Z_p]-\frac{C_{Bcs}}{A_{Bcs}}\frac{1}{D_w}[S_5][Z_w]$$

$$+G\frac{1}{E_aD_wC_p}[M_a][M_w][Z_p]-G\frac{1}{E_aD_w}[M_a][Z_w]-G\frac{D_a}{E_aC_p}[Z_p]+G\frac{1}{E_a}[Z_a]+[T^{n+1}_{5,**}]$$

The Governing Equations And Finite Difference Equations For The Returnline

$$\rho q C_p \frac{\partial T_{rl}}{\partial z} + 2\pi r_{rl} h_{rl}\left(T_{rl} - T_{wrl}\right) = -\frac{\partial}{\partial t}\left(\pi r_{rl}^2 \rho C_p T_{rl}\right) + Q_{rl} = -\pi r_{rl}^2 \rho C_p \frac{\partial T_{rl}}{\partial t} + Q_{rl} \quad \text{Eq(A-38)}$$

$$\rho q C_p \frac{T_{1,j}^{n+1} - T_{1,j-1}^{n+1}}{\Delta z_j} + 2\pi r_{rl} h_{rl}\left(T_{1,j}^{n+1} - T_{2,j}^{n+1}\right) = -\pi r_{rl}^2 \rho C_p \frac{T_{1,j}^{n+1} - T_{1,j}^{n}}{\Delta t} + Q_{rl} \qquad \text{Eq(A-39)}$$

Write these equations in Matrix form, we have

$$\begin{bmatrix} A_{rl} & 0 & 0 & 0 & 0 & 0 \\ B_{rl} & A_{rl} & 0 & 0 & 0 & 0 \\ 0 & B_{rl} & A_{rl} & 0 & 0 & 0 \\ \cdots & \cdots & \cdots & \cdots & \cdots & \cdots \\ 0 & 0 & 0 & B_{rl} & A_{rl} & 0 \\ 0 & 0 & 0 & 0 & B_{rl} & A_{rl} \end{bmatrix} \begin{bmatrix} T_{1,1}^{n+1} \\ T_{1,2}^{n+1} \\ T_{1,3}^{n+1} \\ \cdots \\ T_{1,j-1}^{n+1} \\ T_{1,j}^{n+1} \end{bmatrix} + C_{rl} \begin{bmatrix} T_{2,1}^{n+1} \\ T_{2,2}^{n+1} \\ T_{2,3}^{n+1} \\ \cdots \\ T_{2,j-1}^{n+1} \\ T_{2,j}^{n+1} \end{bmatrix} + D_{rl} \begin{bmatrix} T_{2,1}^{n} \\ T_{2,2}^{n} \\ T_{2,3}^{n} \\ \cdots \\ T_{2,j-1}^{n} \\ T_{2,j}^{n} \end{bmatrix} + \begin{bmatrix} B_{rl} T_{1,0}^{n+1} - Q_{rl} \\ -Q_{rl} \\ -Q_{rl} \\ \cdots \\ -Q_{rl} \\ -Q_{rl} \end{bmatrix} = 0$$

Eq(A-40)

In matrix form

$$\left[M_{rl}\right]\left[T_1^{n+1}\right] + C_{rl}\left[T_2^{n+1}\right] + D_{rl}\left[T_2^{n}\right] + \left[Z_{rl}\right] = 0 \qquad \text{Eq(A-41)}$$

where

$$\left[M_{rl}\right] = \begin{bmatrix} A_{rl} & 0 & 0 & 0 & 0 & 0 \\ B_{rl} & A_{rl} & 0 & 0 & 0 & 0 \\ 0 & B_{rl} & A_{rl} & 0 & 0 & 0 \\ \cdots & \cdots & \cdots & \cdots & \cdots & \cdots \\ 0 & 0 & 0 & B_{rl} & A_{rl} & 0 \\ 0 & 0 & 0 & 0 & B_{rl} & A_{rl} \end{bmatrix}$$

$$\left[T_1^{n+1}\right] = \begin{bmatrix} T_{1,1}^{n+1} \\ T_{1,2}^{n+1} \\ T_{1,3}^{n+1} \\ \cdots \\ T_{1,j-1}^{n+1} \\ T_{1,j}^{n+1} \end{bmatrix}, \quad \left[T_2^{n+1}\right] = \begin{bmatrix} T_{2,1}^{n+1} \\ T_{2,2}^{n+1} \\ T_{2,3}^{n+1} \\ \cdots \\ T_{2,j-1}^{n+1} \\ T_{2,j}^{n+1} \end{bmatrix}, \quad \left[T_2^{n}\right] = \begin{bmatrix} T_{2,1}^{n} \\ T_{2,2}^{n} \\ T_{2,3}^{n} \\ \cdots \\ T_{2,j-1}^{n} \\ T_{2,j}^{n} \end{bmatrix}, \quad \left[Z_{rl}\right] = \begin{bmatrix} B_{rl} T_{1,0}^{n+1} - Q_{rl} \\ -Q_{rl} \\ -Q_{rl} \\ \cdots \\ -Q_{rl} \\ -Q_{rl} \end{bmatrix}$$

For the control volume in the Returnline Wall

$$0=\left(r_a^2-r_{rl}^2\right)\frac{\partial q}{\partial z}+2r_{rl}h_{rl}\left(T_{sea}-T_{rlw}\right)+2r_{rl}h_{rl}\left(T_{rl}-T_{wrl}\right)+\left(r_a^2-r_{rl}^2\right)\rho_{wrl}C_{pwrl}\frac{\partial T_w}{\partial t} \quad \text{Eq(A-42)}$$

$$q=-k\frac{\partial T_{wrl}}{\partial z} \quad \text{Eq(A-43)}$$

$$\begin{aligned}0=&\left(r_a^2-r_{rl}^2\right)\left(\frac{T_{2,j+1}^{n+1}-T_{2,j}^{n+1}}{\Delta z_{j+0.5}}-\frac{T_{2,j}^{n+1}-T_{2,j-1}^{n+1}}{\Delta z_{j-0.5}}\right)+2r_{rl}h_{rl}\left(T_{3,j}^{n+1}-T_{2,j}^{n+1}\right)\\&+2r_{rl}h_{rl}\left(T_{1,j}^{n+1}-T_{2,j}^{n+1}\right)+\left(r_a^2-r_{rl}^2\right)\rho_{wrl}C_{pwrl}\frac{T_{2,j}^{n+1}-T_{2,j}^{n}}{\Delta t}\end{aligned} \quad \text{Eq(A-44)}$$

$$\left[M_{rl}\right]\left[T_1^{n+1}\right]+C_{rl}\left[T_2^{n+1}\right]+D_{rl}\left[T_2^{n}\right]+\left[Z_{rl}\right]=0 \quad \text{Eq (A-41)}$$

$$\left[M_{wrl}\right]\left[T_2^{n+1}\right]+D_{wrl}\left[T_3^{n+1}\right]+E_{wrl}\left[T_1^{n+1}\right]+F_{wrl}\left[T_2^{n}\right]+\left[Z_{wrl}\right]=0 \quad \text{Eq(A-45)}$$

Substituting Eq.(A-41) into Eq.(A-45), we have

$$\begin{aligned}\left[T_{2,*}^{n+1}\right]&=\frac{-1}{C_p}\left\{\left[M_{rl}\right]\left[T_{1,*}^{n+1}\right]+D_{rl}\left[T_{1,*}^{n}\right]+\left[Z_{rl}\right]\right\}\\&=\frac{-1}{C_{rl}}\left[M_{rl}\right]\left[T_{1,*}^{n+1}\right]+\frac{-1}{C_{rl}}D_{rl}\left[T_{1,*}^{n}\right]+\frac{-1}{C_{rl}}\left[Z_{rl}\right]\end{aligned} \quad \text{Eq(A-45)}$$

$$\begin{aligned}\left[T_{3,*}^{n+1}\right]=&\frac{1}{D_{wrl}C_{rl}}\left[M_{wrl}\right]\left[M_{rl}\right]\left[T_{1,*}^{n+1}\right]-\frac{E_{rl}}{D_{rl}}\left[T_{1,*}^{n+1}\right]+\frac{D_{rl}}{D_{wrl}C_{rl}}\left[M_{wrl}\right]\left[T_{1,*}^{n}\right]\\&+\frac{1}{D_{wrl}C_{rl}}\left[M_{rl}\right]\left[Z_{rl}\right]-\frac{F_{wrl}}{D_{wrl}}\left[T_{2,*}^{n}\right]-\frac{1}{D_{wrl}}\left[Z_{wrl}\right]\end{aligned}$$

Eq(A-46)

The derivation for governing equations and fully implicit difference regime of the drilling fluid above the mudline is as same as that for the returnline.

Boundary Conditions

It's necessary to write a discretization equation for the boundary and adjacent node integrated over half the control volume. In our case, we apply Dirichlet boundary condition (known boundary temperature)

$$T_B = T_{known} = T_{ambient} \qquad \text{Eq(A-47)}$$

Initial Conditions

$$T = T_{Thermal\,gradient} \qquad \text{Eq(A-48)}$$

VITA

Name:	Ming Feng
Contact Information:	Department of Petroleum Engineering Texas A&M University 3116 TAMU Richardson Building College Station, TX 77843-3116
Email Address:	mingfeng317@tamu.edu;mingfeng317@hotmail.com
Education:	M.S., Petroleum Engineering, University of Louisiana at Lafayette, 2006 M.S., Mechanical Engineering, Southwest Petroleum University, 2003 B.S. Mechanical Engineering, Southwest Petroleum University, 1999